

Naval Research Laboratory

Washington, DC 20375-5000



2

AD-A247 301



NRL/MR/6505-92-6939

NCS Technical Information Bulletin 91-11

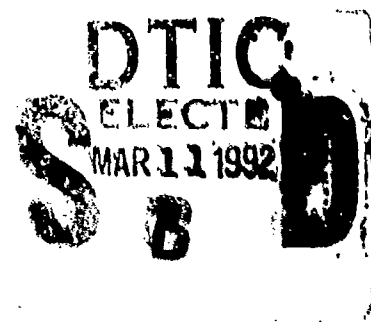
# Correlation of Single Mode Fiber Fabrication Factors and Radiation Response

Final Report  
November 1991

E. J. FRIEBELE

*Optical Sciences Division  
Optical Materials Research Group*

Sponsored by  
National Communications System  
Arlington, VA



February 28, 1992



92-06198



02 3 00 147

Approved for public release; distribution unlimited.

# REPORT DOCUMENTATION PAGE

Form Approved  
OMB No. 0704-0188

Public reporting burden for this collection of information is estimated to average 1 hour per response, including the time for reviewing instructions, searching existing data sources, gathering and maintaining the data needed, and completing and reviewing the collection of information. Send comments regarding this burden estimate or any other aspect of this collection of information, including suggestions for reducing this burden, to Washington Headquarters Services, Directorate for Information Operations and Reports, 1215 Jefferson Davis Highway, Suite 1204, Arlington, VA 22202-4302, and to the Office of Management and Budget, Paperwork Reduction Project (0704-0188), Washington, DC 20503

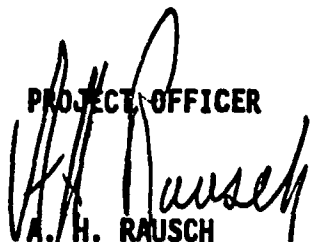
1. AGENCY USE ONLY (Leave blank)	2. REPORT DATE February 28, 1992	3. REPORT TYPE AND DATES COVERED Final	
4. TITLE AND SUBTITLE Correlation of Single Mode Fiber Fabrication Factors and Radiation Response		5. FUNDING NUMBERS	
6. AUTHOR(S) E. J. Friebele		7. PERFORMING ORGANIZATION NAME(S) AND ADDRESS(ES) Optical Sciences Division Naval Research Laboratory 4555 Overlook Avenue, S.W. Washington, D.C. 20375-5000	
8. PERFORMING ORGANIZATION REPORT NUMBER NRL Memorandum Report Number 6939		9. SPONSORING/MONITORING AGENCY NAME(S) AND ADDRESS(ES) Dr. Andre H. Rausch National Communications System 701 S. Courthouse Road Arlington, VA 22204	
10. SPONSORING/MONITORING AGENCY REPORT NUMBER NCS Technical Information Bulletin 91-11		11. SUPPLEMENTARY NOTES	
12a. DISTRIBUTION/AVAILABILITY STATEMENT Approved for public release; distribution unlimited.		12b. DISTRIBUTION CODE	
13. ABSTRACT (Maximum 200 words) The effect of varying single mode fiber fabrication factors such as core and clad dopant concentrations, deposition conditions, and draw parameters on the recovery of the nuclear radiation-induced attenuation at 1.3 $\mu\text{m}$ has been studied. Statistically significant correlations of core factors have been established with a 2 <sup>4</sup> experimental design, and separate one-dimensional experiments revealed the effect of clad [Ge] and [F]. The conclusions from the core effects study have indicated appropriate deposition conditions and fiber draw parameters to maximize recovery and hence minimize the loss induced by low dose rate fallout exposure. Although the effect of the cladding on radiation response is much less than that of core, the one-dimensional study has demonstrated that the best recovery will occur in fibers with pure silica or Ge-F-doped silica matched clads. The worst recovery is experienced in depressed clads with high [F] and low [Ge], which is a significant result since these doping schemes are used for dispersion-shifted and dispersion-flattened fibers for 1.55 $\mu\text{m}$ operation.			
14. SUBJECT TERMS Optical Fibers, Nuclear Radiation, Telecommunications		15. NUMBER OF PAGES 150	
16. PRICE CODE		17. SECURITY CLASSIFICATION OF REPORT Unclassified	
18. SECURITY CLASSIFICATION OF THIS PAGE Unclassified		19. SECURITY CLASSIFICATION OF ABSTRACT Unclassified	
20. LIMITATION OF ABSTRACT Unlimited		21. LIMITATION OF ABSTRACT	

NCS TECHNICAL INFORMATION BULLETIN 91-11


CORRELATION OF SINGLE MODE FIBER FABRICATION FACTORS AND RADIATION RESPONSE

NOVEMBER 1991

PROJECT OFFICER

  
A. H. RAUSCH  
Electronics Engineer

APPROVED FOR PUBLICATION:

  
DENNIS BODSON  
Assistant Manager  
Office of Technology  
and Standards

FOREWORD

The National Communications System (NCS) is an organization of the Federal government whose membership is comprised of 23 Government entities. Its mission is to assist the President, National Security Council, Office of Science and Technology Policy, and Office of Management and Budget in:

- o The exercise of their wartime and non-wartime emergency functions, and their planning and oversight responsibilities.
- o The coordination of the planning for and provision of National Security/Emergency Preparedness communications for the Federal government under all circumstances including crisis or emergency.

In support of this mission the NCS has initiated and manages the Electromagnetic Pulse (EMP) program. The major objective of this program is to significantly reduce the vulnerability of the U.S. telecommunication infrastructure to disabling damage due to nuclear weapon effects in direct support of the survivability and endurability objectives addressed by Executive Order 12472 and National Security Decision Directive 97. Nuclear weapon effects include EMP, Magnetohydrodynamic EMP (MHD-EMP), and fallout radiation from atmospheric detonations. The purpose of this Technical Information Bulletin is to provide the reader with information relating to the effects of fallout radiation on fiber optic cables which will become the predominant transmission media in the 1990's.

Comments on this TIB are welcome and should be addressed to:

Office of the Manager  
National Communications System  
ATTN: NT  
701 S. Court House Road  
Arlington, VA 22204-2199  
703-692-2124

**CORRELATION OF SINGLE MODE FIBER FABRICATION FACTORS  
AND RADIATION RESPONSE**

**FINAL REPORT**

**November 5, 1991**

**E. Joseph Friebele, Principal Investigator  
Optical Sciences Division, Code 6505  
Naval Research Laboratory  
Washington, DC 20375  
(202) 767-2270**

**Andre H. Rausch, Program Manager  
Technology and Standards  
National Communications System  
Arlington, VA 22204  
(202) 692-2124**

**Funded by the National Communications System under MIPR HC1001-8-40216**

## CONTRIBUTING SCIENTISTS

Charles G. Askins  
Michael E. Gingerich  
David L. Griscom  
Calvin C. Harrington\*  
Martin A. Putnam\*\*  
William H. Schmidt\*\*\*

<b>Accession For</b>	
NTIS GRA&I	<input checked="" type="checkbox"/>
DTIC TAB	<input type="checkbox"/>
Unannounced	<input type="checkbox"/>
Justification	
By _____	
Distribution/	
<b>Availability Codes</b>	
Dist	Avail and/or Special
A-1	

\* SFA, Inc., Landover, MD 20785

\*\* University of Maryland Research Foundation, College Park, MD 20770

\*\*\* Michigan State University, E. Lansing, MI 48824

# TABLE OF CONTENTS

EXECUTIVE SUMMARY .....	E1
BACKGROUND .....	E1
PRESENT PROGRAM .....	E2
RESULTS AND CONCLUSIONS .....	E3
TABLE OF CONTENTS .....	ix
1.0 INTRODUCTION .....	1
1.1 BACKGROUND .....	1
1.2 PROGRAM .....	2
1.2.1 Statistical Analysis of Phase I Data. ....	3
1.2.2 Temperature Dependence. ....	3
1.2.3 Clad Studies .....	3
1.2.4 Core Studies .....	4
REFERENCES .....	5
2.0 EXPERIMENTAL IMPROVEMENTS .....	7
2.1 PREFORM FABRICATION FACILITY .....	7
2.1.1 Gas Delivery System .....	7
2.1.2 Scrubber .....	11
2.1.3 Preform Diameter Control .....	14
2.1.4 Computer Control .....	15
2.1.5 Calibration of Vapor Delivery .....	16
2.1.6 Upgrade of the Preform Analyzer .....	18

2.2 FIBER DRAWING FACILITY .....	19
2.2.1 Graphite Draw Furnace .....	19
2.2.2 Diameter Control .....	20
2.2.3 Draw Tension Monitor .....	20
2.2.4 Rapid Cutoff Measurement .....	22
2.3 FIBER MEASUREMENT AND CHARACTERIZATION .....	23
2.4 FIBER IRRADIATIONS .....	24
2.4.1 Upgrade of the <sup>60</sup> Co source .....	24
2.4.2 Stability of the Radiation Damage Measurement System .....	25
2.4.3 Temperature-Stabilized Couplers .....	25
2.4.4 Implementation of a Reference Channel .....	26
REFERENCES .....	26
3.0 STATISTICAL ANALYSIS OF PHASE I DATA .....	31
3.1 PHASE I EXPERIMENTAL DESIGN .....	31
3.2 CONFOUNDING OF THE DESIGN .....	33
3.3 ANALYSIS OF DATA .....	33
3.4 MULTIVARIATE ANALYSIS .....	35
3.4.1 Phase IA Fibers .....	35
3.4.2 Ge-F-Doped Silica Fibers .....	37
A <sub>0</sub> .....	37
A <sub>f</sub> .....	38
n and r .....	38
3.5 ESTIMATED EFFECTS .....	39
3.5.1 Phase IB Fibers .....	40
3.6 DISCUSSION .....	41

REFERENCES .....	43
<b>4.0 TEMPERATURE DEPENDENCE .....</b>	<b>65</b>
4.1 EXPERIMENTAL .....	65
4.2 RESULTS AND ANALYSIS .....	66
REFERENCES .....	68
<b>5.0 EFFECT OF CLAD DOPANTS .....</b>	<b>79</b>
5.1 LEVELS OF THE FACTORS .....	79
5.2 RESULTS .....	80
5.2.1 Silica Clad Fibers .....	81
5.2.2 Effect of Ge Doping .....	82
5.2.3 Effect of F Doping .....	82
5.3 SUMMARY .....	83
<b>6.0 RESPONSE-FABRICATION CORRELATIONS .....</b>	<b>89</b>
6.1 EXPERIMENTAL DESIGN .....	89
6.1.1 Levels of the Core Factors .....	90
6.1.2 Levels of the Clad Factors .....	91
6.2 PREFORM FABRICATION .....	92
6.2.1 Reagent Transfer .....	92
6.2.2 Glass Deposition .....	93
6.2.3 Index Calibration .....	94
6.3 FIBER DRAWING AND MEASUREMENTS .....	96
6.3.1 In-House Draw Facility .....	96
6.3.2 Off-Site High Speed Fiber Drawing .....	97



6.3.3 Fiber Characterization .....	98
6.3.4 Intrinsic Spectral Attenuation .....	98
6.3.5 Mode Field Diameter .....	102
6.3.6 Optical Time Domain Reflectometry .....	103
6.4 IRRADIATIONS .....	104
6.5 ANALYSIS OF DATA .....	105
6.6 ESTIMATED EFFECTS .....	107
REFERENCES .....	109
7.0 CONCLUSIONS .....	131
7.1 SUMMARY OF RESULTS .....	131
7.1.1 Core Effects. ....	131
7.1.2 Clad Effects. ....	132
7.1.3 Temperature Dependence. ....	132
7.2 RADIATION HARD FIBER DESIGN. ....	133
7.2.1 Fallout Radiation Environment .....	133
7.2.2 Delayed Gamma Radiation Environment .....	134
7.3 FUTURE DIRECTIONS .....	134

## **EXECUTIVE SUMMARY**

### **BACKGROUND**

Fiber optic transmission systems, because of their extraordinary channel capacity and decreasing cost, are the preferred terrestrial transmission media of the nation's long distance, inter-city telecommunications infrastructure. Since the commercial telephone network forms the foundation for emergency communication in the event of a national crisis or emergency, additional requirements are placed on the fibers and components of this system. The network must remain operational in the face of such threats as loss of commercial power, disruption by natural causes, violation of physical security, and exposure to the effects of nuclear weapons, including electromagnetic pulse (EMP) and ionizing radiation from the delayed gamma component and fallout.

The most stressing environment for the fiber consists of fallout subsequent to a nuclear attack since the long lengths of fiber can be potentially exposed to high total doses. The susceptibility of some types of commercially available fiber optic cable to optical darkening (and hence increased signal loss and bit error rate) from exposure to ionizing radiation raises serious questions about the survivability of such systems in the reconstitution phase of a nuclear conflict. There is a large body of knowledge available on the effects of gamma radiation on both the older multimode fiber cables and more recent single mode fibers. In spite of the fact that the radiation hardness of fibers has improved through the years, there is a critically important knowledge gap with respect to optimizing the radiation resistance of single mode cables to be employed in the inter-city fiber transmission links in the near future.

There is a continuing need to establish and maintain the data base of single mode fiber radiation responses in order to have the tools necessary to assess the National Security Emergency Preparedness (NSEP) utility of present and future fiber optic systems and to provide guidance on how to decrease their radiation susceptibility. These data will be used in the preparation of a multi-tier specification by the National Telecommunications and Information Administration Institute for Telecommunication

Sciences (NTIA/ITS) for the National Communications System (NCS) to identify the measures to be incorporated into the design of commercial fiber optic networks to meet NSEP survivability needs. The design parameters to be addressed by this specification will be those which tend to minimize disruption of service in the face of the above-mentioned threats and to greatly increase the probability of survival of optical fiber networks.

In the first phase of this program, completed in 1988, a preliminary understanding of the relationship between single mode fiber fabrication parameters and radiation response was developed, and an attempt was made to develop a model so that the behavior of fiber optic waveguides in fallout radiation environments could be quantitatively predicted based on knowledge of fabrication parameters and fiber compositions.

## **PRESENT PROGRAM**

This document is the final report of a 30 month effort, which was the second phase of the program funded by NCS at NRL to study the radiation-induced loss in single mode fibers for telecommunications applications. The experimental and analytical studies carried out in the Phase II program addressed the problem of establishing robust, highly-significant statistical correlations between fiber fabrication factors and the increase in optical loss in single mode fiber optic waveguides that occurs as a result of exposure to fallout from nuclear weapons. Parameters of fiber design and manufacture critical to radiation hardness were identified and provided as input to the specification of fibers for lightwave communications systems capable of satisfying National Security/Emergency Preparedness requirements.

This work is the first statistically robust study of the interrelationship of fiber parameters and radiation-induced loss. The first phase of the program suffered from two deficiencies: 1) confounding of the experimental design resulted in ambiguous interpretation of the observed dependencies; and 2) the experimental design simultaneously addressed both core and clad effects; the latter were masked by the much more dominant core effects. In this second phase clad effects

were investigated in separate, one-dimensional experiment, while core effects were addressed in a strict full-replicate of a  $2^4$  experimental design. The generic radiation environment for the fiber, which was derived in Phase I from literature values and calculations, was used in this study. Fabrication factors having a statistically-significant effect on radiation sensitivity and subsequent recovery have been identified, and the behavior of the fibers has been well-characterized after exposures at  $-35$  C. The  $n^{\text{th}}$  order kinetic model describing the recovery in quantitative terms developed in Phase I was been applied to the data, and the kinetic parameters have been correlated with fabrication factors. In addition, irradiations and recovery measurements have been made over the temperature range from  $-55$  to  $+23$  C, and an analysis has been performed to determine the origin of the temperature dependence of the recovery.

## RESULTS AND CONCLUSIONS

The most significant result of present study is the establishment of highly statistically significant correlations between single mode fiber fabrication factors and recovery parameters. The radiation response and recovery has been quantified by fitting the data to an  $n^{\text{th}}$  order kinetic equation. The "initial" loss  $A_0$  is a measure of the response of the fiber to the delayed gamma component, while the "permanent" incremental  $A_f$  loss, the half-life  $\tau$  of the damage, and the order of the recovery kinetics  $n$  are measures of the fallout response. The statistical significance of the correlations and estimated effects derived from the analysis lay the foundation for a predictive capability whereby the optical attenuation induced by nuclear fallout in a matched clad single mode fiber can be determined via a model whose inputs are core and clad dopant concentrations and fabrication parameters such as draw speed and tension and oxygen-to-reagent ratio ( $O_2/R$ ) used during core and clad deposition.

The conclusions from the study of core effects using the  $2^4$  experimental design have indicated that to maximize recovery and hence minimize the loss induced by low dose rate fallout exposure, the core  $O_2/R$  should be  $\sim 7$ , and the fiber should be drawn at high speed. Either core [Ge]  $\sim 10$  wt% and high fiber draw tension, or core [Ge]  $\sim 14$  wt% and low draw tension will minimize  $A_f$ .

Although the effect of the cladding on radiation response is much less than that of the core, the one-dimensional study has demonstrated that the best recovery, and hence the lowest incremental loss in low dose rate fallout environments, will occur in fibers with pure silica or Ge-F-doped silica matched clads. The worst recovery is experienced in depressed clads with high [F] and low [Ge], which is a significant result since these doping schemes are used for dispersion-shifted and dispersion-flattened fibers for 1.55  $\mu\text{m}$  operation.

Thus, the results of the Phase II program have established the optimum recipe for preform fabrication and fiber drawing to minimize the fallout radiation sensitivity of matched clad single mode fibers operating at 1.3  $\mu\text{m}$ . It is most important to note that the requirements of the recipe can likely be implemented within the intrinsic requirements of the optical fibers and *at very little additional expense!* The latter point is crucial for transition to the telecommunications industry, where cost-effectiveness is a primary concern and it is unlikely that high-cost changes to fiber fabrication would be adopted.

The estimated effects derived from MANOVA provide the basis for developing a model for predicting radiation response from the analyzed core and clad compositions, which can be determined by electron microprobe analysis. In addition, parameters such as oxygen flow during core and clad deposition, draw speed and draw tension are also required as input in some cases. The former parameters can be measured from the fiber, albeit tediously, while the latter must be provided by the manufacturer before the predictive model can be used. Alternatively, fibers to be installed can be specified to have optimum parameters for radiation hardness.

# CHAPTER 1

## INTRODUCTION

### 1.1 BACKGROUND

Currently, telephone companies have installed extensive long line lightwave communication systems using single mode fibers as the data and voice transmission medium. Since the commercial telephone network forms the foundation for communication in the event of a national crisis or emergency, additional requirements are placed on the fibers and components being installed, such as unimpaired operation in the event of power loss, sabotage, disruption by natural causes, EMP, or nuclear fallout. One of the most stressing environments that the fiber might experience consists of the initial prompt gamma rays following a nuclear weapons detonation and the fallout subsequent to a nuclear attack.

In the first phase of this study,[1] an analysis was performed to estimate the total dose/dose rate conditions that a hypothetical telecommunications fiber might experience from both prompt gamma and fallout exposure. The radiation environment was estimated from educated guesses at the survivability of fiber cable exposed to various dynamic overpressures and thermal loads, and the attenuation of the earth for buried cable was considered. In summary, doses of several kilorad rad were deemed reasonable for buried cable exposed to either prompt gamma or fallout, and similar doses were assumed relevant for exposed fiber in bridge crossings and aerial deployments. Thus, the fibers were exposed at an assumed worst-case temperature for the continental US of -35 C to a total dose of 2000 rad. The recovery was monitored for ~24 h after exposure, and the data were fit to an expression for  $n^{\text{th}}$  order kinetics, which has 4 adjustable parameters. The "initial" loss  $A_0$  is a measure of the response of the fiber to the delayed gamma component, while the "permanent" incremental  $A_f$  loss, the half-life  $\tau$  of the damage, and the order of the recovery kinetics  $n$  are measures of the fallout response.

It has been well-established that steady state radiation exposures can induce incremental losses in single mode fibers of at least 0.001 dB/km-rad at 1.3  $\mu\text{m}$ . [1,2] Since most of the commercially-available single mode fibers have intrinsic losses of  $< 0.5$  dB/km at 1.3  $\mu\text{m}$ , a fallout exposure of  $10^4$  rads will result in at least a 3-fold increase in the optical attenuation of the most radiation-resistant fiber! This loss will result in decreased signal at the detector and a concomitant increase in bit error rate. Alternatively, the repeater spacing must be reduced at substantial expense to the system.

There have been numerous characterizations of the radiation sensitivity of both single mode and multimode fiber waveguides, [3-5] but they have been largely qualitative studies of commercial or prototype fibers provided by fiber manufacturers with little or no documentation concerning the fabrication techniques and parameters. More recently, in the first phase of this program, completed in 1988, a preliminary understanding of the relationship between single mode fiber fabrication parameters and radiation response was developed, and an attempt was made to develop a model so that the behavior of fiber optic waveguides in fallout radiation environments could be quantitatively predicted based on knowledge of fabrication parameters and fiber compositions. The first phase of the program suffered from two deficiencies: 1) confounding of the experimental design resulted in ambiguous interpretation of the observed dependencies; and 2) the experimental design simultaneously addressed both core and clad effects; the latter were masked by the much more dominant core effects. Multiple regression and orthogonal matrix analyses were applied to the data in an attempt to elucidate the fabrication-response correlations. Although the deficiencies in the study precluded development of a predictive model, quantitative relationships between preform and fiber fabrication factors and radiation response parameters were demonstrated for the first time.

## 1.2 PROGRAM

The experimental and analytical studies carried out in the Phase II program addressed the deficiencies of Phase I and expanded the environmental parameter space to include a range of temperatures. These studies are summarized below and described in detail in the following chapters.

**1.2.1 Statistical Analysis of Phase I Data.** Because the experimental design used in Phase I was not a part replicate and was not orthogonal, there was confounding of the main effects with two-way and higher order interactions. Both the orthogonal matrix and regression analyses performed in Phase I had limited utility, so additional analysis was performed on the data. To investigate the confounding present in the partial replicate of the full factorial design, a column basis for the full design was used to derive the alias structure. The statistical significance of correlations between fabrication factors and radiation response parameters was then investigated by multivariate analysis of variance, and estimated effects were calculated.

The study showed clearly that the initial induced attenuation was negatively correlated with the concentration of Ge in the core, the final or permanent loss was negatively correlated with the ratio of oxygen to reagent ( $O_2/R$ ) used during core deposition, and the half-life of the incremental loss and the kinetic order of the recovery depended on a two-way interaction of core  $O_2/R$  and draw speed. However, the confounding of the design and the lack of replicates of any fiber precluded additional analysis.

**1.2.2 Temperature Dependence.** In the Phase I study, the fibers' temperature was maintained at -35 C during irradiation and measurement of the recovery of their incremental loss. In a real deployment it is certain that the fibers will experience a range of temperatures, perhaps between -55 and +50 C, and the recovery characteristics will likely vary with temperature. To elucidate these effects, a number of the commercial single mode fibers were irradiated and measured at -55, -35, 0, and 23 C. The data were fit to  $n^{\text{th}}$  order kinetics, and an analysis of the temperature dependence of the recovery parameters was performed. It was determined that temperature dependence was primarily expressed in the number of color centers, i.e.  $A_0$  and in the half-life of the attenuation.

**1.2.3 Clad Studies.** Because any effect of the cladding on radiation response would be masked in an experimental design that included variations in both core and clad factors, two one-dimensional studies of clad effects alone were undertaken. A common fiber core and draw conditions were used in all fibers. In the first study, a series of matched clad fibers was fabricated where the clad [Ge] and



[F] were varied from pure silica to the maximum available from the NRL gas delivery system. This set confirmed the anomalously large values of  $A_0$  observed in silica clad fibers in Phase I and determined that only slight Ge doping was needed in the clad to suppress  $A_0$ . Further increases in clad [Ge] decreased  $A_0$  slightly. The second experiment involved increasing the clad [F] while holding the concentration of Ge constant at a low level so that depressed clad fibers with increasing values of  $\Delta$  were fabricated. It was found that the excess F doping in these fibers resulted in substantially longer recovery times due to increased kinetic order and half-lives.

**1.2.4 Core Studies.** The core effects on matched clad fiber radiation response were investigated using a full-replicate of a  $2^4$  experimental design. The core [Ge],  $O_2/R$  used during core deposition, draw speed and draw tension were each varied over 2 levels while the clad composition and deposition were held constant. Replicates of each of the 16 fibers were fabricated and measured, and the good quality control resulted in a number of statistically significant correlations between fabrication factors and radiation response parameters.

The results of the Phase II program have established the optimum recipe for preform fabrication and fiber drawing to minimize the fallout radiation sensitivity of matched clad single mode fibers operating at 1.3  $\mu\text{m}$ . It is most important to note that the requirements of the recipe can likely be implemented within the intrinsic requirements of the optical fibers and *at very little additional expense!* The latter point is crucial for transition to the telecommunications industry, where cost-effectiveness is a primary concern and it is unlikely that high-cost changes to fiber fabrication would be adopted.

The estimated effects derived from MANOVA provide the basis for developing a model for predicting radiation response from the analyzed core and clad compositions, which can be determined by electron microprobe analysis. In addition, parameters such as oxygen flow during core and clad deposition, draw speed and draw tension are also required as input in some cases. The former parameters can be measured from the fiber, albeit tediously, while the latter must be provided by the

manufacturer before the predictive model can be used. Alternatively, fibers to be installed can be specified to have optimum parameters for radiation hardness.

#### REFERENCES

1. E.J. Friebele, "Radiation Response Prediction of Single Mode Fibers," NCS Tech. Bull. 88-1 (National Communications System, Arlington, VA, 1988).
2. E.J. Friebele, K.J Long and M.E. Gingerich, "Radiation Response of Single Mode Optical Fibers," Appl. Opt. 22 1754-1757 (1983).
3. E.J. Friebele, "Optical Fiber Waveguides in Radiation Environments," Opt. Eng. 18 552-561 (1979).
4. E.J. Friebele, C.G. Askins, M.E. Gingerich, and K.J. Long, "Optical Fiber Waveguides in Radiation Environments II," Nucl. Inst. Meth. in Phys. Res. B1 355-369 (1984).
5. E.J. Friebele, K.J. Long, C.G. Askins, M.E. Gingerich, M.J. Marrone, and D.L. Griscom, "Overview of Radiation Effects in Fiber Optics," Crit. Rev. Tech.: Opt. Materials in Radiation Environments (SPIE Vol. 541), P. Levy and E.J. Friebele, Ed. (SPIE, Bellingham, WA, 1985), pp. 70-88.

## CHAPTER 2

### EXPERIMENTAL IMPROVEMENTS

Throughout the period of performance of the Phase II program, a number of improvements to the experimental apparatus used to fabricate the preforms, draw the fibers, characterize their optical properties, and determine their radiation response were implemented. Some were funded by the program, while others benefitted from other programs. In any event, all had a positive impact on the Phase II program and are summarized in this chapter.

#### 2.1 PREFORM FABRICATION FACILITY

**2.1.1 Gas Delivery System.** Prior to the Phase I program, the Optical Materials Research Group had purchased a Modified Chemical Vapor Deposition (MCVD) gas delivery system in 1981 from Tylan, Inc. to provide the capability to generate fiber optic waveguide preforms. The system was intended to represent a typical industry facility for the production of telecommunications optical fibers. Over the ensuing years, in-house modifications to the system became necessary and were incorporated to permit experimentation with MCVD techniques which did not exist at the time of purchase. Extensive control alterations were also implemented to correct design short-comings in the original apparatus. The modified system was employed to fabricate preforms for several material studies, including Phase I of the radiation response prediction program.

Throughout the several years of operation, the Tylan system was exposed to a low-level corrosive environment of the MCVD laboratory, which consisted of low concentrations of HCl vapors formed by reaction of slight quantities of the  $\text{SiCl}_4$  and  $\text{GeCl}_4$  reagent vapors with humidity in the atmosphere. The effects of this atmosphere were exasperated in the Tylan system because the electronics cabinet was directly above the reagent cabinet which held the bubblers, and neither was sealed from the room atmosphere or each other. The corrosive exposure had degraded the electrical

control connections to the point that auxiliary monitoring electronics had to be appended. The stability and accuracy of the flow-metering devices began to suffer from age, and it was felt that the stainless steel plumbing of the delivery manifolds was beginning to be compromised. Although useful experimentation continued with this equipment, waning reliability had substantially reduced the yield of valid samples. The death knell for the Tylan system occurred the summer after the initiation of the Phase II study when a steam line ruptured in the basement of the building, pouring high humidity into the laboratory for several weeks before NRL Public Works fixed it.

Since the Tylan system was now completely unreliable, a survey and evaluation began for identifying both the appropriate replacement gas delivery technology and a suitable supplier. Although seriously considered, in-house design and construction of a replacement apparatus was rejected as an option after projecting the expenditure of time required for such a non-research undertaking. The survey identified a set of specifications for the procurement that addressed the weaknesses of the original facility, anticipated the flexibility required for further in-house innovation, and reflected the current state-of-the-art in MCVD gas delivery. These (and other) guidelines, which determined the eventual supplier, were:

- 1) The source of liquid chemicals such as  $\text{SiCl}_4$ ,  $\text{GeCl}_4$  and  $\text{POCl}_3$  which are evaporated into an oxygen gas stream must be either a reflux bubbler or a supplemental temperature-controlled bubbler to provide accurate reagent concentration via accurate vapor pressure determination. To maintain accuracy of the mass flow controllers and to minimize corrosion, only the input of the oxygen carrier gas was to be metered by mass flow controller. Differential mass flow measurement of the vapor was not acceptable because of the potential for drift and degradation of the sensing device exposed to the reagent.
- 2) The vapor source containers and connections (valves, plumbing) must be enclosed in a dry, nitrogen-purged cabinet with the capability of maintaining water vapor content *in the cabinet* below 1 ppm. The enclosures for the vapor sources and the reactive gaseous sources ( $\text{SiF}_4$ ,  $\text{Cl}_2$ , and  $\text{BCl}_3$ ) must provide visual access, lighting, and glove ports so that valves can be

manipulated without opening the container to the atmosphere. Fittings and tubing must be Teflon to ensure resistance to attack by the reactive chemicals (which would result in unacceptable impurity levels in the fiber preforms) and to enable simple replacement and modification of plumbing as required. The older technology based on stainless plumbing had visibly corroded in the Tylan system, which promised ultimate leakage and contamination during servicing.

3) The NRL Safety Office and safe standard operating procedures require that the chemical cabinet enclosure provide a reservoir with the capacity to contain the total volume of highly reactive liquid chemicals in the event of spillage or breakage. The earlier enclosures violated the requirement for containment of liquid chemicals, and vapor leakage was not controlled.

4) The reagent gas sources ( $O_2$ , He, Cl, etc.) must have drying columns and gettering furnaces (as applicable) which can be renewed with commercially-available, standard stock replacement parts. All bottle and bubbler connections must have cross-purge tees and pressure regulators which are chemically inert relative to any reactive reagent. Each cross-purge tee must be provided with dry nitrogen gas for purging. Although water contamination was managed by use of high purity starting gases in the original system, a monetary and time savings results from the ability to use and purify lower grade gases.

5) All parts of the system plumbing except the interior of chemical source containers must be capable of being purged by dry nitrogen gas, both under operator control and as a default in the event of loss of power to the control electronics. The useful life of the original system was extended by this measure, and residual contaminants are minimized by preventing stagnant lines.

6) The control electronics, plumbing (valves, tubing, flow controllers) must be in clean, dry cabinet enclosures. The laboratory environment in the vicinity of the chemical deposition is too harsh for unprotected mechanisms and electronics. Past experience with the Tylan System

demonstrated that the high humidity, dirt, and occasional chemical leaks combined to fatally degrade exposed components.

7) The deposition torch must be controlled to a temperature setpoint monitored by an Iacon 7000 series pyrometer (used for previous work and incorporated into the new system).

8) The gas delivery system shall be one which has been demonstrated both in research and production in the telecommunications industry so that the results of the NRL program are directly transferrable to industry. For example, fibers fabricated from preforms must have demonstrated minimum metallic and water impurity levels in commercial volume so that optical losses at 0.85 and 1.3  $\mu\text{m}$  are below 3 and 0.5 dB/km, respectively, and the maximum loss in the 1.4  $\mu\text{m}$  water absorption has been routinely demonstrated to be less than 5 dB/km.

The system selected was manufactured by Special Gas Controls, Ltd., based in the U.K. with a U.S. representative. As installed, the assembly comprises three separate cabinets enclosing: hazardous gas sources and liquid reagent reservoirs for refill, a set of five gas driers, and the central liquid chemical dry-box with control manifolds, flow metering and electronics. All cabinets provide protected internal environments ranging from filtered air at positive pressure to complete closed-cycle air conditioning. The liquid reagents are immersed in external oil baths whose temperatures regulate the vapor pressures and therefore the rate of vapor transport per unit of carrier gas. Refill is accomplished through permanently plumbed and continuously purged lines inside purged enclosures so that the chemical vessels and fittings are never exposed to a humid environment.

The new gas delivery system has provided reliable operation over the course of the Phase II study and appears to be a fundamentally sound apparatus. The installation and early operation was, however, characterized by complications and delays. The equipment was delivered 1-1/2 months later than prescribed by the contract due to vendor delays. Once on site, installation continued nearly non-stop for over one month with progress slowed by the cramped laboratory space. As portions of the complex assembly were brought on-line, engineering flaws appeared which either limited or

prevented operation. Most problems reflected customizations to meet our specifications, or adaptations to US standards and codes. Because the specified capacity for separate thermal control of the multiple liquid sources required individual oil baths and controllers, a large heat load had to be dissipated. The vendor's engineering did not sufficiently consider this load, and repeated attempts at solving the cooling problem stretched over the following year. Power failed internally on two occasions when connections to a step-up transformer overheated. As late as Spring 1991, logic circuit faults were resulting from a power supply adjusted for British line voltages.

In the midst of return service calls and on-the-fly re-engineering of the cooling problem, the system was brought into operation. Reagent bubblers were filled on February 21, 1990, three months after the apparatus was uncrated. The first deposition (and calibration test) occurred the following week on the 28th. Subsequent progress was interleaved with stoppages from failures of varying severity. Examples range in magnitude from loose signal wires connecting the torch translation motor, to the implosion of the glovebox window after a power outage allowed the interior to cool and the resulting pressure drop caused cracks to initiate at improperly polished glass edges. As drastic as these events seem in retrospect, the fundamental apparatus is sturdy, and each appearing problem has been amenable to permanent correction; a large step beyond the condition of its predecessor. Months of successful operation have included periods averaging an unprecedented three preforms per week.

**2.1.2 Scrubber.** There are three noxious and/or hazardous by-products of the MCVD process, i.e. silica dust, chlorine, and fluorine gas, which must be scrubbed from the effluent before exhausting it into the environment. Operators of MCVD facilities are compelled to responsibly process the exhaust products in a manner that is neutral to the environment, so that the vicinity of the process is not noxious to other personnel. Although successful preform deposition is not physically dependent on scrubber function, consistent neutralization of byproducts with underdesigned equipment consumes an inordinate amount of operator time. In light of the limited personnel available for Phase II and the large number of consistent preforms required, it was deemed essential that the scrubber be a turn-key system that would consume as little attention as possible.

Several commercial scrubbers are available for addressing this problem. One such system was purchased from one of the better-rated manufacturers, but due to poor design it failed after a short time. It was decided that a robust scrubber would be designed and built in-house after learning from the faults of the industrial design. The commercial system employed high velocity nozzles to spray an aqueous, highly caustic KOH solution ( $\text{pH} > 12$ ) into the effluent gas stream and onto a dense nylon mesh. The KOH sprayed over a large surface area to react with and neutralize the  $\text{Cl}_2$  and  $\text{F}_2$  gases and keep the silica soot in solution, rather than having it form a gel. After the gas/liquid mixture interacts in the nylon mesh, the gas was exhausted and the liquid was recycled *via* a pump. In spite of frequent efforts to clean the mesh, this system eventually failed due to clogging and was replaced by the first of two scrubbers designed and built in-house.

The first scrubber consisted of a tall cylindrical tower filled with hundreds of high surface area plastic packing spheres, a large volume polyethylene tank, a chemical recirculating pump and a high velocity blower. The KOH solution was pumped from the holding tank up to the top of the tower through chemically resistant tubing, where it was propelled into a circulating sprayer, evenly wetting the plastic balls. After percolating down through the column, the neutralizing solution fell back into the tank for recirculation. The blower was employed to draw the gases from the MCVD lathe up through the tower (opposite to the flow of the solution) before exhausting the chemical and particulate-free gas to the outside.

By comparison with the purchased scrubber, the in-house system provided an enlarged capacity and a sharp increase in the time between servicing. The improvement can be attributed to the replacement of the nylon mesh with high surface area spheres. Although the two media have comparable areas, the size of the spheres prevents clogging with captured particulate, which rapidly disabled the commercial design. An expanded holding tank provided improved settling of solids due to lowered flow velocity, and the avoidance of fine aperture nozzles extended the time required for cumulative clogging to seriously impair the scrubbing capacity.



Several years of constant use weakened the first in-house scrubber by constant vibration and chemical corrosion. A replacement scrubber was then constructed near the beginning of Phase II, approximately at the same time that the Tylan gas delivery system was replaced. Most of the first in-house scrubber concept was incorporated into the second; the most significant improvements involved the use of more chemically-inert materials. For example, the new version replaced welded polyethylene joints with glued PVC. Both polyethylene and PVC are considered chemically-inert in the presence of high pH solutions such as KOH, but polyethylene is relatively difficult to work with. Joints and seals on the original polyethylene parts were made by constructing various complex fittings from Teflon or PVC plumbing and sealing them with silicon RTV. Over time these joints loosened and leaked. For this reason both the holding tank and the two-section polyethylene tower of the earlier scrubber were replaced by a seamless PVC tower and a tank with glued joints. The new PVC tank sits inside of the original polyethylene tank, which functions as a backup containment vessel.

The recirculating pump utilized two pieces of polished graphite to form a rotational seal between the impeller and the motor shaft, and it suffered numerous failures from chemical corrosion. These seals had a tendency to wear out quickly, exposing metal bearings and windings to the KOH solution, so that the pump would required replacement several times a year. The new scrubber employs a pump with a sealed impeller magnetically coupled to the motor shaft, and it has proven to be 100% reliable, not requiring replacement over the last two years.

An improvement yielding the most dramatic reduction in scrubber repair frequency was the placement of a water droplet trap just downstream of the blower. On the preceding scrubber, water spray drawn from the tower into the blower eroded the flexible fabric impeller at a rate which consumed impellers after less than two months use. The first attempt at designing a baffle chamber entirely from PVC completely removed all traces of spray from the exhaust stream before contacting the impeller. The original gadget has been in place for nearly two years, and no further impeller replacements have been necessary.

The net result of all improvements to the scrubber has been more than a year's operation of the MCVD system with processing of the effluent reduced to a nearly forgotten, yet reliable, function.

**2.1.3 Preform Diameter Control.** Fabrication of axially-consistent preforms is critical to minimize length-to-length variations in the fiber drawn from the preform. However, due to nonuniform axial deposition rates, which are characteristic of the MCVD process and therefore unavoidable, significant diameter fluctuations along the 0.5 m length of the substrate tube typically evolve over the course of depositing many layers. Without compensation, the substrate tube will continuously shrink (as it does during the collapse phase of the process) at a rate governed by the temperature of the glass, material composition, geometry and pressure inside the tube.

The elevated temperatures used for deposition of the glass layers in the MCVD process are sufficient to cause the glass substrate tube to soften. But if the pressure inside the tube exerts a force identical to the surface tension force acting to shrink it, the tube will remain at constant diameter; greater pressures will expand the tube and lesser pressures will allow the tube to contract. A system to monitor and control the preform diameter was designed and constructed in-house at the onset of Phase I of this study. Theory of operation and improvements made to the system during Phase II are described below.

The diameter controlling unit, or "puffer," consists of a line scan camera, control electronics, a flow regulating valve, and an exhaust tube interface assembly. As the torch traverses the preform in the lathe, a camera mounted to the same moving platform monitors the instantaneous diameter of the preform in the region of the hot zone. Pressure in the substrate tube (used to increase the diameter of the tube in the hot region) is achieved by metering back-flow of nitrogen gas into the exhaust tube through an interface assembly with an electrically-controlled valve. Information regarding the diameter is acquired by the camera, fed back to the control electronics, which then adjusts the back-flow of nitrogen accordingly to either expand or contract the diameter of the preform.

The harsh environment of the MCVD laboratory took its toll on the puffer during Phase I, and over time significant maintenance and repair was required to continue operation. Changes made to

the puffer were aimed at increasing efficiency of preform fabrication rather than improving control performance. Minor repairs of the camera and electronics were required, but the exhaust assembly needed to be redesigned and constructed. The original concept of a flexible exhaust assembly was abandoned for a more rigid, all-machined design with fewer moving parts in return for ease of set up and long term reliability. The new system has resulted in time savings of as much as 3/4 hr per preform, which has played a significant role in increasing our maximum sustained production rate from 1 preform every two days to 1 preform per day, as well as increasing our yield of acceptable preforms from 1 in 4 to 1 in 2.

**2.1.4 Computer Control.** In order to ensure reproducible preform fabrication conditions while maintaining a high degree of flexibility, all aspects of the MCVD process must be computer-controlled, either directly or indirectly. These include all chemical flows, traverse speeds, and the temperatures of deposition and collapse. Although it would be desirable to also control the preform diameter by computer, this has not been implemented to date.

The SGC gas delivery system utilizes the multitasking capabilities of a DEC PDP-11/53 microcomputer with an extensive interface to automate the fabrication process. Through the use of a high level programming language (PCM-465) developed by SGC, flexible configuration and control of all the fabrication parameters can be achieved. However, as supplied there was no convenient control code.

The process control software developed by us and written in the high level language (PCM-465) is divided into two sections: the main control program and the menu routine. The main program determines the sequence in which calls to interface routines are made, and the menu contains a list of values used by the main program to set flow rates, temperatures, and traverse speeds specific to the preform being fabricated. Process automation is made flexible in this way by requiring a separate menu routine but only one main program for each type of preform. While creating or editing a menu is significantly less difficult and time-consuming than editing the whole process control program for each preform, it is not necessarily trivial and can often be an arduous task.

Streamlining the often cumbersome task of editing or creating menu files was achieved by developing an IBM PC-compatible program that is capable of generating values for flow rates, temperatures, and deposition speeds in a format compatible with the process control software. Files created by this program are then downloaded to the PDP-11 into a menu file and subsequently used for the fabrication of a particular preform.

**2.1.5 Calibration of Vapor Delivery.** The previous Tylan MCVD system incorporated differential mass flow controllers for direct measurement and control of each vaporized reagent. This required sensors in the corrosive gas downstream of the bubblers, which are glass containment vessels filled with the appropriate liquid reagent, and was one of the causes of the unreliability of the system. Controlled reagent vapor delivery is achieved in the SGC system by monitoring only the flow of carrier oxygen ahead of the glass frit submerged in the bubbler.

Mass transport rate of the vapor (in units of g/min) is governed by not only the flow rate of the carrier oxygen (in units of  $\text{cm}^3/\text{min}$  or sccm), but also by the temperature of the reagent bubbler and the liquid level of the chemical (see Chapter 6). Because most production in the fiber optic industry involves the repeated fabrication of nearly the same fiber design, most "recipes" are determined through an iterative trial-and-error process and are rarely changed. Considering this approach to preform engineering along with the tendency to guard proprietary recipes, there is little motivation to convert flow rates to the absolute units of g/min.

For this work, accurate conversion from carrier oxygen flow to reagent mass flow was necessary for two reasons. First, the Phase II results should be directly comparable with and expand upon Phase I results obtained using the Tylan system, where mass transport was measured in g/min. Second, it was considered essential that the telecommunications industry be able to use the results of Phase II in the fabrication of and improvement of radiation-hard fiber. Reporting the fabrication factors as carrier gas flows would make the transfer of the information virtually impossible. Although calibration of mass transport can be achieved for a particular system if all other variables mentioned above are held constant, transfer of this information to industry could only be accomplished if all

parameters are specified in absolute terms, i.e. in g/min. Without calibration the results of this report could not be easily applied to any other MCVD facility. Thus, it was necessary to calibrate the SGC system in terms of mass transport.

One option for calibration is the use of expensive, dedicated mass flow meters for each reagent. This approach may be considered attractive because of the ease of implementation, especially if the mass flow meters are already available or where their cost is considered incidental. As an alternative, we designed and built an apparatus almost identical to the condenser stage of a distillery.

The ability of a gaseous mixture to absorb and retain vapor is directly related to the temperature of the gas, and as the temperature of a gas is lowered, its ability to retain vapor decreases, resulting in a new equilibrium condition where some of the vapor condenses. If the temperature approaches the freezing point of the reagent, nearly all of the vapor originally contained in the gas will precipitate as liquid.

The vapor transport rate of the SGC gas delivery system was calibrated by diverting its output from the preform substrate tube to a condenser unit and measuring the accumulation rate of the condensate. The apparatus consists of two coils of stainless steel tubing submerged vertically in an ethanol-dry ice slurry, which maintains the temperature near -60 C. At the bottom of the column, the tubes enter a sealed graduated cylinder which terminates in a stop-cock. Warm gas entering the first coil cools, and the reagent vapor condenses onto the walls of the tube. Under gravity, the liquid trickles into the glass graduated cylinder at a rate identically equal to the mass flow rate of the reagent vapor. The second coil exhausts the gas and provides additional path length through the cold bath to ensure that all vapor has condensed out of the carrier gas.

As each transported reagent was introduced to the distiller, a period of many minutes elapsed before the filling rate of the graduated cylinder stabilized. This was attributed to the need for all internal surfaces to be wetted so that any further condensate could drain. Careful timing of the accumulation of 1-2 cm<sup>3</sup> of reagent permitted an accuracy of ~1 %. Accumulation times were recorded over a range of carrier flow rates for each of the vapor sources. The results agreed well with

a rough method based on gauging the rate of level change in the bubblers with a scaled, magnifying sight.

**2.1.6 Upgrade of the Preform Analyzer.** The York Technology preform analyzer serves as the primary tool for evaluating the geometry and index structure of newly-fabricated preforms. Estimates of dopant levels and calibration of flow rates may be based on the indicated index steps. Estimates of the proper fiber diameter to achieve the desired cutoff wavelength is calculated from the profiler's analysis. At the end of Phase I, the apparatus had been in service for six years and was evidencing need for service.

The optical path of the analyzer includes a cell filled with an index-matching oil in which the preform is immersed. Between samples, the cell is emptied into an internal reservoir for removal of the preform, then refilled. The plumbing, level sensors, and pump were in varying states of decrepitude due to long exposure to the oil, and many optical surfaces had become contaminated from leaks. Functional impairment included a binding focus mechanism and the need for an external pump, neither of which compromised the optical analysis. The degradation and gradual misalignment of the optics, however, had contributed to serious distortions in the calculated index profiles. Figure 2.1 is a result of profiling a preform with the machine in this condition; asymmetry of the trace is pronounced, which is purely an artifact of the analysis error. Because the profile is known to be nominally step-like, relative index amplitudes may still be inferred, and the diameters of the structures remain reliable.

The instrument was aligned and recalibrated in April, 1989, and an upgrade of the plumbing and operating software in July improved the speed of operation from a slow crawl to a pleasant experience. The index profile of Figure 2.2 demonstrates the regular features typical of an accurate analysis. A standard preform section was purchased as a means to monitor the instrument calibration.

## 2.2 FIBER DRAWING FACILITY

The need for improved efficiency in the fiber draw process became apparent as the results of Phase I were critically evaluated during the planning of Phase II. Because of the intensive and lengthy process involved in generating each MCVD preform, no waste of samples due to errors or inefficiency during fiber drawing could be tolerated. Elucidation of statistically-significant draw-induced effects depended upon the successful draw of multiple, well-specified, long continuous lengths of fiber from each preform. The required four draw conditions encompassing two levels of draw tension and speed (see Chapter 6) had to be established quickly and held stable so that usable fiber lengths were generated before the preform was exhausted. Toward this purpose, major changes were made to the furnace, diameter measurement and control, tension measurement, and cutoff wavelength determination.

**2.2.1 Graphite Draw Furnace.** All fiber samples for the single-variable cladding studies (Chapter 5) and the 2<sup>4</sup> Phase II design (Chapter 6) were drawn using graphite resistance furnaces. The furnaces at both the contracted high-speed draw facility and the NRL silica draw tower were the same model, manufactured by Thermal Technologies, Inc. The furnace was installed on the NRL draw tower after five years of operating an RF induction furnace employing a zirconia susceptor. While the RF furnace was equally capable of drawing quality fibers, typical operation entailed frequent rebuilding of the susceptor/insulator envelope. The ceramic element densified rapidly when operated at temperatures over 2100 C, resulting in uneven heating and vulnerability to thermal stress and fatiguing. The element often required changing after as few as three draw sessions because an aged element would crack as the furnace temperature was changed, which rapidly degraded the strength of the drawn fiber. In order to avoid servicing the element the furnace would be "idled" at 1800 C over the (sometimes) weeks-long periods between draws.

The graphite resistance furnace is capable of cycling from cold to > 2200 C hundreds of times, with each cycle requiring no more than one half hour. In contrast, bringing the RF furnace up to temperature once it had been turned off consumed most of a single day. Temperature changes within

the operating range had to be ramped at less than  $10^{\circ}/\text{min}$  to prevent stressing the suscepting element. When drawing a single preform at several speeds and tensions, most of the useful sample would be consumed while arriving at a new temperature setpoint. The graphite furnace, on the other hand, has permitted draw over a large range of tensions and speeds while consuming a minimum of preform length, largely because temperature steps greater than 100 C can be effected within five minutes.

**2.2.2 Diameter Control.** The fiber diameter control apparatus used for Phase I (LaserMike by Techmet) was replaced by an Anritsu laser micrometer linked by a standard IEEE-488 data bus to a computer for control of the draw speed. The Techmet instrument suffered from increasingly frequent electronic failures in the middle of otherwise monotonous draw sequences, thereby necessitating immediate manual overriding of the process. Repeated repairs and in-house fixes began to seriously reduce the productive time available for drawing fibers.

The Anritsu instrument extended the controllable fiber diameter downward from a minimum of 70 to 40  $\mu\text{m}$ ; the latter dimension being relevant to the development of sensor fibers. The new combination of instrument and computer permits rapid diameter setpoint changes, with stabilization achieved in under 15 seconds for a 20  $\mu\text{m}$  step. A similar change in setpoint with the older arrangement would require several minutes, as well as manual control during the transition. This rapid arrival at equilibrium contributes to the successful generation of specified fiber samples from a limited preform length.

**2.2.3 Draw Tension Monitor.** The tension under which a preform is drawn into an optical fiber must be controlled, to maintain reproducible fiber draw conditions and to attain the set points prescribed by the Phase II study. In Phase I, tension was measured mechanically during drawing by passing the fiber through a series of three rollers; the force applied to the second roller to deflect the fiber by a fixed distance is measured with a sensitive load cell. The tension is determined by prior calibration of the device by hanging various weights from a fiber threaded through the 3 rollers.

It is necessary to measure the tension on the uncoated section of fiber to avoid the influence that the coating has on the result. Mechanical measurement has at least two disadvantages: (1) because the



rollers contact the fiber, the fiber strength is degraded, and the measurement cannot be performed on a section of fiber intended for service; and (2) unless extreme care is taken, the fiber often breaks in the rollers, especially under high draw tension.

A method for determining draw tension without contacting the fiber, which was developed during the Phase II project, avoids the limitations of the technique described above. It is based on detecting the resonant vibrational frequency of the fiber during draw using the position output of the fiber diameter monitor and requires no specialized circuitry.

The first vibrational mode of a fiber of length  $L$  (the distance in meters between the preform neckdown and coating cup), mass per unit length  $\mu$  (kg/m) and axial tension  $S$  (Newtons) resonates at a frequency  $f_1$  (Hz) defined by

$$f_1 = \frac{1}{2L} \sqrt{\frac{S}{\mu}} = \frac{1.2 \times 10^4}{Ld} \sqrt{S} \quad (2.1)$$

where  $\rho$  has been taken as the density of silica =  $2.2 \times 10^3$  kg/m<sup>3</sup> and  $d$  ( $\mu$ m) is the fiber diameter. Thus, the tension  $s$ , measured as an equivalent mass (kg) attached to the fiber can be calculated from

$$s = 7.1 \times 10^{-10} (f_1 L d)^2 \quad (2.2)$$

In the case of our draw tower, the fundamental resonant frequency is approximately 58 Hz for a 115  $\mu$ m diameter fiber drawn under 0.010 kg tension. Figure 2.3 shows the spectrum of the fiber measured during draw: the intense peak at 27 Hz is from the tractor motor, that at 13 Hz is due to a building vibration; and the weak fundamental fiber resonance is seen near 75 Hz. We applied a small puff of nitrogen from an electrically-actuated valve to reproducibly excite the fiber resonance; a typical spectrum of the excited fiber during draw is shown in Fig. 2.4.

It is clear that the fundamental fiber resonance is clearly separable from extrinsic resonances and that excellent data are obtained in spite of the fact that the ends of the fiber are in viscous media.

L was first estimated as the length from the entrance to the coating cup to the point in the neckdown where significant beading was noted when the preform was held horizontally. This estimation agreed within a few mm of the effective fiber resonant length L determined from Eq. 2.2 using fiber tensions measured by the conventional 3 roller technique.

To automate the fiber tension measurement and integrate it into the existing apparatus, a section of code was added to the Fortran PC-based computer program which controls the draw tower. The fiber is puffed slightly before data acquisition, and the position output from the diameter monitor is amplified and fed to an A/D board (Metrabyte DASH-8) at rates up to 4000 points/sec. A fast Fourier transform is performed on the data, and the resultant spectrum is displayed on the monitor. Using 1024 points, the FFT requires only 1.3 sec on a 12 MHz 80286 machine with a math coprocessor. The fiber tension is then calculated from Eq. 2.2. If added computational speed is desired, a 80386 machine and/or an array processor board could be used; in the latter case the FFT is virtually instantaneous on either an 80286 or 80386 machine.

Obviously, the maximum amplitude of the fundamental resonance occurs at the midpoint of the tower, but diameter monitors are typically located near the top just below the furnace. Especially in the case of long draw towers, the amplitude of the fundamental at this point may be quite small, and a puffer located near the monitor could excite primarily higher order modes. These also can be used to determine draw tension provided a calibration to identify the frequencies of the fundamental and higher order modes has been performed using a weighted static fiber.

The non-contact fiber draw tension measurement technique has been published[1] and is now the subject of a patent application (Navy Case #73613). Several commercial vendors have already expressed interest in licensing the system for production.

**2.2.4 Rapid Cutoff Measurement.** To insure that each fiber sample operated as a single-mode waveguide at 1.3  $\mu\text{m}$ , a measurement must be performed concurrently with continuing draw as soon as a fiber section of stable dimension has been drawn. From this evaluation, a correction is made in the setpoint diameter for drawing the remainder of the preform. The essentials of the measurement

entail the launch of white light into a section of fiber, and spectral resolution of the power transmitted. A bend in the fiber produces changes in the spectrum which indicate the cutoff wavelength (a description in greater detail appears in Chapter 6).

The conventional cutoff measurement requires two complete spectral measurements of the attenuation in a short length of fiber, a process requiring 10 to 20 minutes. At a draw speed of 1 meter per second, over one kilometer of fiber can be wasted while awaiting the measurement results. A method reducing the actual measurement time to approximately two minutes was conceived and implemented by imaging the fiber endface *via* a stationary dispersing grating onto a prototype InGaAs linear array, so that a complete, real-time spectrum is available for inspection in the form of a video signal. When displayed on a calibrated oscilloscope, the position of motion along the spectrum due to bending the fiber indicates the cutoff wavelength. By speeding the test, it becomes reasonable to take multiple readings to improve certainty.

### **2.3 FIBER MEASUREMENT AND CHARACTERIZATION**

An optical fiber characterization system made by Photon Kinetics was added to the Division's facilities in the summer of 1990 in response to a need for a packaged, turnkey method of evaluating the large volume of fiber samples processed by Code 6505. Up to that time, measurements of spectral attenuation, mode field diameter, and cutoff wavelength had been performed on specialized in-house instruments in effective but non-standard configurations. Successful analysis depended heavily upon the operator's familiarity with the nature of each measurement, and a theoretical understanding of critical conditions. Because simultaneous investigations often required borrowing or adjustment of critical components, reassembly was frequently required and operation was rarely routine. The addition of the commercial unit has freed research personnel from the task of repetitive but fundamental sample characterization. In addition, the instrument assures compliance with standard methods, thereby easing interlaboratory comparison and transition to industry.

The advantages brought by the Photon Kinetics instrument to each measurement complement the goal of standardizing the fabrication of each sample fiber for statistical comparison. (The physical basis and relevance of the intrinsic fiber properties are more fully discussed under Chapter 6.) For all measurements, the fiber must be prepared so that the maximum light signal can be injected into the sample fiber. The operator is relieved of the tedious alignment associated with single mode fibers by a semiautomatic registration and cleaving procedure. Both the input and output cleaved endfaces can be visually inspected for cleanliness and absence of hackle, both of which affect launching efficiency and the validity of the results. Fine alignment proceeds as an automated and reproducible task. The software prompts the operator to perform any manipulations required in the proper order. The separate measurements are executed by a single device, requiring only one alignment of a single sample. In executing the analyses of spectral attenuation, cutoff wavelength and mode field diameter, a standardized, automated procedure produces results which are relatively free of operator bias.

The system's accuracy and compliance with standardization has been rigorously checked by measurements of an NIST standard single-mode fiber which circulates between laboratories. After installation, this procedure indicated excellent agreement with inter-laboratory values for attenuation from 0.7 to 1.6  $\mu\text{m}$  ( $< 0.05$  dB/km discrepancy), cutoff wavelength ( $< 0.02$   $\mu\text{m}$ ) and mode field diameter ( $< 0.1$   $\mu\text{m}$ ).

## **2.4 FIBER IRRADIATIONS**

**2.4.1 Upgrade of the  $^{60}\text{Co}$  source.** Near the end of the Phase I project, the  $^{60}\text{Co}$  source which was used to irradiate the fiber specimens had degraded from its original activity of 20 kCi to about 800 Ci. At this level, it was impossible to obtain the requisite dose rate of 4000 rad/min, even in the highest dose rate position in the source. As a result, the source was upgraded in September 1988 with a source of 17,948 Ci activity. The same sample carousel was used, and it was simply a matter of replacing the old pencils of  $^{60}\text{Co}$  with new, higher activity pencils. This increased our available dose rate by about a factor of 9. By positioning the samples at a proper distance, the dose rate for

irradiating NCS fibers was still achievable, now in the outer ring sample positions where lower dose rates are available. Since the half life of  $^{60}\text{Co}$  is 5.26 years, the source has lost about 7 Ci per day from its initial activity; the current activity computes to approximately 12.1 kCi.

**2.4.2 Stability of the Radiation Damage Measurement System.** The loss induced in the fiber samples as they damage and recover from exposure to the  $^{60}\text{Co}$  source is monitored with the help of lock-in amplifiers (LIA's). The radiation-induced attenuation  $\alpha(t)$  is calculated from the logarithm of the change in received power, i.e.

$$\alpha(t) = \log(P_o/P_t), \quad (2.3)$$

where  $P_o$  is the optical power at the output end of the fiber prior to irradiation and  $P_t$  is the power at any time  $t$  during (growth) or following (recovery) the exposure. The units of  $\alpha$  are dB. During and preceding Phase I, the logarithm function was performed by analog circuit modules built into the lock-in amplifiers, and their outputs were digitized by computer. The gain of these log-ratio amplifiers was discovered to have sufficient thermal drift that the small, long term signal changes due to fiber properties were obscured or distorted. Additionally, small nonlinearities passed a certain amount of the optical source drift, which was nominally removed by ratioing with a reference detector. These errors were identified, and to avoid them in Phase II, the data sets are derived from the linear outputs of the LIA's which are digitized directly. The outputs of the signal and reference LIA's were fed directly into an IBM PC, and the logarithm function was calculated digitally, thereby avoiding the drift and non-linearity of the log-ratio modules. Improved rejection of fluctuations in source power is evident in comparing raw data traces from the two methods.

**2.4.3 Temperature-Stabilized Couplers.** The Aster couplers that are being used have a thermal coefficient specification of  $< 0.003$  dB/C for each output. Since the signal of one output is ratioed to the other, the effect is twice as large as the coefficient for a single arm. Further, since the output of the first coupler is input into a second coupler to achieve two signal arms, the total temperature coefficient for the coupler group adds to as much as  $\approx 0.01$  dB/C. For a typical variation in the ambient room temperature of  $\pm 2$  C and a fiber sample length of 50 m, the apparent loss change of 0.8

dB/km will result. Therefore, it was essential to temperature stabilize the couplers by mounting them to a copper block which was then insulated in a block of styrofoam. Water from the temperature-controlled bath, which is used to stabilize the heat radiation side of the thermoelectric cooled Ge detectors, was circulated through tubes in the block to stabilize its temperature. The bath temperature is maintained at  $20 \pm 0.01$  C. Assuming a worst-case temperature control of the couplers within  $\pm 0.25$  C, the apparent loss change due to temperature drift is  $< 0.1$  dB/km.

**2.4.4 Implementation of a Reference Channel.** To further minimize sources of drift and error, the computer program which performs the data acquisition was modified to acquire  $P_o$  from the reference channel along with  $P_i$  for the two fibers under test. In this way common mode drifts due to fluctuations in laser output or other sources are eliminated, and the reference channel could be analyzed along with the computed signal data to determine trends of all three signals and increase the confidence of the data results. This comparison is normally done only when there is questionable results with the data.

#### REFERENCES

1. C.G. Askins, M.A. Putnam and E.J. Friebele, "Noncontact measurement of optical fiber draw tension," J. Lightwave Tech. 9 (1991) 945-947.

Measurement: 0032, at 00:11 on ?? ?? ??  
Sample code: NRL 880920 CEN

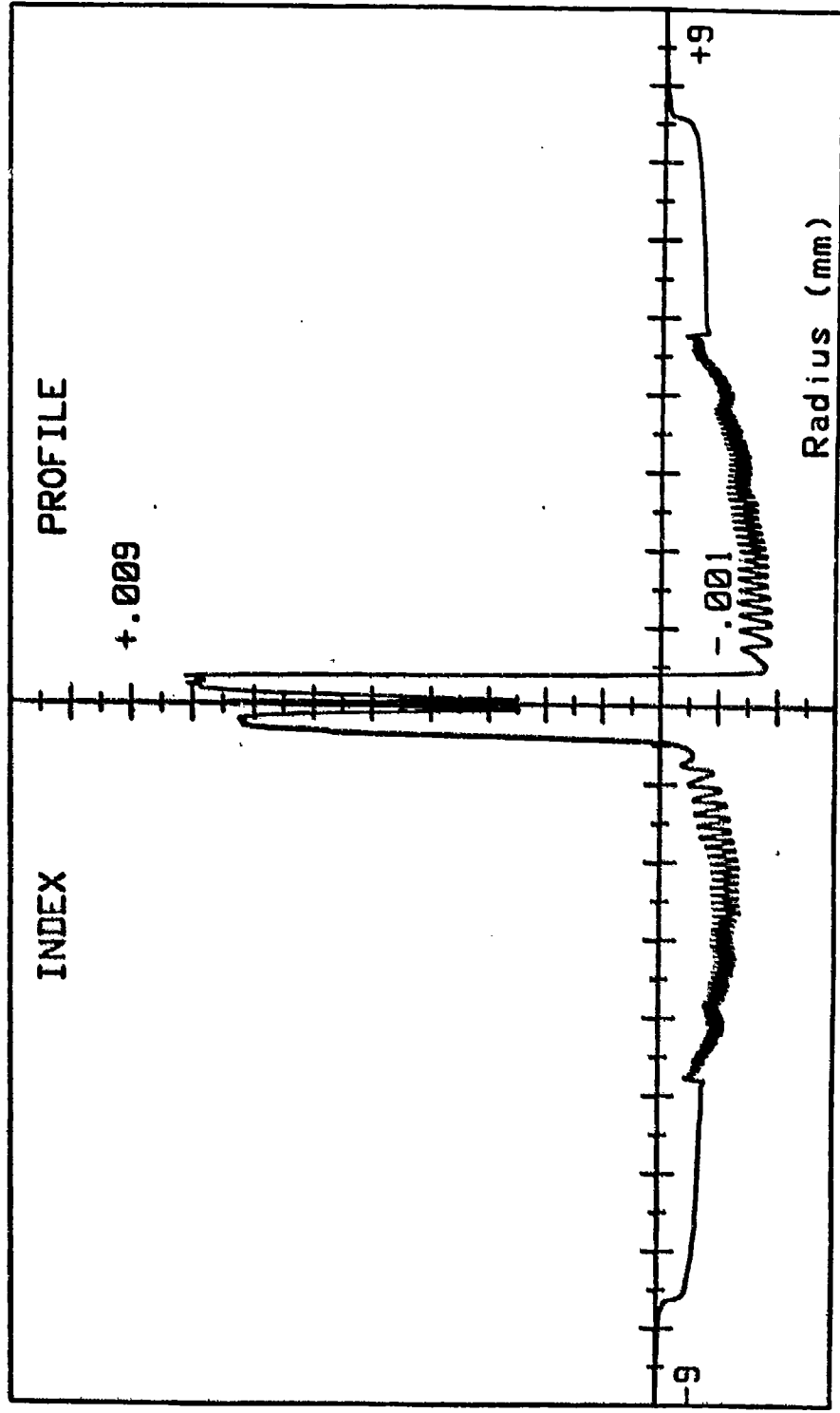


Figure 2.1. Refractive index profile of a preform prior to upgrading the York Technology preform profiler. Note the appearance of a sloping baseline due to the misalignment of the optics.

Measurement: 0027, at 18:42 on 1 OCT 98; Step size: 15 microns  
PIB Ser. no.: 01000, Sample code: NPL300020\_MID 0 DEG  
Axial position: 10 mm, Angle: 0 degs

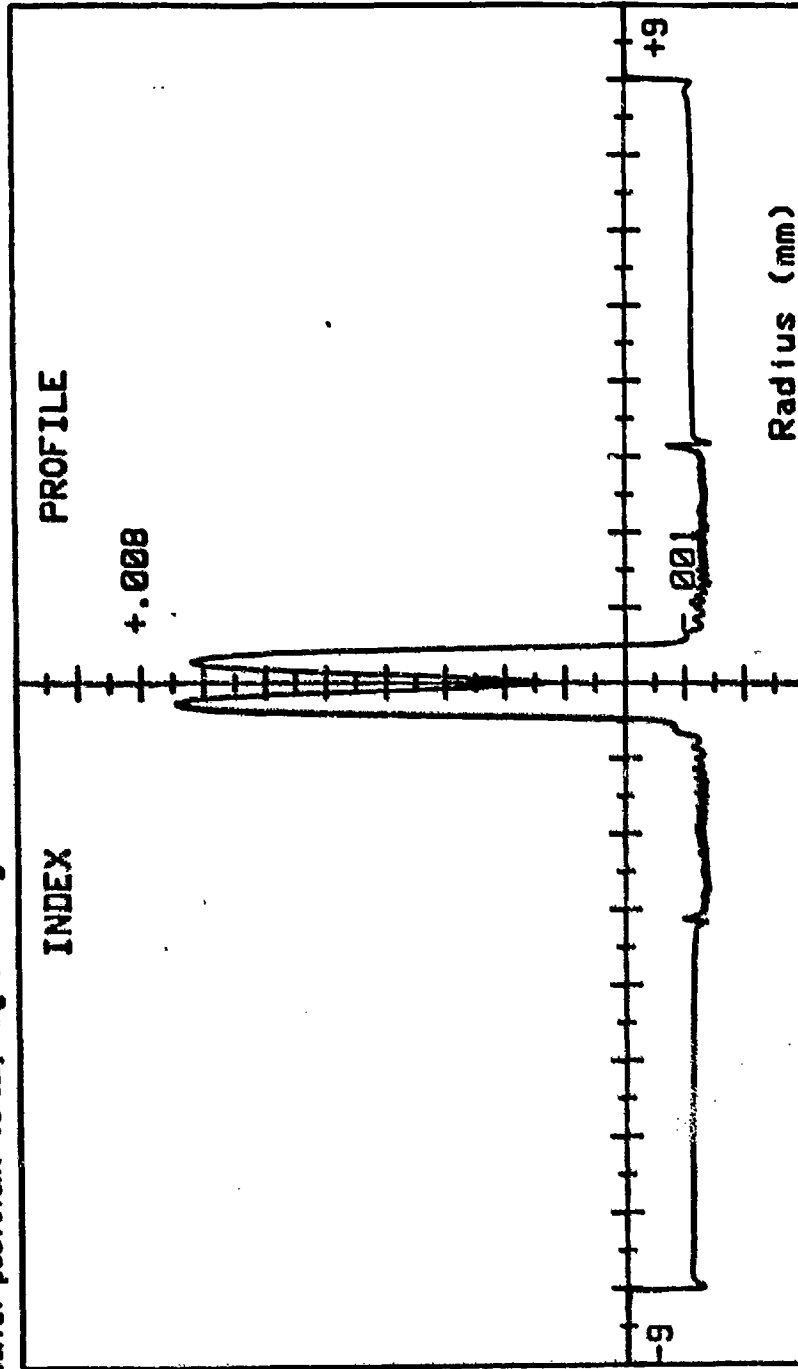


Figure 2.2. Refractive index profile of a preform after upgrading the York Technology preform profiler.



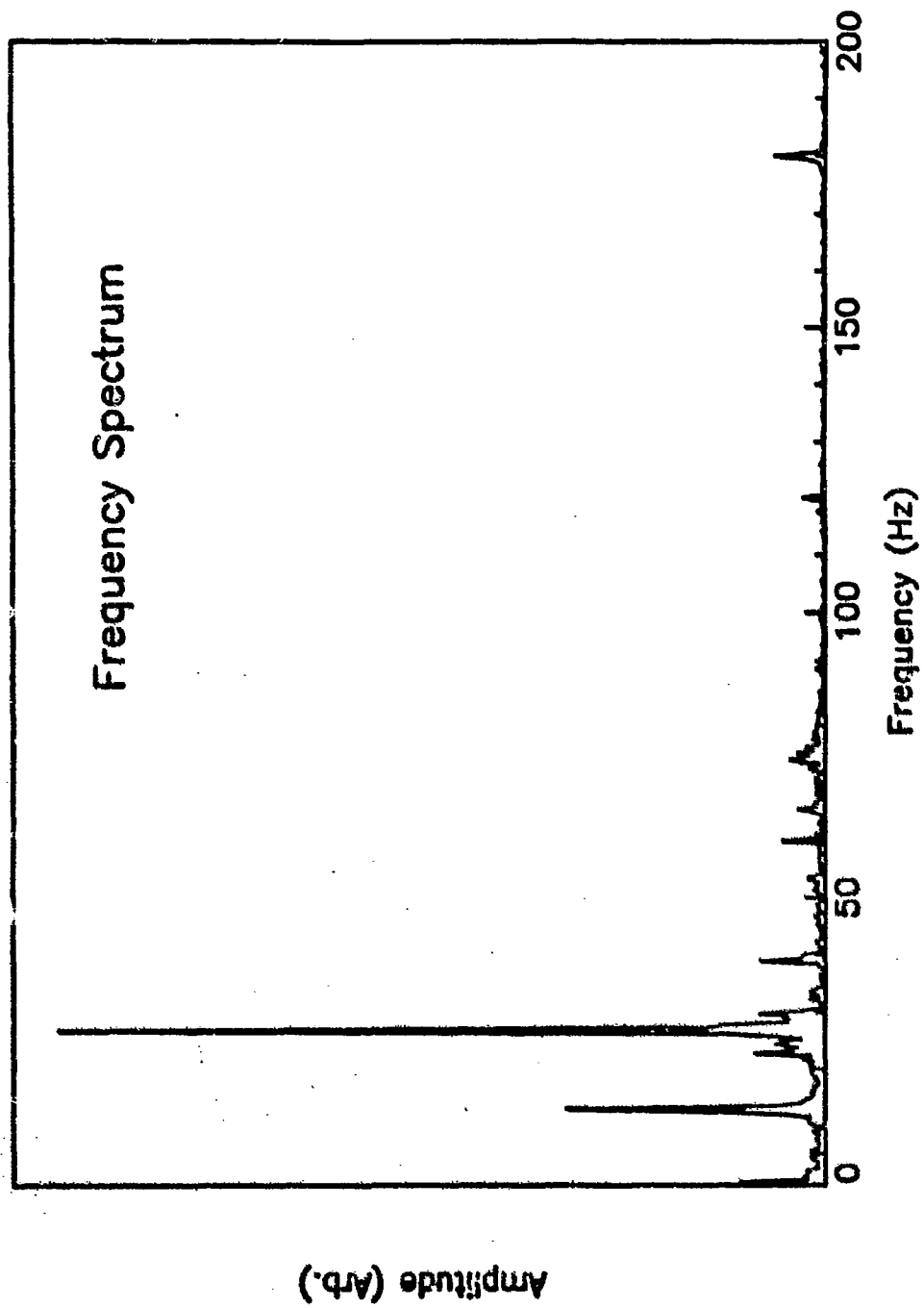


Figure 23. Vibrational spectrum of a 125  $\mu\text{m}$  fiber during draw without excitation. The fundamental resonance of the weakly-vibrating fiber is seen near 75 Hz.

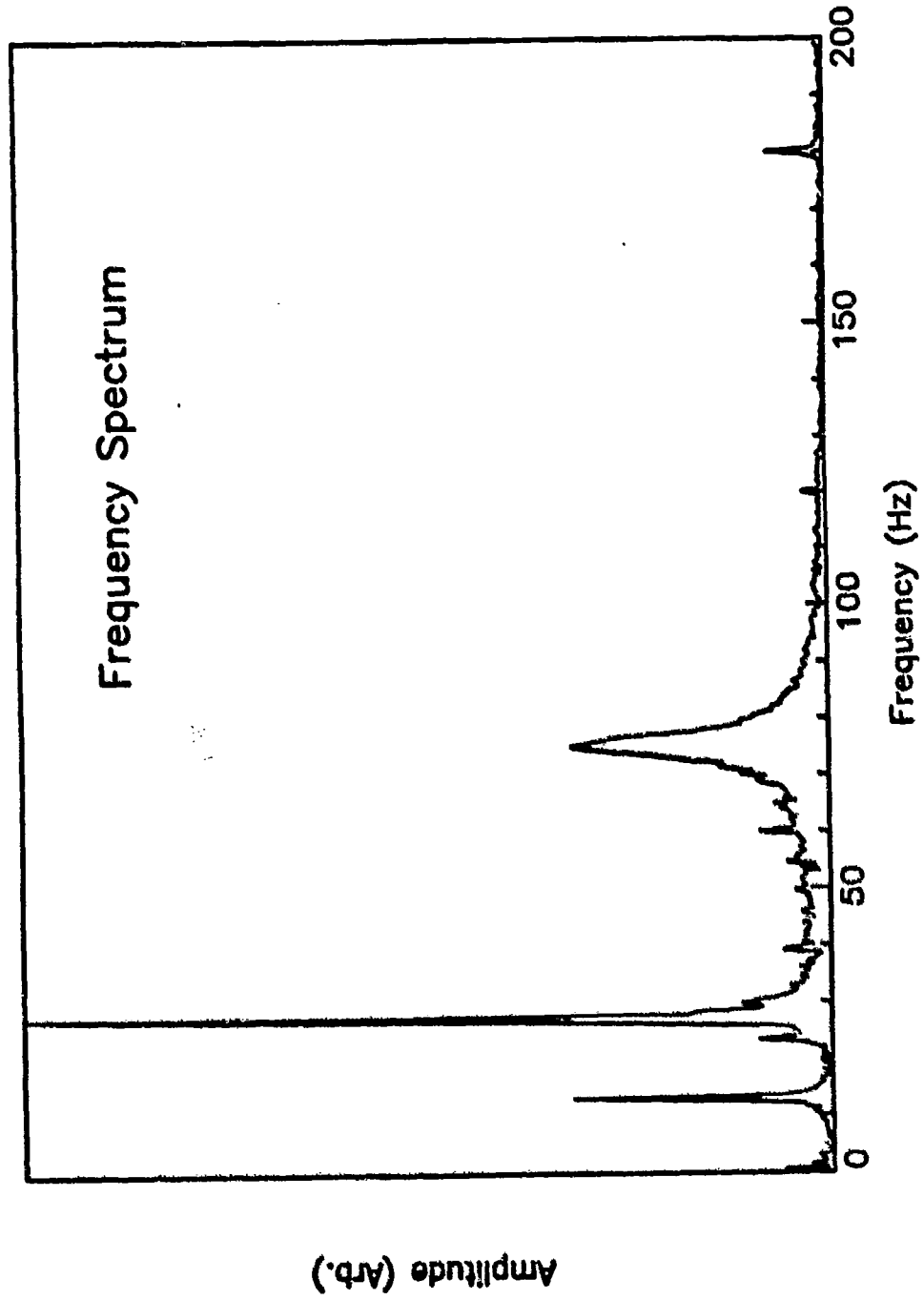


Figure 2.4. Vibrational spectrum of a 125  $\mu\text{m}$  fiber during draw following excitation by a puff of dry nitrogen gas. The fundamental resonance of the fiber is now clearly seen near 75 Hz.

## CHAPTER 3

### STATISTICAL ANALYSIS OF PHASE I DATA

#### 3.1 PHASE I EXPERIMENTAL DESIGN

Fabrication of matched clad single mode fibers by the MCVD method involves experimental factors such as core and cladding dopants, oxygen flows during deposition, draw tension, and draw speed. To demonstrate a relationship between these experimental parameters and the resultant radiation response would involve varying each factor among two or more levels. In principle, one could attempt to vary one factor at a time (full permutation), but such a procedure is not always desirable or practical. In the Phase I study shown in Table 3.1, 6 factors were chosen of which three vary over three levels and three over two levels. The total number of experiments (i.e. fibers to be fabricated and irradiated) required to establish a relationship between the selected fabrication parameters and radiation response is  $3^3 \times 2^3 = 216$  if only one factor is varied per experiment--an extremely expensive and time-consuming process.

In the Phase I study, a fractional factorial design was implemented to reduce the required number of experiments. Since considerable effort is expended in the fabrication of an MCVD preform with the desired core and clad dopant levels, drawing an optical fiber, and performing the radiation test, the basis of the design to be used is a  $2^4$  orthogonal array, of 16 experiments intended to address all main effects and some interactions between two factors.

A  $2^4$  orthogonal array has the property that when the results of the experiments are summed for a given level in any column, all the levels of the other columns are summed with equal frequency, and thus appear as a constant offset. This orthogonal array can be used for designing experiments to study phenomena involving four two-level factors, including all possible interactions between two, three and four factors, and a half-replicate of this array (i.e. 8 experiments) can be used to rigorously determine all main effects and two-way interactions. The  $2^4$  orthogonal array can also be modified

to study phenomena involving factors with three levels. One of these modified designs is shown in Table 3.2, which is the factorial design used in Phase I of our experiments. In addition to revealing the dependence of the radiation response on single factors, some of the interactions between two factors (DF, CF, and BC) can also be studied. Note, however, that the factorial design of Table 3.2 is not orthogonal due to the presence three-level factors A, B, and E (level 2 appears twice as often as levels 1 and 3).

The Phase I design shown in Table 3.2 includes those parameters which are expected to exhibit contributions to the radiation-induced loss, such as Ge concentration in the core and clad, and oxygen stoichiometry in the core and clad. Also included in the scope of this study are fiber draw parameters, i.e. draw speed and draw tension. However, it is well established that phosphorus doping in the core and/or cladding has a large effect on the radiation response of single mode fibers.[1,2] A second, separate design (Phase IB) was implemented mainly to observe the effect of phosphorus doping on the radiation-induced loss. Mies and Soto [2] have reported a one-dimensional study of the effect of only phosphorus variations on radiation response. Linear regression of the Mies and Soto data shows a high degree of correlation between the radiation sensitivity  $\alpha$ (dB/km-krad) induced by low dose rate (2.3 rad/h) exposure and  $[P]_{eff}$ :

$$\alpha_{1.3 \mu m} = 2.98[P]_{eff} + 0.17 \quad R^2 = 0.994 \quad (3.1)$$

$$\alpha_{1.53 \mu m} = 4.63[P]_{eff} - 0.09 \quad R^2 = 0.982. \quad (3.2)$$

The Phase IB design expands this work to include the effects of other fabrication parameters and possible cross correlations. Since phosphorus has been shown to have a large effect on the radiation response, it has been isolated to this second phase so as not to mask the effects of the other parameters.

The parameters for the Phase IB study include phosphorus concentration in the clad, oxygen stoichiometry in the clad, draw speed, and draw tension. The parameter levels are given in Table 3.3, together with the corresponding parameter values. The number of preforms required for the Phase IB study has been decreased to 8 by limiting the number of experimental parameters, as shown in the

experimental design table in Table 3.4. It should be noted that the core composition for all fibers of the phosphorus experiment was chosen to be that of fiber 1 in the non-phosphorus experiment (Phase IA) shown in Table 3.2, i.e. 6.5 wt% Ge with low oxygen flow during deposition. The nonorthogonal nature of the design of Phase IB is clearly evident.

### 3.2 CONFOUNDING OF THE DESIGN

If the variation in factors A, B, and E in the Phase IA experimental design in Table 3.2 had been limited to 2 levels, an experiment in which variation of one factor at a time was performed would allow independent determination of all main effects and higher order interactions.[3] However, this would have required the fabrication of  $2^6$  fibers. A half-replicate of a  $2^6$  design, i.e. 32 fibers, can be implemented to allow independent determination of all main effects and two-way interactions.[3] However, the design in Table 3.2 is not orthogonal due to the presence of 3-level factors. To investigate the confounding present as a result of the partial replication of the full factorial design, a column basis for the full design was used to derive the alias structure. Confounding occurs where one or more main effects contrasts and/or interactions are estimated from the data in an identical manner. Table 3.5 shows the confounding of the design in Table 3.2. It is apparent that there is no confounding of main effects with other main effects, while several of these contrasts are confounded with two-way interactions, thus clouding their interpretation. There is additional confounding with 3-way, 4-way, 5-way and higher order interactions; since it is considered unlikely that these would have a significant effect, they have been omitted from further consideration.

### 3.3 ANALYSIS OF DATA

Each set of recovery data for the 24 fibers of the Phase I study has been fit to the empirical kinetic model described in Chapter 7 of the Phase I final report.[4] In summary, the radiation-induced attenuation  $A(t)$  at time  $t$  following exposure is described by

$$A(t) = (A_0 - A_f)[1 + ct]^{-1/(a-1)} + A_f \quad (3.3)$$

where  $c = (1/\tau)[2^{n-1} - 1]$ . The parameters of the fit are the initial and final, or permanent, induced attenuations,  $A_0$  and  $A_f$ , the half-life of the incremental loss  $\tau$ , and the kinetic order of recovery  $n$ . Theoretical plots of Eq. 3.3 with varying  $n$  for constant  $A_0$ ,  $A_f$  and  $\tau$  are shown in Fig. 3.1. It is obvious that the goal of increasing recovery of the incremental loss, which is equivalent to decreasing the response of fiber optics to low dose rate fallout radiation[4] can be accomplished by decreasing  $n$ ,  $\tau$ , and  $A_f$ .

The parameters of the fits for the 24 fibers of Phase I are shown in Table 3.6. In some cases slight trade-offs could be made between  $A_f$ ,  $n$ , and  $\tau$  without visibly degrading the fit; we used the criterion of minimum least squares deviation between experiment and fit to obtain the parameters in Table 3.6. The fits in general are quite good, as evidenced by the low standard deviations of  $< 0.86$  dB/km for the fibers with low radiation response. Of course, the standard deviations are higher for those with large initial losses, but in all cases they are  $< 1\%$  of  $A_0$ .

As is evident by comparing the data, the behaviors span a broad range--the initial damages in the pure silica clad fibers are quite high, while those of the other waveguides are substantially lower. It is interesting to note that the initial damage in the pure silica clad fibers varies considerably from sample to sample. Fiber #1 with the lowest [Ge] in the core shows the greatest damage, while #5 with the second level of [Ge] shows the least. Unfortunately, there are no pure silica clad fibers with the third level of [Ge] in the core in this design to ascertain if this trend of decreasing  $A_0$  with increasing core [Ge] continues.

Even in the case of doped claddings, there is a range of initial responses, and some fibers show good long term recovery while others do not. Of course, one would expect inhibited long term recovery and enhanced permanent attenuation in the P-doped clad fibers, and this is indeed the case. However, some of the other fibers which do not contain P in the cladding show substantial long term attenuation, indicating that the measured radiation response results from a complex interaction of all the fabrication parameters.

Other than to note the large initial induced attenuation in the pure silica clad fibers, without further analysis it is impossible to relate the observed responses to fabrication parameters because of the fact that multiple parameters are changed between any two fibers.

The analysis of the Phase I data described in the Phase I final report was made using orthogonal matrix analysis (OMA). Because the success of OMA depends on a complete averaging of the contributions of all factors other than the one under consideration, anomalous values of response for one or two cases tend to be highly-weighted in the final result. Although OMA provides estimations of the dependencies of the radiation response parameters on the fabrication factors, there is no indication of the validity of these results as described by statistical significance. In addition, the part-replicate used in the Phase IA experimental design is not orthogonal, so the effects are not statistically independent. For these reasons multivariate analysis was applied to the data.

### 3.4 MULTIVARIATE ANALYSIS

Multivariate analysis of variance (MANOVA) was performed with the PC version of Multivariate,[5] a computer code which is attractive because it is statistically robust and it allows a great deal of control of the procedures. The analysis was performed in an iterative fashion, beginning with the full set of 15 fibers of Phase IA.

**3.4.1 Phase IA Fibers.** Table 3.7, which contains the correlation matrix for the radiation response parameters of this experiment, shows that there is a high degree of correlation between  $n$  and  $\tau$ , and these in turn are negatively correlated with  $A_1$  to a significant degree. In contrast, there is no correlation of  $n$ ,  $\tau$ , or  $A_1$  with  $A_0$ .

An analysis of variance (ANOVA) was performed on the Phase I results to determine which interactions had statistical significance. Because of the extremely small sample size in the analysis, it seems reasonable to relax the usual criterion of statistical significance somewhat from  $\leq 0.05$  to  $\approx 0.10$ ; indeed, probabilities of as much as 0.25 may be significant. The results shown in Table 3.8 indicate that, at the least, the potentially significant main effects are: core [Ge] (factor A) and possibly

clad oxygen (factor D) on  $n$ , clad [Ge] (factor B) on  $A_0$  and  $A_r$ , core oxygen (factor C) and possibly clad oxygen on  $r$ , and draw tension (factor E) on  $A_r$ . However, with the exception of factor B on  $A_0$ , none of these appear to be *highly* significant ( $p < 0.05$ ). Since a much greater fraction of the light travels in the fiber core than clad, it would be expected that the core oxygen-to-reagent ratio would be more significant than that of the clad. Thus, the result that D is more significantly correlated with  $n$  and  $r$  than is C seems physically unreasonable.

The effect of some of the two-way interactions was also studied in this ANOVA, and these results are at the bottom of Table 3.8. However, as shown in Table 3.5, many of the two-way interactions in the Phase I experimental design are confounded with main effects and therefore cannot be unambiguously interpreted. Nevertheless, the results for the two-way interactions in Table 3.8 show that CF (core oxygen-to-reagent ratio and draw speed) seems to have the most significant effect on the radiation responses, and Table 3.5 indicates confounding of this interaction with 3-way and higher order interactions. It is encouraging that other two way interactions have high null probabilities, so that values of  $p = 0.2$  for the CF interaction may be significant.

The strong effect of clad [Ge] on  $A_0$  evident in Table 3.8 comes about because of the extremely large initial incremental loss in the pure silica clad fibers (level 1 of factor B), as shown in Table 3.6. Because  $A_0$  is so much larger at this level, the effect of B on  $A_0$  appears to be highly significant in the omnibus test of all contrasts shown in Table 3.8. However, in testing the individual contrasts, the effect is found to be significant only in the contrast between levels 1 and 2. The  $B_2$ - $B_3$  contrast is definitely not significant at the 0.67 level.

These results are consistent with the suggestion that fibers with pure silica clads comprise a separate genre from those with doped clads. Radiation damage processes in silica have been extensively studied,[6] and it is well-known that the defect centers are associated with the silicon-oxygen glass network or impurities such as OH. In contrast, doping with percentage quantities of Ge provides copious traps for the radiolytic electrons and holes, and the defect centers associated with these dopants dominate the radiation damage process.[7] (Note that to maintain a matched-clad



condition, F is codoped with Ge in the clad, likely providing additional trapping sites.) Since the damage associated with the pure silica clad is so great in this study, the B effect dominates the analysis. Thus, a second ANOVA was performed without these outlying cases (removing the first level of factor B).

**3.4.2 Ge-F-Doped Silica Fibers.** The correlation matrix for this experiment (Table 3.9) shows a high degree of correlation between  $n$  and  $\tau$  and between  $A_o$  and  $A_f$ , while the negative correlations of  $A_f$  with  $n$  and  $\tau$  are much weaker. These results indicate that: 1) the speed of recovery determined by  $n$  and  $\tau$  is independent of the amount of induced attenuation and 2) fibers with lower initial incremental loss can be expected to have lower permanent loss, as well.

**$A_o$ .** The results of the omnibus test in Table 3.10 show that there is a significant effect of core [Ge] (factor A) on  $A_o$  at the 0.12 level, and perhaps an effect of clad oxygen (factor D) at the 0.09 level. (Since CF was not significant in determining  $A_o$  and  $A_f$ , as shown in Table 3.10, the interaction term was added to the residual error, thus increasing the available degrees of freedom for the analysis of the main effects on  $A_o$  and  $A_f$ .) This is shown in more detail in the least squares estimates for the individual contrasts found in Table 3.11, where the significant A effect is concentrated in the first contrast associated with A (between levels 1 and 3). Note also from Table 3.5 that this contrast is confounded only with three-way and higher order interactions. The second contrast is not significant ( $p < 0.45$ ), but it is confounded with the DE and FB two way interactions. Since the analysis has established that the D effect on  $A_o$  is significant (Table 3.10), the low null probability of the  $A_2$ - $A_3$  contrast could be due to a cancellation of any effect between levels 2 and 3 by the effects of the DE and FB two-way interactions.

As shown in Table 3.5, the D effect is also confounded with AE, and since the A effect is strong, it seems likely that D itself is the reason for the observed statistical significance but rather the interaction of core [Ge] with draw tension. Intuitively, this seems correct since it would be difficult to imagine clad oxygen stoichiometry (factor D) having a stronger effect on attenuation than core oxygen stoichiometry (factor C). Thus, the analysis has shown that  $A_o$  is primarily affected by the

core [Ge] and that the most significant decrease in  $A_o$  occurs upon changing from the lowest to the highest Ge concentrations. For this reason, it is to be expected that fibers with high  $\Delta^+$ 's, such as the bend-resistant fibers, would have initial incremental losses which are at least no higher than equivalent conventional telecommunications fibers. Indeed, recent measurements support this result.

The trend of the effect of A on  $A_o$  derived from MANOVA is consistent with that of OMA described in the previous section, as shown in Fig. 3.2, where increasing the [Ge] in the core resulted in a significant decrease in incremental loss. However, the induced loss predicted by OMA is almost an order of magnitude greater than the estimated effect from MANOVA, especially at the first level of core [Ge]. It is likely that the OMA results are skewed because of the necessity of including the pure silica clad fibers in the analysis.

$A_f$ . It is interesting to note that the same trends of significance observed for  $A_o$  between the first and second contrasts of A in Table 3.11 are evident for  $A_f$  as well. The first contrast is more significant, and although the significance of the first contrast at the 0.25 level is marginal, the strong effect of core [Ge] on  $A_o$  indicates that further study of its effect on  $A_f$  is in order.

Clearly, core oxygen stoichiometry (factor C) has the most significant effect on  $A_f$  with a null probability of 0.09. Since C is confounded only with four way and higher interactions, the attribution is relatively straightforward. Interestingly, C does not have any statistically significant effect on  $A_o$  ( $p < 0.57$ ).

n and r. From the previous ANOVA using all Phase I fibers the CF interaction was found to be the most significant of the two-way interactions. It is apparent from Table 3.10 that its effect on r in the limited ANOVA is significant, especially in view of the fact that the CF effect is confounded only with three-way and higher interactions (Table 3.5), all of which are considered negligible and/or unlikely. The high degree of correlation between n and r shown in Table 3.9, together with the relatively significant probability of the CF effect on n in Table 3.10 imply that these radiation response parameters are determined by a two-way interaction of oxygen stoichiometry used during core deposition and draw speed.

### 3.5 ESTIMATED EFFECTS

Thus far, the ANOVA has established that the parameters describing the recovery of the radiation-induced attenuation are correlated with certain fabrication factors in a statistically significant manner. The estimated effects of the A and C contrasts on initial and final induced attenuations are shown in Table 3.11.

As shown in Table 3.11,  $A_0$  decreases by 7.3 dB/km between levels 1 and 3 of core [Ge], and 1.2 dB/km between levels 2 and 3. Since the estimated effects are contrasts, they can predict only the relative differences between the levels. The actual estimated values shown in Fig. 3.2 for the three levels of  $A_0$  were derived by fitting the appropriate main class model to the data. The estimation of  $A_0$  at the second level is problematic because of the confounding of the  $A_2$ - $A_3$  contrast with two-way interactions (Table 3.5). Note the similarity of the MANOVA and OMA results shown in Fig. 3.2 where in both cases increasing the [Ge] in the core resulted in a large decrease in  $A_0$ . The effects estimated from OMA are much larger than those from MANOVA, however, likely due to the skewing of OMA from the pure silica clad fiber data. Likewise, the trend of the null probabilities and estimated effects of the two contrasts of A on  $A_0$  and  $A_f$  is consistent--there is a greater effect with higher significance in the first contrast than in the second. Although the significance of the first contrast of A on  $A_f$  is marginal ( $p < 0.25$ ), the strong effect of core [Ge] on  $A_0$  indicates that further study of its effect on  $A_f$  is in order.

The estimated effect of changing oxygen/reagent flow during core deposition on  $A_f$  is shown in Fig. 3.3, where it is evident that an increase from a ratio of 5 to 15 results in a substantial decrease in  $A_f$  of 3.8 dB/km. (The estimated values were again derived through the statistical fitting of the appropriate main-class model.) Note also that the effect estimated from OMA of 2.8 dB/km is in good agreement with the MANOVA result.

The  $n$  and  $r$  effects on the two-way interaction of core oxygen stoichiometry and draw speed CF are shown in Fig. 3.4. It is apparent that at low draw speed core oxygen does not have an effect on these recovery parameters while draw speed does not have an effect at high core oxygen ratio.

Clearly, if fibers are to be drawn at high speed, their cores must be deposited with high oxygen flows to enhance the recovery of the radiation damage. At the higher draw speed, the effect of core oxygen is estimated to be similar by both MANOVA (Fig. 3.4) and OMA (Fig. 3.5), although OMA estimates less of a difference for both  $n$  and  $\tau$ . Likewise, at the lower oxygen level, OMA relatively underestimates the difference in  $n$  and  $\tau$  between low and high draw speed (Fig. 3.6 *vis a' vis* Fig. 3.4).

**3.5.1 Phase IB Fibers.** The analysis of the recovery data of the P-doped silica clad fibers is complicated by the fact that two of the 8 fibers in this design have pure silica clads, and the design is not orthogonal since it is  $4 \times 2 \times 2 \times 2$  (Table 3.4). After removing the pure silica clad outliers from the analysis, there were only 6 fibers in the sample population; rather than attempt to extract too much information from these data, the analysis was limited to only the main effect, i.e. [P] in the clad.

Table 3.12 contains the null probabilities for the P effect on the radiation response parameters. In this case we have performed the same MANOVA as before, but the contrasts have been parameterized for a polynomial fit of the data. There is no confounding of the main effect, but the results may be oversimplified if the P effect interacts with other fabrication factors since these have been omitted from the analysis.

From the omnibus test it is apparent that there is a significant effect of P on  $n$  ( $p < 0.16$ ), while there is no effect on the other parameters. The estimates of the individual contrasts show that the significant P effect is isolated in the first contrast, i.e. the slope of the linear trend across the different levels of [P] in the clad, and that there is no significance associated with the nonlinear effect. Although Table 3.12 also suggests that there may be an effect of the first contrast of P on  $\tau$  ( $p < 0.24$ ), the probability of the omnibus test is so large ( $p < 0.40$ ) to obviate this possibility.

Note that the relative effect of the first contrast of P on  $n$  derived from MANOVA and shown in Table 3.12 is similar to the linear trend from OMA for all fibers except those with the first level of P, i.e. 0% (Fig. 3.7). The estimated effect of [P] on  $n$  from the MANOVA shown in Fig. 3.7 has an identical slope with the OMA results, again showing the consistency between MANOVA and OMA.

It should be mentioned here that the Phase IB design was clearly inadequate for more than the most preliminary determination of fabrication effects on the radiation response of P-doped silica clad fibers. In addition to being nonorthogonal, there are significant confoundings of the main effects with two-way and higher order interactions. A more serious flaw was the choice of the first levels of core [Ge] and oxygen flow for the core since subsequent analysis of the Phase IA results has shown this to have the poorest radiation resistance and to be the most susceptible to microbending loss because of the low  $\Delta$ .

### 3.6 DISCUSSION

The results described above have shown that there are statistically-significant correlations between the recovery parameters and certain fabrication factors of matched clad single mode fibers. These correlations were derived in spite of the very small sample sizes and the deficiencies in the experimental design, which led to confounding of some main effects.

The levels of the fabrication factors were chosen to encompass as wide a variation as possible. In some cases, such as the low core [Ge] and low core and clad oxygen stoichiometry levels, it was difficult to fabricate fibers of good quality. Although these were clearly out of the range that would be encountered in commercial production, they are useful in revealing the presence of significant effects of fabrication factors on recovery parameters. Variations of core [Ge] and oxygen in subsequent experiments over a smaller range around the higher levels might not result in substantial changes in  $A_0$  and  $A_1$ , respectively. Certainly, the higher null probability of the second contrast of A vs. the first contrast indicates that there may not be much reduction in  $A_0$  when the core [Ge] is increased from 10.4 to 15.4 wt%.

Although statistically-significant correlations were established in this part of the study, the confounding of the experimental design makes a clear interpretation of the results difficult. It is clear from Table 3.11 that the first contrast of  $A_0$  on core [Ge] (factor A), which is unconfounded, is a main effect. However, the interpretation of the low null probabilities of clad oxygen (D) on  $A_0$  and

the second contrast of draw tension (E) on  $A_0$  are clouded by their confounding with two-way interactions involving A, as shown in Table 3.5.

The results of the Phase IB design have indicated a statistically significant correlation of [P] and kinetic order. In contrast, Mies and Soto[2] showed that the attenuation induced by low dose rate exposure, which is equivalent to  $A_f$  in the present study, is highly correlated with  $[P]_{eff}$ , as described by Eqs. 3.1 and 3.2. This discrepancy may be due to the fact that Mies and Soto irradiated their fibers at room temperature (23 C). In addition, to isolate the effect of P, they created a depressed clad with F-doping and then added P in varying amounts while holding the F level constant. In our case, both the P and F concentrations were varied in concert in order to maintain a matched clad condition. As will be seen in Chapter 5, increased levels of F doping of the clad have been found to increase  $\tau$ . However, in the Phase IB study only slight F doping was used, and there is no effect of P (and F) on  $\tau$ .

The variation in doping levels used by Mies and Soto were different from ours, and the numerical apertures of their fibers varied, whereas ours were constant. Additional studies are in order to resolve these discrepancies.

It is interesting to note from Table 3.13 that Eq. 3.1 predicts  $A_f$  within 15% for the Phase IB fibers fabricated with the first level of clad oxygen stoichiometry, i.e. fibers 19, 21, and 23. The fact that there is such good agreement in spite of the difference in temperatures of the two experiments is attributed to the presence of P, which is known to reduce the temperature dependence of the incremental attenuation.[1,8] In contrast, Table 3.13 shows that the prediction from Eq. 3.1 for fibers with the second level of oxygen stoichiometry, i.e. fibers 20, 22, and 24, is significantly less than experiment. The difference between the results for the two groups of fibers, which suggests that Mies and Soto may have used low oxygen stoichiometry during clad deposition, clearly shows the danger of one-dimensional studies. Although they derived a highly significant correlation of  $[P]_{eff}$  on radiation response, other factors, held constant in such an experiment, can apparently influence

the result almost as strongly as the one which was varied. It should also be noted that the effect of clad oxygen on  $A_f$  is not significant in this study.

The Phase I work, which is the first reported multidimensional study of the effects of fabrication parameters on response to ionizing radiation, has shown that statistically-significant correlations can be derived, in spite of deficiencies in the original experimental design.

It is tempting to try to extract additional information from this study, such as a capability for *predicting* radiation-induced attenuation from fabrication parameters, and the estimated effects described above represent a first-order attempt. However, the confounding in the experimental design and the very small sample populations of Phase IA, and particularly Phase IB, preclude such an effort.

## REFERENCES

1. E.J. Friebele, M.E. Gingerich and K.J. Long, "Radiation damage of optical fiber waveguides at long wavelengths," *Appl. Opt.* **21**, 547-553 (1982).
2. E.W. Mies and L. Soto, "Characterization of the radiation sensitivity of single-mode optical fibers," in Proc. ECOC '85 (Venice), 1985.
3. C.R. Hicks, Fundamental Concepts in the Design of Experiments, Holt, Rinehart and Winston, New York, NY, 1964.
4. E.J. Friebele, Radiation Response Prediction of Single Mode Fibers (NCS Tech. Bull. 88-1), National Communications System, Arlington, VA, 1988.
5. Multivariate, distributed by Scientific Software, Inc., Mooresville, IN.
6. D.L. Griscom, "Nature of defects and defect generation in optical glasses," in Radiation Effects in Optical Materials (SPIE Volume 541), Edited by P.W. Levy, SPIE, Bellingham, WA, 1986, pp. 38-59.

7. E.J. Friebele and D.L. Griscom, "Color centers in glass optical fiber waveguides," in Defects in Glasses (MRS Proceedings Volume 61), Edited by F.L. Galeener, D.L. Griscom and M.J. Weber, Materials Research Society, Pittsburgh, PA, 1986, pp. 319-331.
8. E.J. Friebele, C.G. Askins, M.E. Gingerich, and K.J. Long, "Optical fiber waveguides in radiation environments, II," Nucl. Inst. Meth. in Phys. Res. B1, 355-369 (1984); E.J. Friebele, K.J. Long, C.G. Askins, M.E. Gingerich, M.J. Marrone, and D.L. Griscom, "Overview of radiation effects in fiber optics," in Crit. Rev. Tech.: Opt. Materials in Radiation Environments (SPIE Vol. 541), Edited by P. Levy and E.J. Friebele, SPIE, Bellingham, WA, 1985, pp. 70-88.



Table 3.1  
Fabrication Parameters Phase IA

Parameter	Level			
	1	2	3	
A. Ge in Core	6.5	10	14	wt%
B. Ge in Clad	0	2.4	3.8	wt%
C. Core O <sub>2</sub> /R	5	15		
D. Clad O <sub>2</sub> /R	5	10		
E. Draw Tension	80	50	20	grams
F. Draw Speed	0.5	4.0		m/sec

Table 3.2

Experimental Design Table for 6 Factors. N is the Fiber Number, and

$R_i$  are the Radiation Response Parameters.

N	A	B	C	D	E	F	$R_i$
1	1	1	1	1	1	1	$R_1$
2	2	1	2	2	1	2	$R_2$
3	1	2	2	2	2	2	$R_3$
4	2	2	1	1	2	1	$R_4$
5	2	1	1	1	2	2	$R_5$
6	1	1	2	2	2	1	$R_6$
7	2	2	2	2	1	1	$R_7$
8	1	2	1	1	1	2	$R_8$
9	2	2	2	1	2	1	$R_9$
10	3	2	1	2	2	2	$R_{10}$
11	2	3	1	2	3	2	$R_{11}$
12	3	3	2	1	3	1	$R_{12}$
13	3	2	2	1	3	2	$R_{13}$
14	2	2	1	2	3	1	$R_{14}$
15	3	3	1	2	2	1	$R_{15}$
16	2	3	2	1	2	2	$R_{16}$

Table 3.3

Fabrication Parameters Phase IB

Parameter	Levels				
	1	2	3	4	
A. P in Clad	0	0.5	1.0	2.0	wt%
B. Clad O <sub>2</sub> /R	5	10			
C. Draw Tension	80	20			grams
D. Draw Speed	0.5	4.0			m/sec

Table 3.4

Experimental Design for Phase IB. N and  $R_i$  as in Table 3.2

N	A	B	C	D	$R_i$
17	1	1	1	1	$R_{17}$
18	1	2	2	2	$R_{18}$
19	2	1	1	2	$R_{19}$
20	2	2	2	1	$R_{20}$
21	3	1	2	1	$R_{21}$
22	3	2	1	2	$R_{22}$
23	4	1	2	2	$R_{23}$
24	4	2	1	1	$R_{24}$

Table 3.5  
**Confounding of Main Effects Contrasts with Higher Order Interactions**  
**in the Phase 1 Experimental Design.**

$A_{1-3}$		$D_{1-2}$	$AE$ $FBE$ $DFAB$
$A_{2-3}$	$DE$ $FB$ $DFABE$	$E_{1-3}$	$FABE$
$B_{1-3}$	$DABE$	$E_{2-3}$	$DA$ $DFB$ $FABE$
$B_{2-3}$	$FA$ $DFE$ $DABE$	$F_{1-2}$	$AB$ $DBE$ $DFAE$
$C_{1-2}$	$CDAE$ $CFAB$ *	$CF$	$CAB$ $CDBE$ *

---

\* Indicates 6-way interaction.

Table 3.6

Analyzed Fiber Compositions (wt%), Oxygen-to-Reagent Ratio ( $O_2$ ) Used During Deposition, Draw Tension (g), Draw Speed (m/sec), and Radiation Recovery Parameters. Initial and Final Loss,  $A_0$  and  $A_f$  in dB/km; Half-Life  $\tau$  in sec.

N	Core			Clad				Draw		Recovery Parameters			
	[Ge]	[F]	$O_2$	[Ge]	[F]	[F]	$O_2$	Tens	Speed	n	$\tau$	$A_0$	$A_f$
1	7.5	0.07	5	0.0	0.0	0.00	5	6.6	0.5	1.8	12	420.0	10.0
2	9.4	0.06	15	0.0	0.0	0.00	10	7.3	4.0	2.0	15	260.0	10.0
3	7.4	0.10	15	2.5	0.0	0.55	10	3.5	4.0	4.0	70	12.2	0.3
4	10.3	0.20	5	2.4	0.0	0.50	5	4.0	0.5	3.0	100	1.9	1.5
5	10.2	0.10	5	0.0	0.0	0.00	5	5.0	4.0	2.0	20	60.0	7.0
6	6.2	0.04	15	0.0	0.0	0.00	10	5.3	0.5	2.3	22	243.0	0.0
7	11.4	0.24	15	2.5	0.0	0.51	10	7.7	0.5	4.0	25	7.0	0.0
8	6.2	0.14	5	2.3	0.0	0.53	5	6.6	4.0	4.0	350	9.1	6.9
9	12.0	0.18	15	2.5	0.0	0.49	5	4.7	0.5	4.0	75	4.9	0.1
10	15.2	0.26	5	2.4	0.0	0.54	10	5.9	4.0	10.0	60000	4.8	0.0
11	9.8	0.26	5	3.8	0.0	0.87	10	2.1	4.0	4.0	20000	5.7	2.6
12	15.4	0.27	15	3.9	0.0	0.84	5	2.2	0.5	4.0	80	4.0	0.6
13	16.0	0.19	15	2.4	0.0	0.53	5	2.4	4.0	4.0	70	4.5	0.0
14	8.6	0.16	5	2.4	0.0	0.50	10	1.8	0.5	4.0	2000	11.4	7.2
15	15.0	0.28	5	3.9	0.0	0.83	10	4.8	0.5	4.0	100	5.1	4.7
16	11.8	0.26	15	4.0	0.0	0.82	5	3.7	4.0	3.5	15	3.7	0.0
17	7.5	0.02	5	0.0	0.0	0.00	5	6.6	0.5	1.8	12	420.0	10.0
18	7.4	0.03	5	0.0	0.0	0.00	10	1.6	4.0	2.3	28	237.0	0.5
19	7.5	0.12	5	0.0	0.4	0.17	5	6.4	4.0	4.0	300	8.0	1.0
20	8.0	0.01	5	0.0	0.5	0.17	10	1.6	0.5	4.0	50	4.3	2.8
21	6.5	0.02	5	0.0	1.2	0.25	5	1.5	0.5	4.0	60	5.6	2.6
22	7.4	0.11	5	0.0	1.5	0.25	10	6.4	4.0	3.0	20	7.5	4.5
23	7.3	0.05	5	0.0	1.9	0.34	5	1.4	4.0	3.0	25	5.2	3.7
24	6.6	0.01	5	0.0	2.2	0.32	10	6.6	0.5	2.0	25	6.5	2.8

Table 3.7

Correlation Matrix for Radiation Response Parameters of Phase 1--All Cases.

	n	$\tau$	$A_o$	$A_f$
n	1.00			
$\tau$	0.95	1.00		
$A_o$	0.04	0.27	1.00	
$A_f$	-0.64	-0.74	-0.07	1.00

Table 3.8

Probabilities of Individual Null Effects and Interactions  
 For the Phase 1 Design--All Fibers.

	n	$\tau$	$A_o$	$A_f$
A	0.17	0.43	0.40	0.88
B	0.93	0.78	0.01	0.14
C	0.42	0.24	0.94	0.41
D	0.22	0.25	0.89	0.91
E	0.45	0.75	0.35	0.07
F	0.31	0.27	0.27	0.81
CA	0.27	0.39	0.25	0.63
CB	0.53	0.74	0.99	0.99
CD	0.27	0.39	0.25	0.63
CE	0.27	0.39	0.25	0.63
CF	0.22	0.27	0.22	0.18



Table 3.9

Correlation Matrix for Radiation Response Parameters of Phase 1  
 For Reduced Design of Ge-F-Doped Silica Clad Fibers.

	n	$\tau$	$A_o$	$A_f$
n	1.00			
$\tau$	0.95	1.00		
$A_o$	0.14	-0.16	1.00	
$A_f$	-0.22	-0.50	0.92	1.00

Table 3.10

Probabilities for Individual Null Effects of Phase 1 Design  
 For Reduced Design of Ge-F-Doped Clad Fibers.

	n	r	A <sub>o</sub>	A <sub>f</sub>
A	0.31	0.39	0.12	0.44
B	0.54	0.72	0.21	0.90
C	0.66	0.43	0.57	0.09
D	0.33	0.29	0.09	0.55
E	0.80	0.80	0.42	0.50
F	0.39	0.31	0.49	0.65
CF	0.21	0.12	0.73	0.52

Table 3.11

Probabilities for Individual Null Effects And Selected Estimated Effects  
 For Reduced Phase 1 Design of Doped Silica Clads.

Contrast	n	Probabilities			Estimated Effects	
		$\tau$	$A_o$	$A_f$	$A_o$	$A_f$
$A_1-A_3$	0.19	0.21	0.05	0.25	-7.3	-4.0
$A_2-A_3$	0.23	0.45	0.45	0.77	-1.2	-0.5
$B_2-B_3$	0.36	0.50	0.47	0.67		
$C_1-C_2$	0.66	0.42	0.57	0.09		-3.8
$D_1-D_2$	0.42	0.43	0.08	0.85		
$E_1-E_3$	0.61	0.78	0.32	0.79		
$E_2-E_3$	0.44	0.54	0.19	0.31		
$F_1-F_2$	0.29	0.19	0.50	0.34		

Table 3.12

Probabilities for Null Effect of P And Estimated Effect  
 For Reduced Phase 2 Design of P-Doped Silica Clads.

Contrast	Probabilities				Estimated Effect
	$\alpha$	$\tau$	$A_0$	$A_f$	$\eta$
Linear	0.08	0.24	0.88	0.32	1.1
Higher Order	0.65	0.55	0.74	0.39	0.2
A (omnibus)	0.16	0.40	0.93	0.41	

Table 3.13

Comparison of  $A_f$  (dB/km) of the Phase 2 Fibers Determined  
Experimentally with that Predicted by Eq. 1

<u>N</u>	<u>[P]<sub>eff</sub></u>	<u>A<sub>f</sub> (pred)</u>	<u>A<sub>f</sub> (meas)</u>
19	0.09	0.9	1.0
20	0.14	1.2	2.8
21	0.44	3.0	2.6
22	0.39	2.7	4.5
23	0.53	3.5	3.7
24	0.66	4.3	2.8

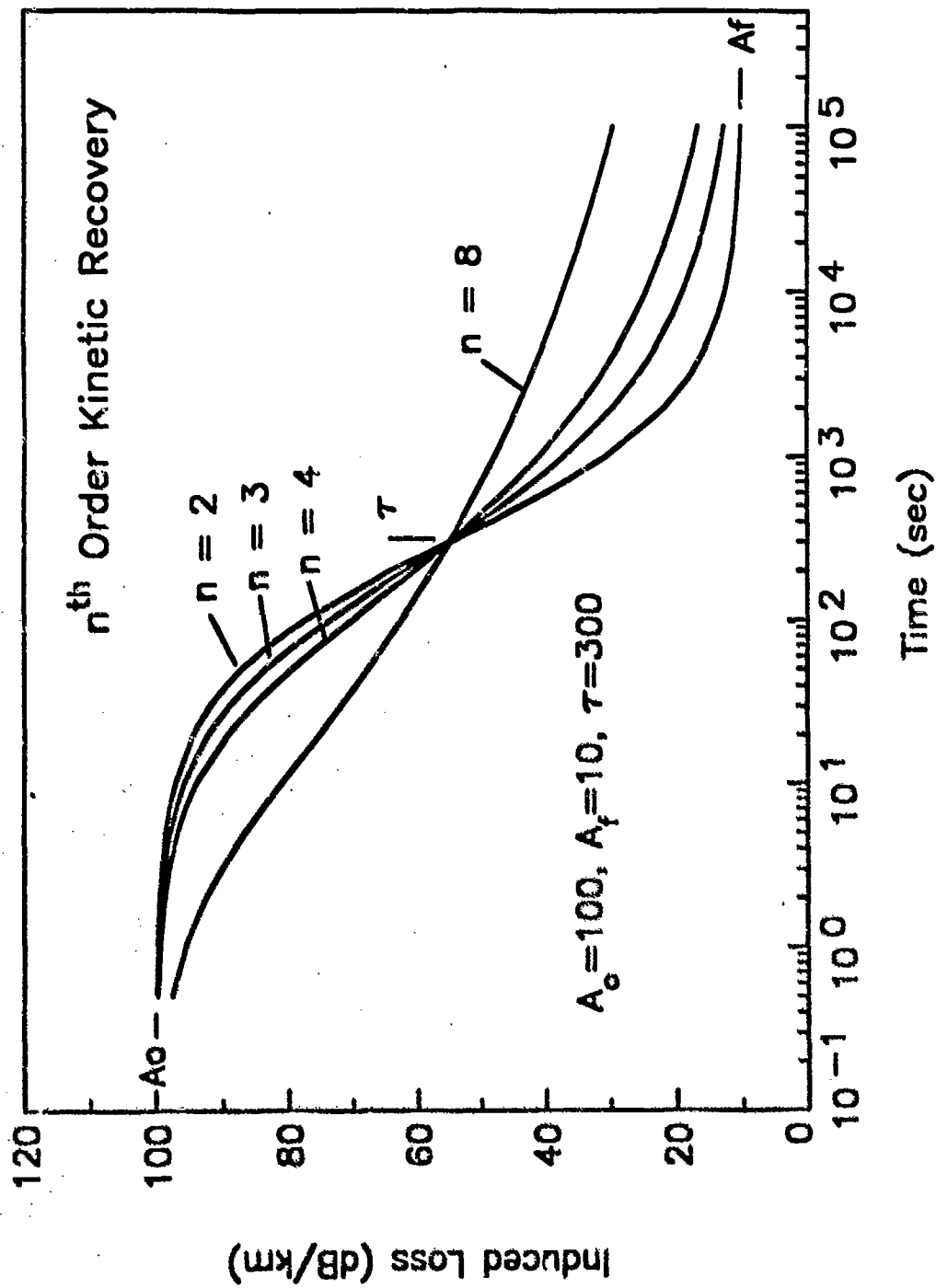


Figure 3.1. Plots of  $n^{\text{th}}$ -order kinetic recovery behavior (Eq. 3.3) for various values of kinetic order  $n$ .

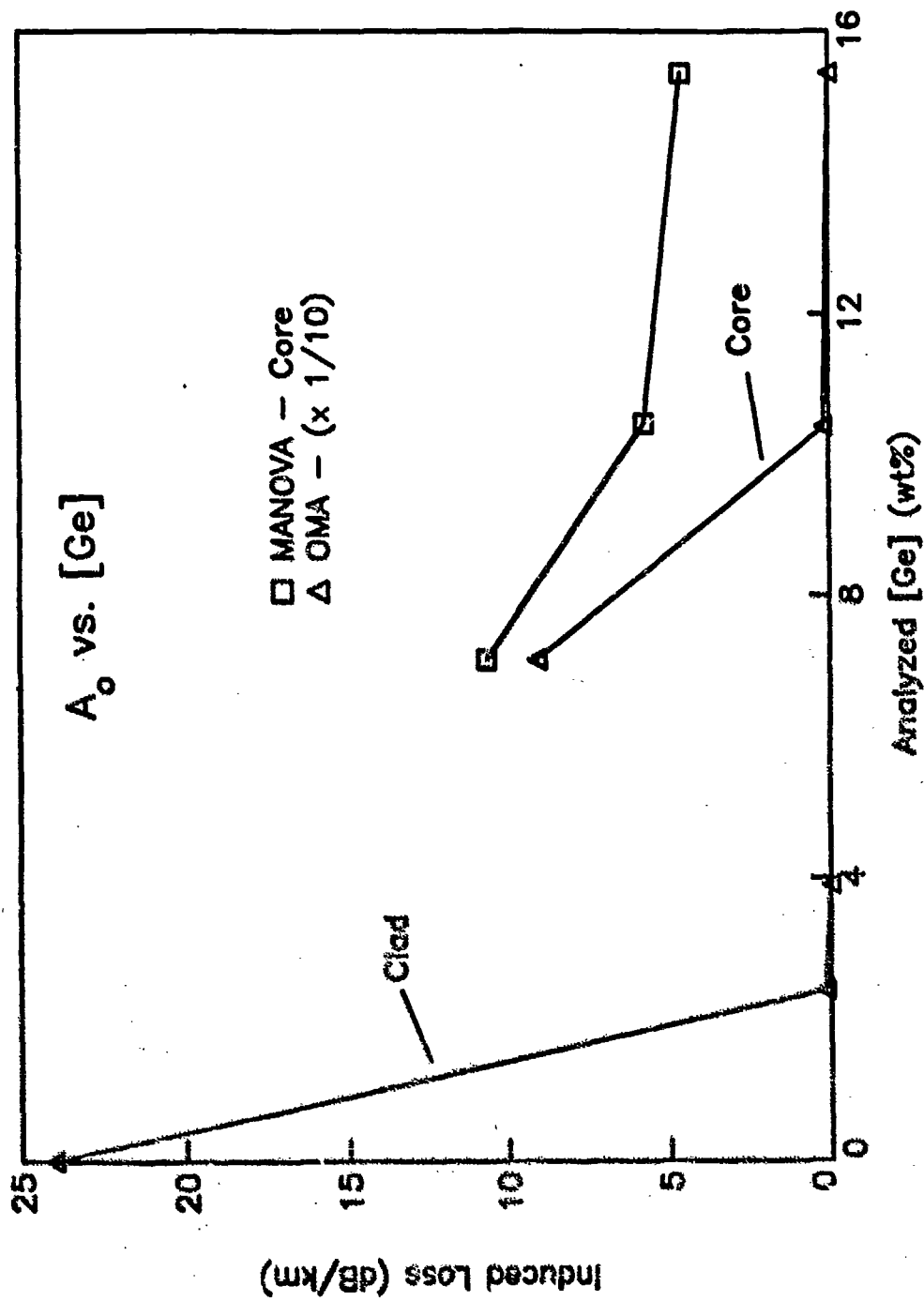


Figure 3.2. Effect of core [Ge] and clad [Ge] (target levels from Table I) on  $A_0$  derived from OMA and MANOVA. The values of  $A_0$  derived from OMA are plotted relative to the smallest value since it is impossible to quantitatively determine the correct offset. Note that F is codoped with Ge in the clad in order to maintain index matching with the silica substrate.

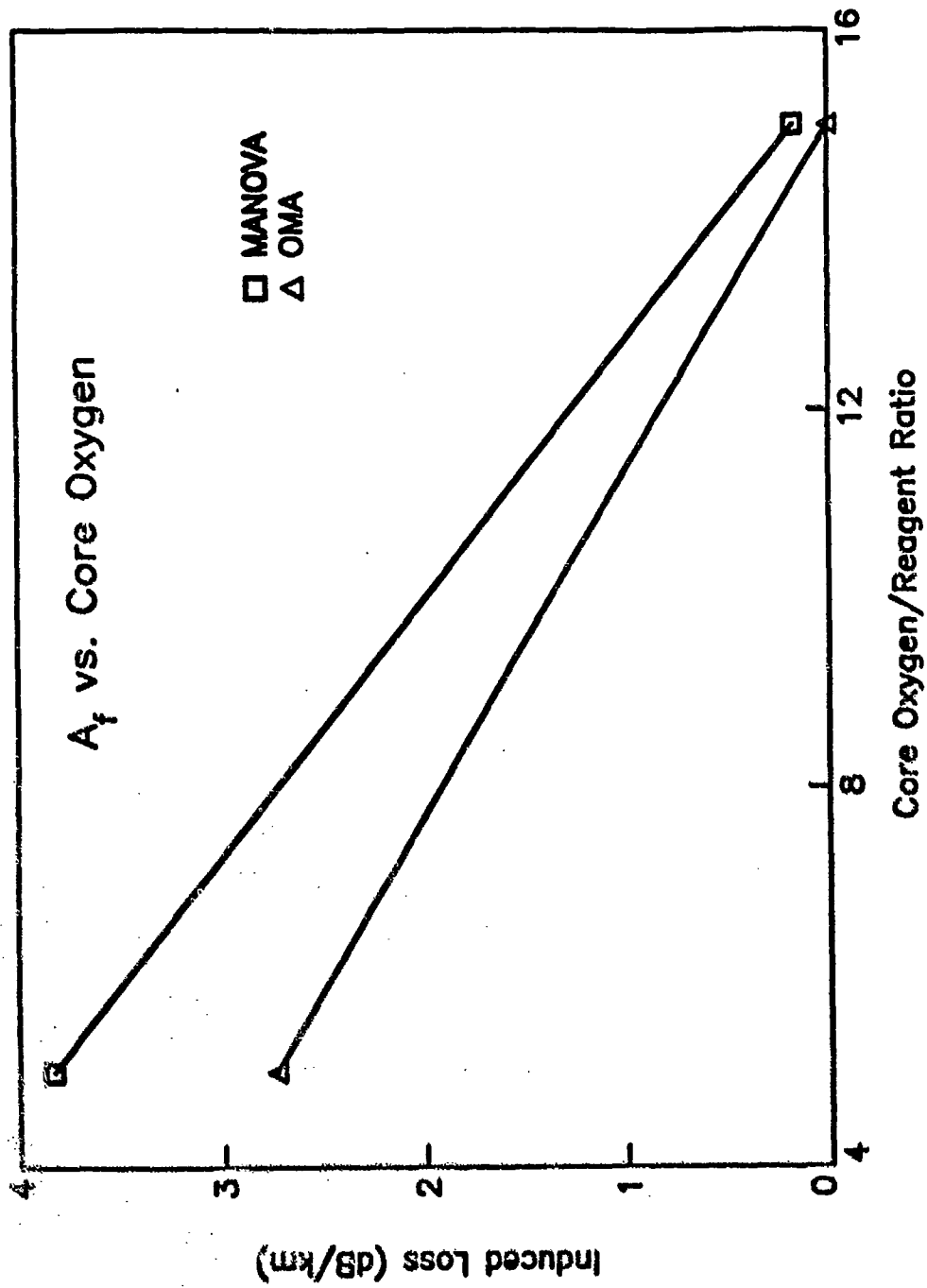


Figure 3.3. Effect of oxygen/reagent ratio used during core deposition on A<sub>f</sub> derived from OMA and MANOVA. Relative values are plotted for the OMA results (see caption for Fig. 3.2).



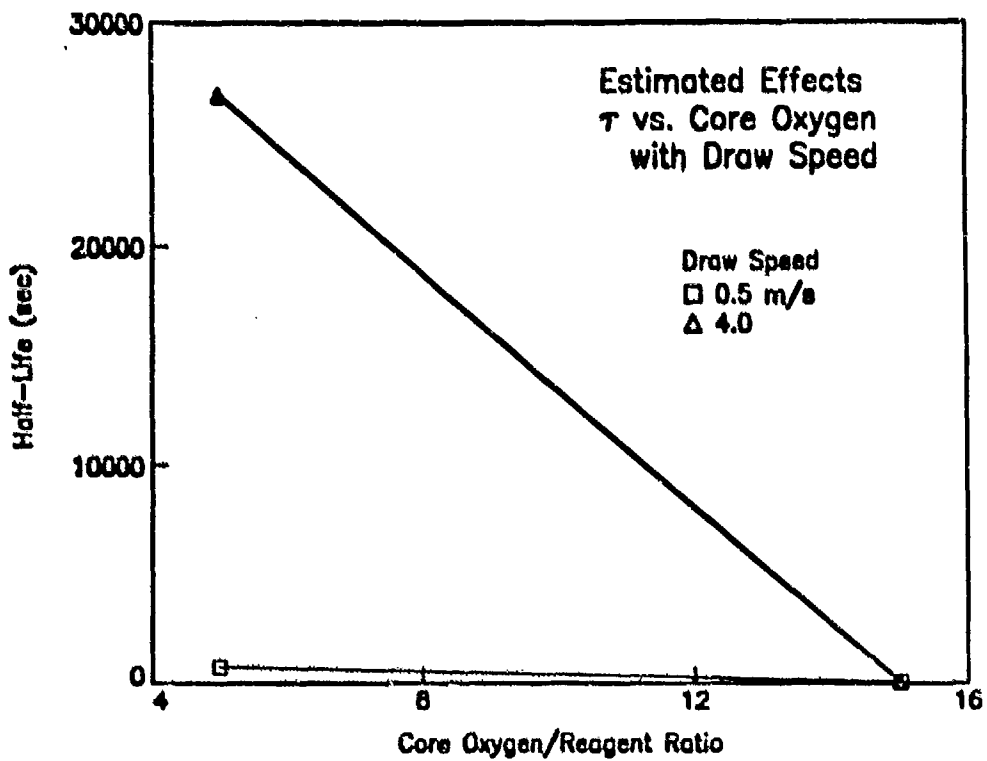
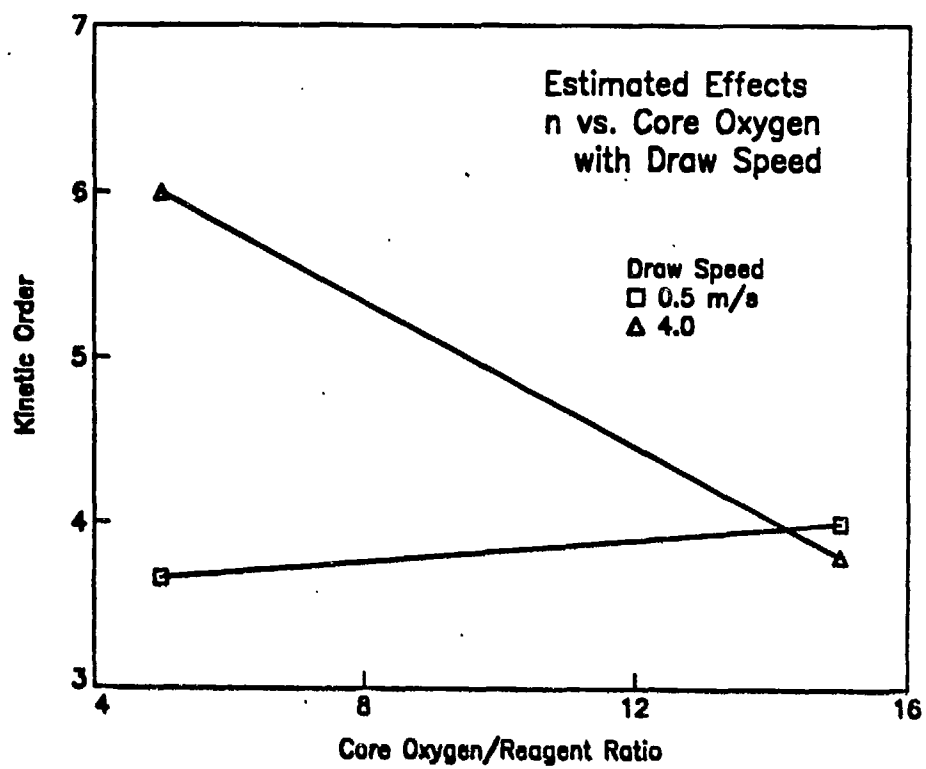


Figure 3.4. Estimated effect of draw speed and oxygen to reagent ratio used during core deposition on (a)  $n$  and (b)  $\tau$  derived from MANOVA.

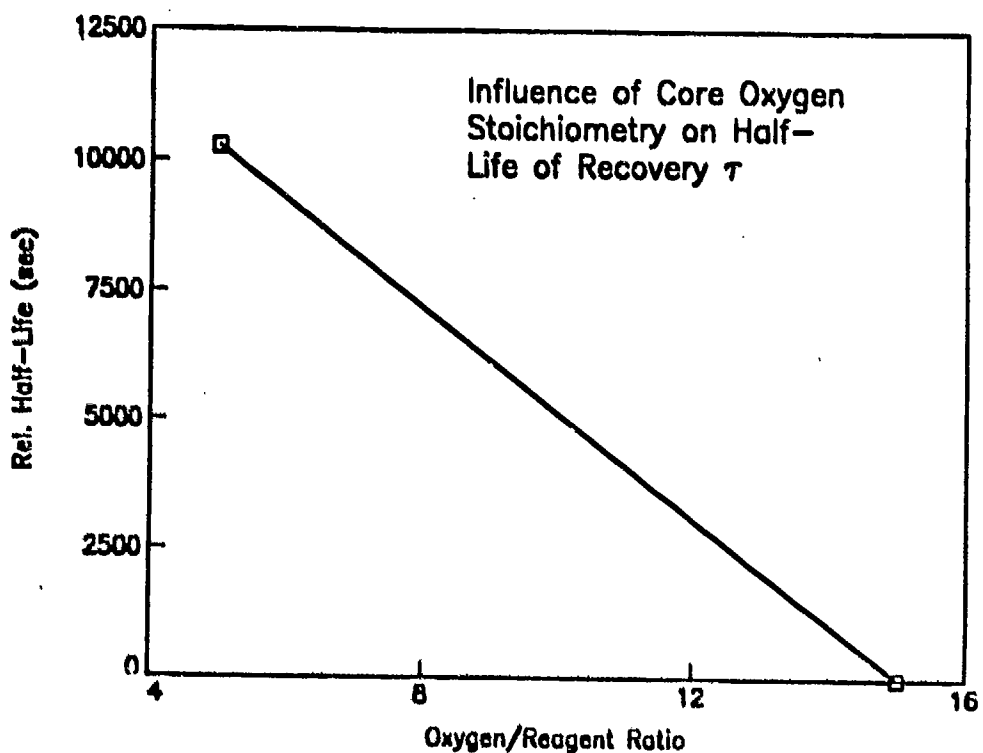
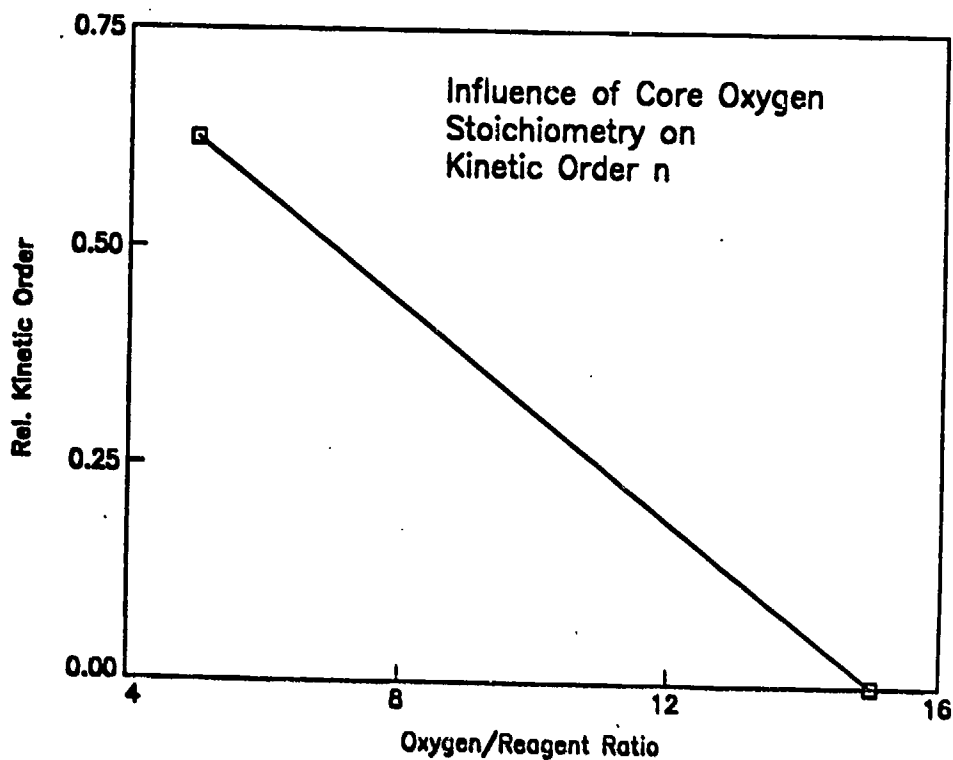


Figure 3.5. Effect of oxygen/reagent ratio used during core deposition on (a)  $n$  and (b)  $\tau$  derived from OMA.

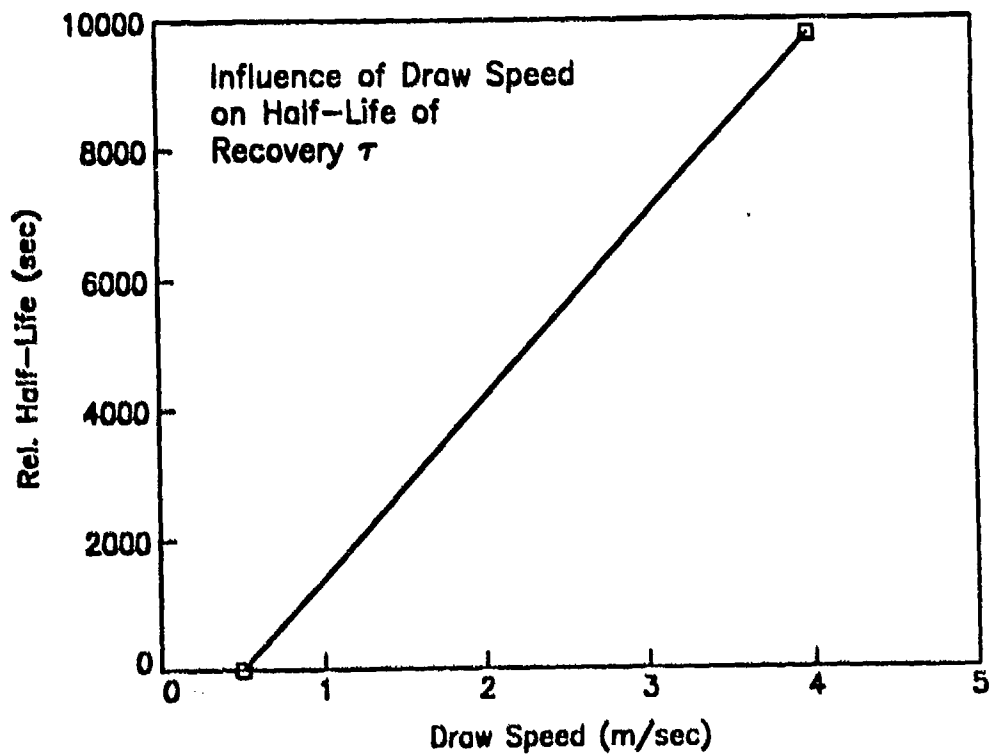
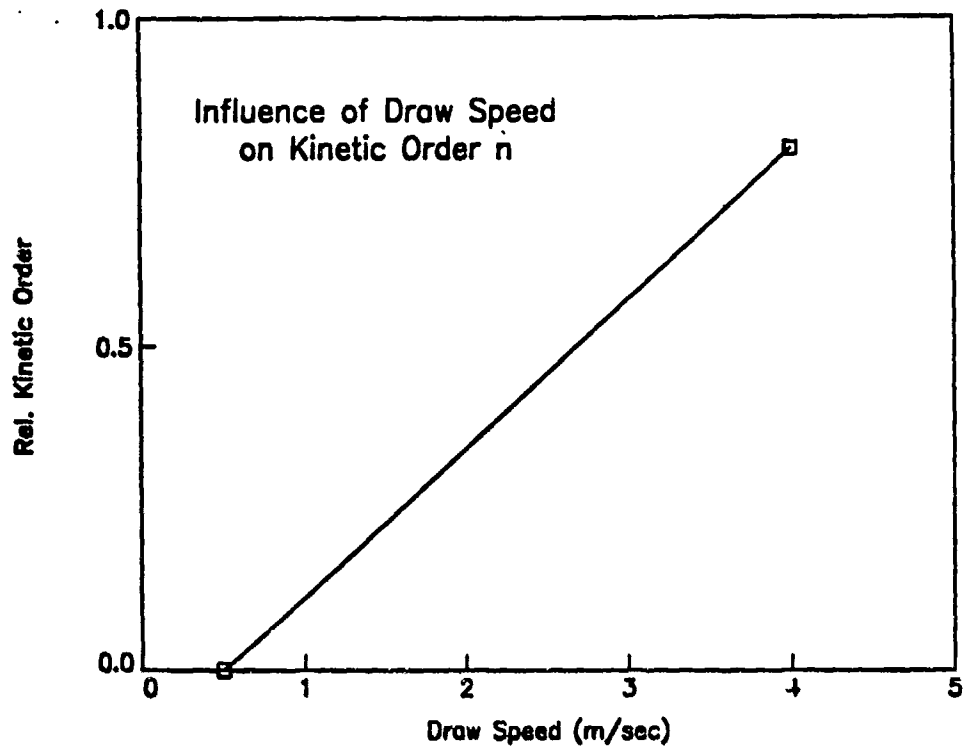


Figure 3.6. Effect of draw speed on (a)  $n$  and (b)  $\tau$  derived from OMA.

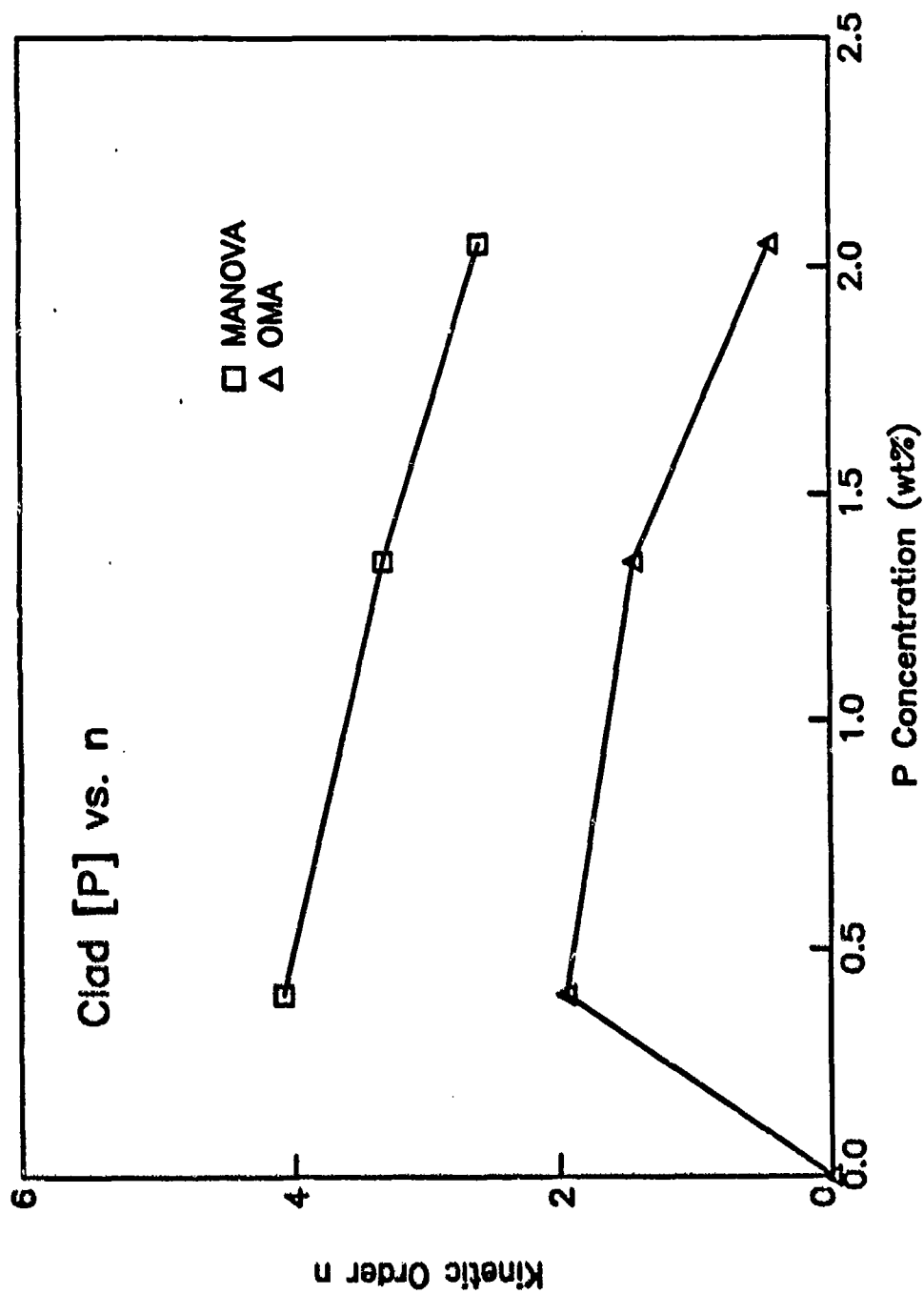


Figure 3.7. Effect of clad [P] (target level from Table 3.3) on  $n$  derived from OMA and MANOVA. Relative values are plotted for the OMA results (see caption for Fig. 3.2).

## CHAPTER 4

### TEMPERATURE DEPENDENCE

The measurements of radiation-induced attenuation in the Phase I and Phase II fibers fabricated in-house at NRL were carried out at the presumed worst-case temperature for buried cables on the continental United States of  $-35\text{ C}$ , as discussed in the Phase I final report. However, deployed fiber links will be subjected to a wide variation in temperature, and it is important to characterize the temperature dependence of the incremental loss.

The initial intent of this task was to study all the Phase I fibers over a range of temperatures, and then develop models of the radiation response that incorporated both temperature dependence *and* fabrication factors. But the lengths of fiber remaining after the  $-35\text{ C}$  exposures were in general too short for subsequent tests. Because of difficulties with the Tylan gas delivery system described in Chapter 2, it was not feasible to fabricate additional Phase I preforms, and the Phase I high speed drawing would have to have been carried out under contract at AT&T Engineering Research Center, Princeton, NJ, at some expense to the program. However, there were still remaining substantial lengths of the commercial single mode fibers, which had been provided to NRL by FiberTrak and which had been irradiated at  $-35\text{ C}$ , as described in Chapter 5 of the Phase I report. Thus, it was decided to perform initial studies of temperature dependence on these fibers.

#### 4.1 EXPERIMENTAL

It was straightforward to irradiate the commercial fibers at a variety of temperatures using the temperature-controlled sample can which had been used for the  $-35\text{ C}$  measurements. The temperature was maintained at the desired set point during the exposure to the  $^{60}\text{Co}$  source and for the  $10^4$ - $10^5$  sec recovery period. As in the case of the  $-35\text{ C}$  measurements, each set of recovery data was fit to the expression for  $n^{\text{th}}$ -order kinetics,

$$A(t) = (A_0 - A_f)[1 + ct]^{-1/(n-1)} + A_f \quad (4.1)$$

where  $c = (1/\tau)[2^{n-1} - 1]$ . The parameters of the fit are the initial and final, or permanent, induced attenuations,  $A_0$  and  $A_f$ , the half-life of the incremental loss  $\tau$ , and the kinetic order of recovery  $n$ . The fibers were irradiated and measured at -55, -35, 0, and 23 C. Table 4.1 contains a summary of the recovery parameters.

## 4.2 RESULTS AND ANALYSIS

Although it is apparent from inspection of Table 4.1 that some of the parameters, e.g.  $A_0$ ,  $\tau$ , and in some cases  $A_f$ , do vary considerably with temperature, the nature of this dependence has been explored by fitting the data to Arrhenian behavior,

$$K = K_0 e^{-E/kT}, \quad (4.2)$$

where  $K$  and  $K_0$  represent the recovery parameter under analysis,  $E$  is the activation energy,  $k$  is the Boltzmann constant, and  $T$  is the temperature. Figures 4.1-4.6 are plots of  $\log(K)$  vs.  $1000/T$ , so that straight lines represent fits to Eq. 4.2, and the slope of the fit is the activation energy. (This analysis was carried out only for those fibers where there was sufficient length that irradiations could be performed at a minimum of 3 different temperatures.) Table 4.2 contains a summary of the activation energies for the 4 parameters. Because  $A_f = 0.0$  at several temperatures in the Corning 1521, 1524 and Sumitomo Standard fibers, the temperature dependence of the final attenuation could not be fit to Eq. 4.2 for these waveguides.

Figures 4.1-4.6 show that there is little temperature dependence of the kinetic order  $n$  in any of the fibers studied, regardless of their core and clad composition. The small values for  $E$  in Table 4.2 confirm this result.

By contrast, the half-life  $\tau$  is thermally-activated in all fibers. With the exception of the Northern Telecom waveguide, which has phosphorus doping in the clad, and the Sumitomo Z fiber, which has a pure silica core, the activation energies are positive. As described in Chapter 6 of the

Phase I report, Eq. 4.1 is derived from chemical kinetics. The general kinetic equation for time-dependent systems is

$$-\frac{dq}{dt} = \lambda q^n \quad (4.3)$$

where  $q$  is the concentration of the reactant,  $t$  is the time,  $\lambda$  is a constant and  $n$  is the order of the reaction. Eq. 4.3 can be integrated to give

$$q = q_0 [1 + (n-1)q_0^{n-1} \lambda t]^{1/(1-n)} \quad (4.4)$$

for  $n > 1$ , and

$$q = q_0 e^{-\lambda t} \quad (4.5)$$

for  $n = 1$ . In reaction processes, the rate constant  $\lambda$  is usually given by the Arrhenius expression

$$\lambda = \lambda_0 e^{-E_A/RT} \quad (4.6)$$

From Eq. 4.1 and 4.4,

$$c = \left(\frac{1}{\tau}\right) [2^{(n-1)} - 1] = (n-1)q_0^{n-1} \lambda \quad (4.7)$$

Thus, the thermal activation of  $\tau$  is understood as arising from the Arrhenian behavior of the rate constant  $\lambda$ , described in Eq. 4.6.

The temperature dependent behavior of  $A_0$  and  $A_f$  arises as a result of the temperature dependence of the color center concentration, i.e.  $A_0$  decreases with increasing temperature because of the electron-hole recombination and color center annihilation which occurs simultaneously with the darkening during radiation exposure.

The negative activation energy of  $\tau$  for the Northern Telecom fiber is a result of the P doping in the fiber cladding. As described in detail in the literature,[1] incorporation of P results in a variety of radiation-induced color centers. As the thermally-unstable phosphorus-oxygen-hole center releases its trapped holes with increasing temperature, they are retrapped by the  $P_1$  defect center, which gives

rise to the radiation-induced absorption at 1.3 and 1.5  $\mu\text{m}$ . [1,2] The negative activation energy is a reflection of this retrapping process, which leads to color center *formation*, rather than bleaching, with increasing temperature. It is interesting to note that the activation energy of  $A_0$  is *positive* for this fiber; presumably this is due to the fact that the core is Ge-doped silica so that the initial attenuation is not affected by the presence of P in the clad. Only after the attenuation associated with the core anneals does the inverse bleaching associated with the clad become a factor.

The origin of the negative activation energy of  $\tau$  for the pure silica core Sumitomo Z fiber is not understood at this time. Further studies of the color centers contributing to the 1.3  $\mu\text{m}$  incremental loss in this fiber will no doubt yield a consistent model based on the kinetics of radiation-induced defect center annealing.

In past studies, [3,4] only qualitative relationships of the temperature dependence of the radiation damage in optical fiber waveguides were established. Although by no means complete, the initial analysis discussed in this chapter has shown that the temperature dependence of the recovery process is primarily expressed in the half-life due to the temperature dependence of the rate constant governing recovery. In addition, the initial and final attenuations are temperature dependent because the concentration of color centers induced during steady state exposure is affected by the recovery that occurs with the darkening. Further studies are clearly in order to more fully characterize these behaviors, in particular in low dose rate environments.

## REFERENCES

1. D.L. Griscom, E.J. Friebele, K.J. Long and J.W. Fleming, "Fundamental defect centers in glass: Electron spin resonance and optical absorption studies of irradiated phosphorus-doped silica glass and optical fibers," J. Appl. Phys. 54 (1983) 3743-3762.
2. E.J. Friebele and D.L. Griscom, "Color centers in glass optical fiber waveguides," Defects in Glasses (MRS Proceedings Volume 61), F.L. Galeener, D.L. Griscom and M.J. Weber, Ed. (Materials Research Society, Pittsburgh, PA, 1986), pp. 319-331.



3. E.J. Friebele, C.G. Askins, M.E. Gingerich, and K.J. Long, "Optical fiber waveguides in radiation environments, II," Nucl. Inst. Meth. in Phys. Res. B1 (1984) 355-369.

4. E.J. Friebele, K.J. Long, C.G. Askins, M.E. Gingerich, M.J. Marrone, and D.L. Griscom, "Overview of radiation effects in fiber optics," Crit. Rev. Tech.: Opt. Materials in Radiation Environments (SPIE Vol. 541), P. Levy and E.J. Friebele, Ed. (SPIE, Bellingham, WA, 1985), pp. 70-88.

**Table 4.1**  
**Temperature Dependence of 1.3  $\mu\text{m}$  Recovery Parameters of Commercial**  
**Single Mode Fibers (Dose = 2000 rad)**

Fiber	T (C)	A <sub>0</sub> (dB/km)	A <sub>f</sub> (dB/km)	n	$\tau$ (s)
Corning 1521	-55	23.1	0.0	5.2	256
	-35	28.6	1.0	4.9	25
	0	5.5	0.0	4.2	89
	27	3.4	0.2	4.1	20
Corning 1524	-55	32.1	0.1	6.9	492
	-35	17.5	0.0	5.4	111
	0	13.9	0.0	4.6	17
	23	4.6	0.4	5.0	70
Sumitomo Std.	-55	14.0	0.0	5.2	156.4
	-35	8.8	2.1	2.1	34.2
	23	6.1	0.0	3.7	4.8
LTI 1754	-35	8.6	0.5	6.3	200
	23	3.0	0.0	4.1	48
No. Telecom	-55	5.9	2.3	4.6	33
	-35	4.4	2.1	3.2	106
	0	2.1	2.0	5.0	1000
	28	3.5	2.3	9.0	100000
NRL 860815	-35	2.5	0.2	3.8	44
	27	3.2	2.8	9.0	1000
Philips	-55	11.0	1.0	4.4	100
	-35	18.0	0.0	5.4	186
	0	2.6	0.6	5.8	20
	28	1.2	0.4	2.8	50
Spectran RH	-35	9.9	0.0	4.0	10
	23	3.3	1.3	5.7	9000
Sumitomo Z	-55	23.4	1.7	3.1	2.1
	-35	9.3	1.4	2.2	28.0

**Table 4.1**  
**Temperature Dependence of 1.3  $\mu\text{m}$  Recovery Parameters of Commercial**  
**Single Mode Fibers (Dose = 2000 rad)**

	0	5.9	0.0	3.6	4.0
	23	3.2	0.1	3.5	9.2
Mitsubishi	-55	11.6	1.0	2.9	4
	27	4.0	0.5	1.7	4

**Table 4.2**  
**Core and Cladding Dopants and Activation Energies (eV) of the Recovery Parameters of Commercial Single Mode Fibers Irradiated at Various Temperatures to 2000 rad.**

Fiber	Core			Cladding				Recovery Parameters			
	Ge	F	Ge	P	F	A <sub>0</sub>	A <sub>f</sub>	n	τ		
Corning 1521	X					0.131		0.019	0.159		
Corning 1524	X		X			0.121		0.024	0.171		
Sumitomo Std.	X				X	0.056		0.012	0.240		
No. Telecom	X			X	X	0.050	0.131	-0.048	-0.512		
Philips	X	X	X		X	0.147	0.060	0.022	0.095		
Sumitomo Z					X	0.131	0.214	-0.019	-0.093		

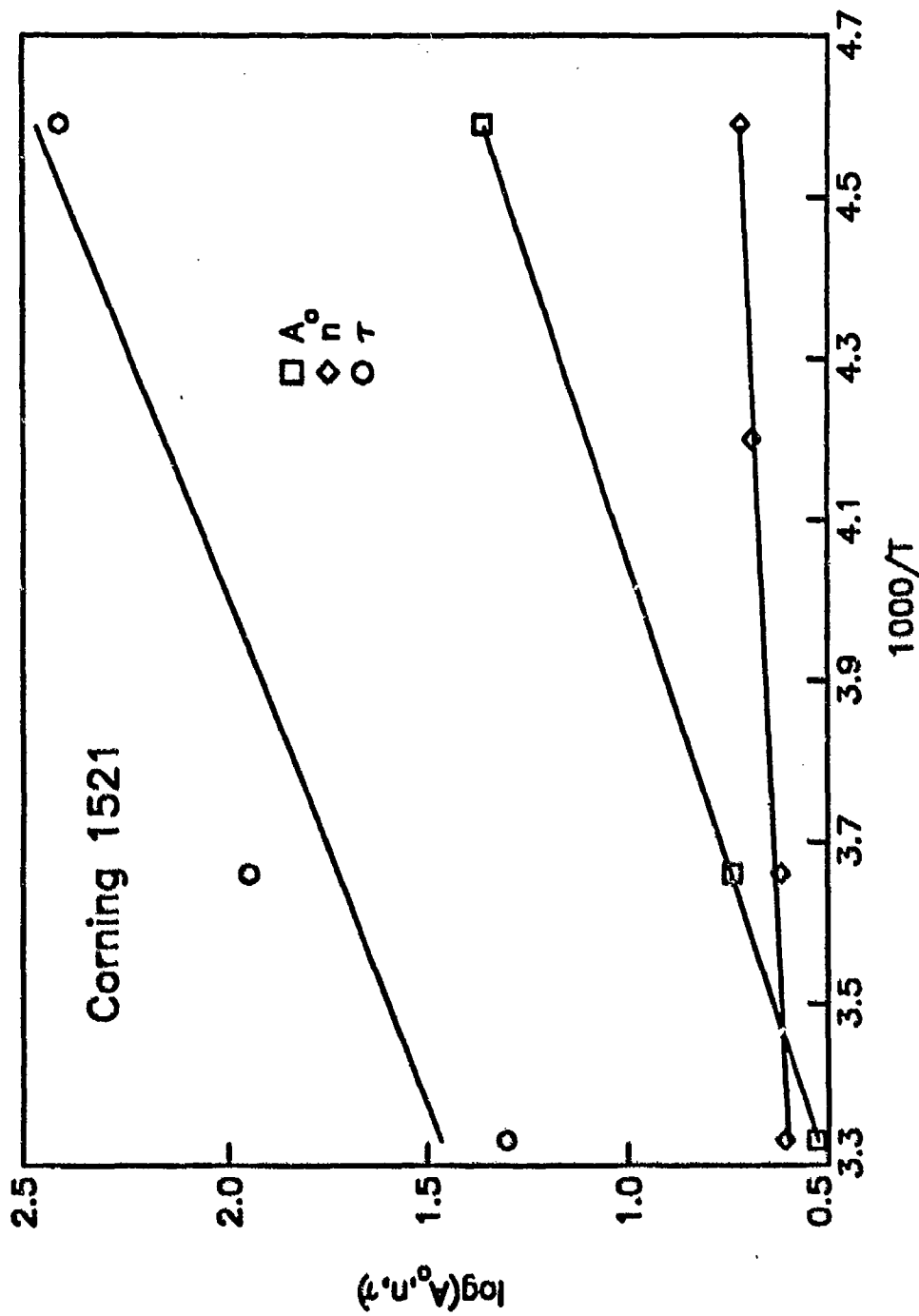


Figure 4.1. Temperature dependence of the recovery parameters of the radiation-induced attenuation in Corning 1521 (points) and fits to Arrhenius behavior (lines).

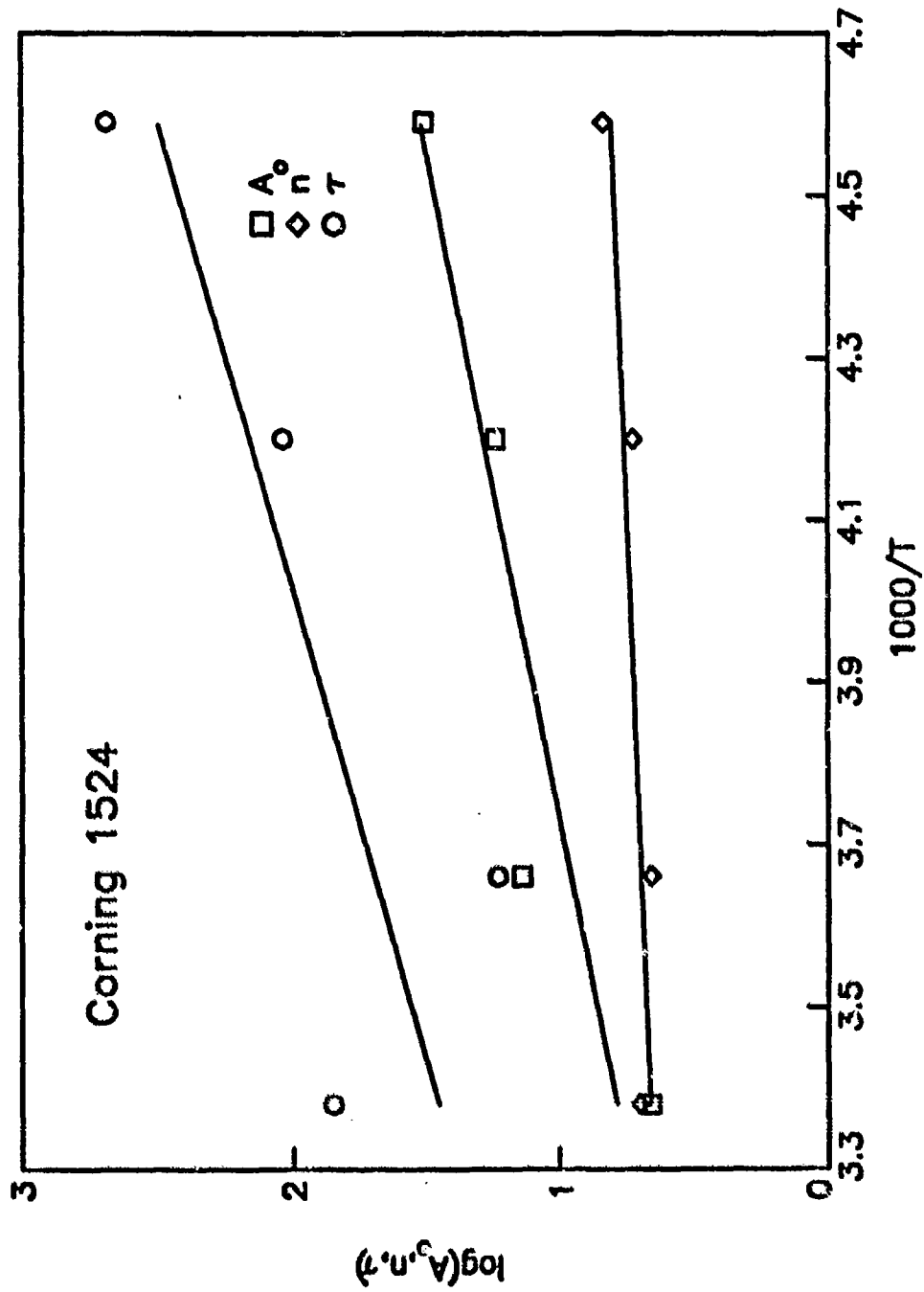


Figure 4.2. Temperature dependence of the recovery parameters of the radiation-induced attenuation in Corning 1524 (points) and fits to Arrhenius behavior (lines).

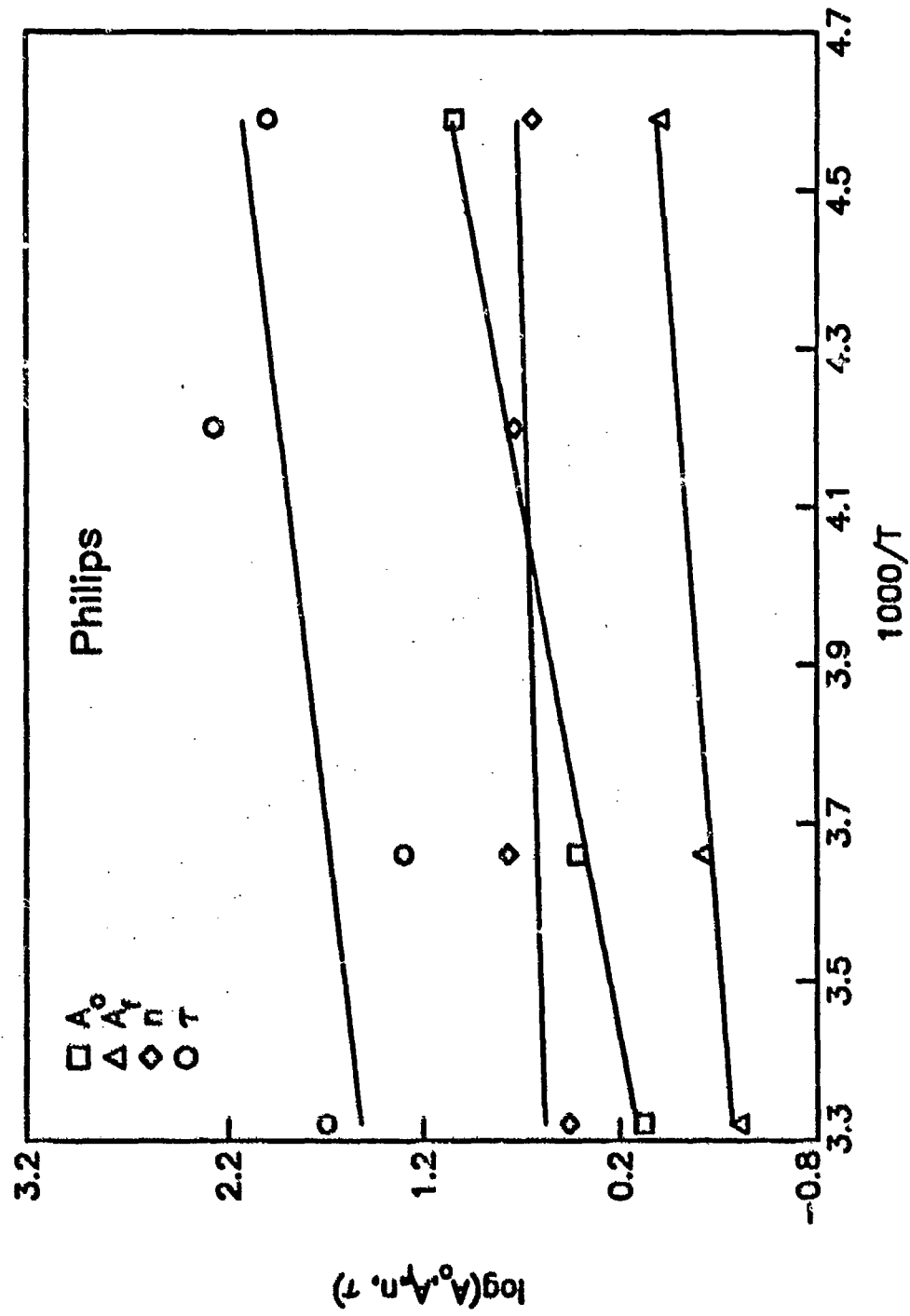


Figure 4.3. Temperature dependence of the recovery parameters of the radiation-induced attenuation in the Philips single mode fiber (points) and fits to Arrhenius behavior (lines).

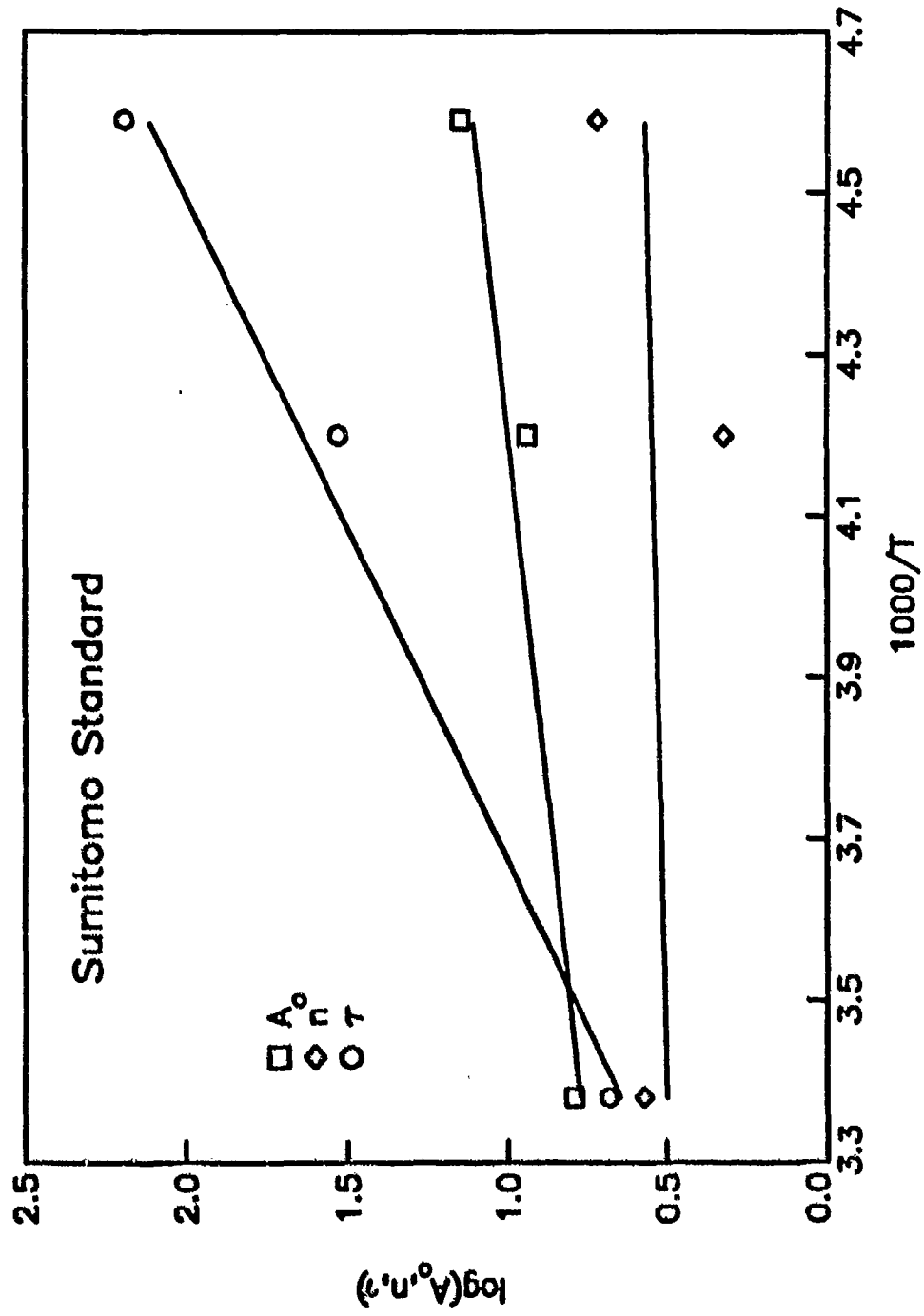


Figure 4.4. Temperature dependence of the recovery parameters of the radiation-induced attenuation in the Sumitomo standard single mode fiber (points) and fits to Arrhenius behavior (lines).



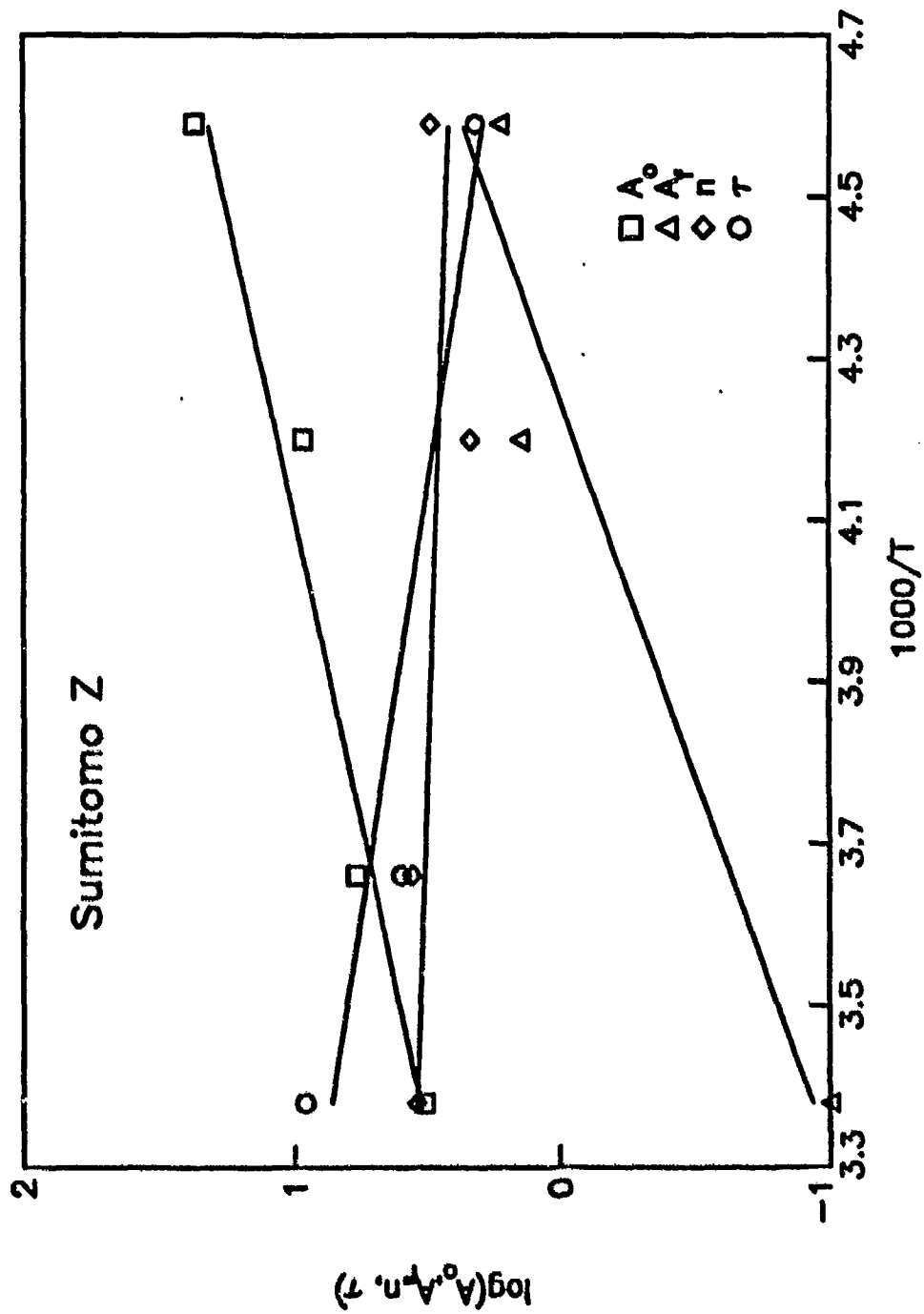


Figure 4.5. Temperature dependence of the recovery parameters of the radiation-induced attenuation in the Sumitomo Z pure silica core fiber (points) and fits to Arrhenius behavior (lines).

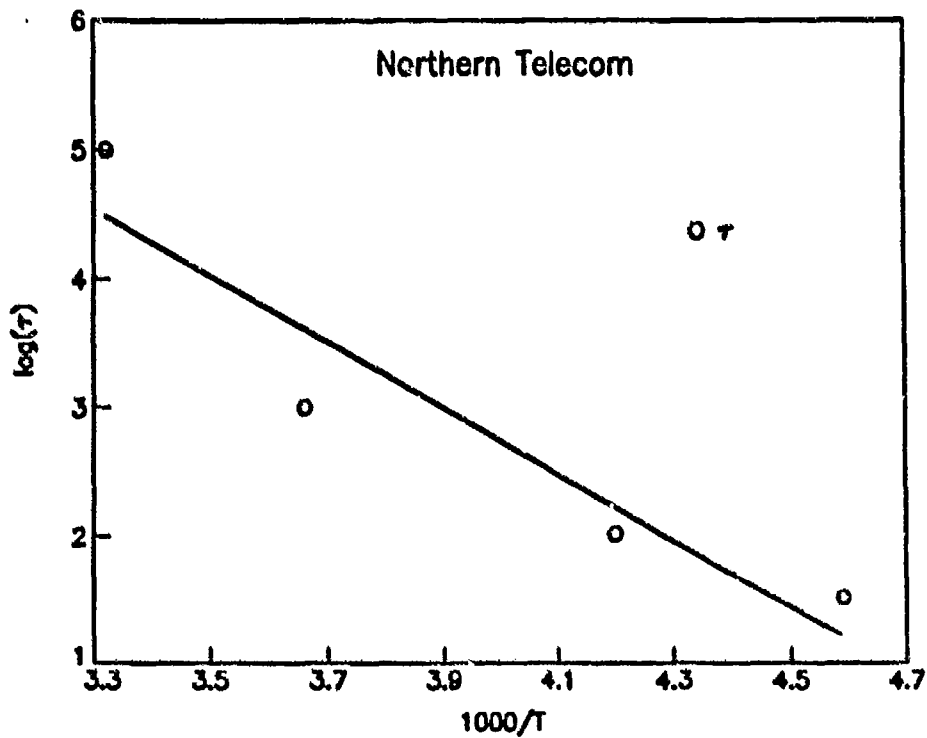
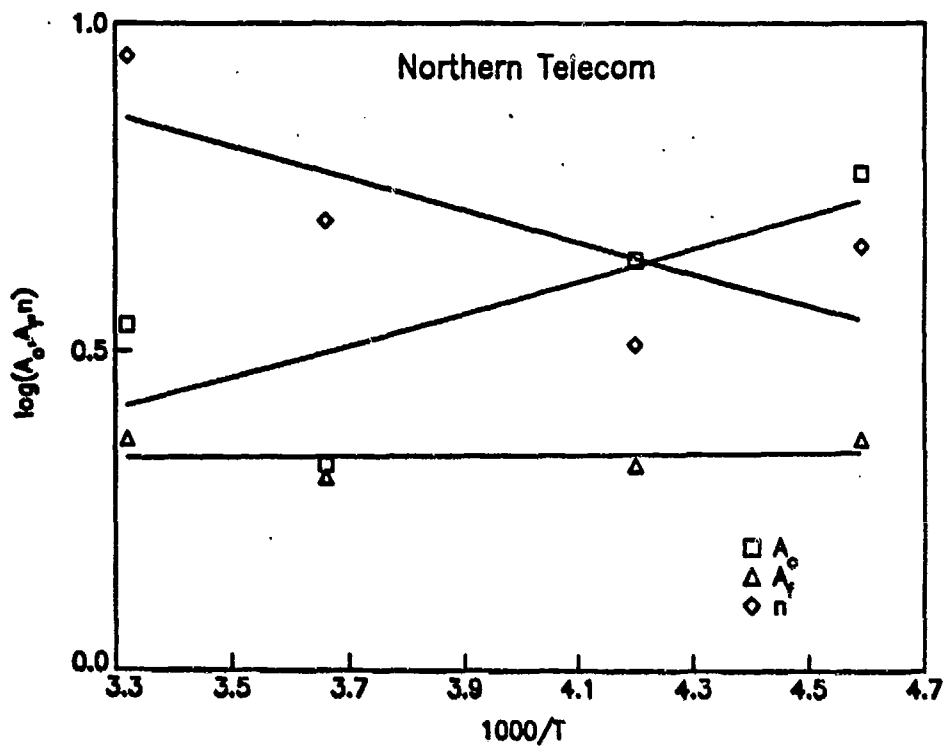


Figure 4.6. Temperature dependence of the recovery parameters of the radiation-induced attenuation in the Northern Telecom single mode fiber (points) and fits to Arrhenius behavior (lines).

## CHAPTER 5

### EFFECT OF CLAD DOPANTS

In the multidimensional Phase I study of matched clad single mode fiber waveguides described in Chapter 3, both core and clad fabrication factors were varied, i.e. clad [Ge], the oxygen/reagent ratio ( $O_2/R$ ) used during core deposition, clad [Ge], and clad  $O_2/R$ . Because the experimental design used in this prior study was not orthogonal, there was confounding of the main effects associated with the clad with two-way (and higher order) interactions, as shown in Table 3.5. In addition, the core factors exerted a much stronger influence on the fibers' radiation response, since the largest fraction of optical power travels in the core. Nevertheless, attenuation in the clad will be deleterious to the overall radiation hardness of the fiber since as much as 20-25% of the optical power is in the cladding as an evanescent wave. Although subtle, the cladding radiation response will significantly affect the overall radiation response of the fiber.

#### 5.1 LEVELS OF THE FACTORS

There were primarily two outstanding questions from Phase I which this one-dimensional study addressed: First, in the earlier work  $A_0$  was substantially greater in fibers with pure silica clads than in those with 2.4 wt% [Ge], the lowest amount of Ge doped into the clad. However, in the Phase I experimental design (Table 3.2), all of the fibers with pure silica clads (fibers 1, 2, 5, and 6 with level 1 of factor B) had either the first or second levels of core [Ge]. As it turned out, 3 of the 4 fibers were poorly guiding with as much as 40% of the optical power in the clad due to the small  $\Delta^+$  in the fibers 1 and 6, which had the lowest level of core [Ge] (Table 3.5d in the Phase I final report). It was not clear whether the origin of the high values of  $A_0$  could be solely attributed to the pure silica clads.

A second question revolved around the fact that as the clad [Ge] increased, F had to be codoped in increasing amounts in order to maintain the refractive index of the cladding matched to that of the silica support tube. It was assumed in Phase I that any effects of the clad on the radiation response would be due to variations in [Ge]. However, because of the F codoping, it was desirable to separate the effects of changes in clad [Ge] from changes in [F]

The fiber preforms were fabricated using the MCVD method, and all fibers were drawn at 0.5 m/s with 50 g draw tension with the exception of the pure silica clad fiber, which was also drawn at 20 and 80 g tension. (All tensions are normalized to a 125  $\mu\text{m}$  diameter fiber.) Electron microprobe analysis with a resolution of 1  $\mu\text{m}$  was used to determine the concentration of Ge and F in the cores and clads. The core [Ge] and  $\text{O}_2/\text{R}$  were maintained constant for all fibers at ~8 wt% and 10, i.e. level 2 of Phase IA core [Ge] and a level of  $\text{O}_2/\text{R}$  intermediate between levels 1 and 2 of Phase IA. Two sets of experiments were undertaken: As shown in Table 5.1, matched clad fibers 25-28 had increasing concentrations of Ge (and F) in the clad, while depressed clad fibers 29 and 30 investigate the effect of increasing clad [F] when compared with fiber 26. (The fibers are numbered consecutively, following the first 24 fibers investigated in the Phase I study.) The clad [Ge] of fiber 26 was obtained with the lowest possible flow of  $\text{GeCl}_4$  vapor in order to determine if  $A_0$  decreased uniformly with clad [Ge] or whether the decrease would occur with even the slightest amount of Ge.

As in Phase I, the fibers were irradiated to 2000 rad at a dose rate of ~3000 rad/min; the temperature was maintained at -35 C during exposure and for ~ $10^5$  sec recovery. The incremental attenuation at 1.3  $\mu\text{m}$  was monitored *in situ* during this period, and the recovery of the incremental loss was fit to  $n^{\text{th}}$  order kinetics, Eq. 3.3.

## 5.2 RESULTS

Figures 5.1 and 5.2 show the recovery data and the fits to Eq. 3.3; it is apparent that the agreement is quite good, and the behavior of all fibers is adequately described by the 4 radiation response parameters. A summary of the parameters is shown in Table 5.1. As expected from the

results of Phase I, and the Phase I 2<sup>4</sup> experimental design described in Chapter 6, the final attenuation  $A_f$  of all fibers is relatively low since all fiber cores were deposited with high oxygen/reagent ratio.

**5.2.1 Silica Clad Fibers.** Likewise, in agreement with Phase I, the initial loss  $A_0$  of the pure silica clad fibers (Fig. 3.1 and fiber 2.5 in Table 5.1) is substantially greater than that of those with doped silica clads. In contrast, the kinetic order is  $\sim 3$  and the half-life is  $\sim 10$  sec, which are both substantially less than the Ge-doped clad fibers. Note also the significant effect of draw tension on the initial attenuation; a similar dependence has not been revealed in Ge-doped silica clad fibers, as discussed in Chapter 6 (see Table 6.7).

One of the most intriguing effects in the study of radiation damage in optical fibers is light-induced annealing or photobleaching of the incremental loss either by the data signal itself or by an additional optical signal of a different wavelength. Many of the variations in radiation sensitivity reported by different laboratories for nominally identical fibers can be traced to differences in optical power used to make the measurement. Photobleaching over a range of optical powers is demonstrated in Fig. 5.3 for a pure silica core multimode fiber. Here, the requisite power was maintained in the fiber during irradiation and recovery. The data labeled "Dark" were obtained using a 100 nW source which was turned off during exposure and shuttered on for  $\sim 2$  s for each measurement plotted. Similar effects have been observed for Ge-doped silica core fibers, although the extent of the light-induced annealing is much less.

It is clear from Fig. 5.3 that increasing the optical power greatly enhances the recovery. What was not recognized until recently was that there is a significant change in the kinetics between the cases where the fiber is dark and where it is transmitting even the least amount of power. Note from the fits that the order of the kinetics changes from 7.5 to 2 when the fiber transmits light, implying that even 300 nW ( $-35$  dBm) of  $0.85 \mu\text{m}$  light is sufficient to activate the diffusing species. Similar effects of photobleaching have been observed at  $1.3 \mu\text{m}$ .

Although the photobleaching obviously affects the recovery of the radiation-induced loss in pure silica core fibers, such as the multimode fiber in Fig. 5.3 or the Sumitomo Z fibers studied in Phase I, there is apparently a similar effect in pure silica *clad* fibers. The kinetic order of Ge-doped silica core-pure silica clad fibers, such as fiber 25 in Table 5.1, is not 2, presumably because the kinetic order of the recovery of the incremental attenuation in the Ge-doped silica core is on the order of 4-5. Nevertheless, both  $n$  and  $\tau$  are significantly less in pure silica than in Ge-F-doped silica clad fibers, indicating faster recovery in fibers with pure silica clads.

**5.2.2 Effect of Ge Doping.** Doping the clad with even the slightest amount of Ge results in a significant decrease in  $A_0$  and increases in  $n$  and  $\tau$ , as shown for fiber 26 in Table 5.1. However, further increases in [Ge] decrease both  $A_0$  (fibers 26, 27, and 28). This result is in accord with the results of the Phase I where  $A_0$  decreased with increasing *core* [Ge], as shown in Fig. 3.2. In this one-dimensional study with the core [Ge] held constant, a similar effect is noted for clad [Ge].

**5.2.3 Effect of F Doping.** Finally, consider fibers 26, 29 and 30 where the clad [Ge] was held constant and [F] was increased. Although  $A_0$  and  $A_f$  are unchanged, depressing the clad with increased [F] causes an immediate increase in  $n$  from  $\sim 4.5$  to  $\geq 6$  and in  $\tau$  from  $\sim 100$  to  $\sim 550-700$  sec, (Fig. 5.4 and Table 5.1) and hence a significant increase in the time required for recovery. (As shown in Fig. 5.2, the recovery data of fibers 29 and 30 are quite similar. Because of the long term drift, it is impossible to state definitively that the values of  $n$  and  $\tau$  are greater for fiber 29 than for 30, and they may in fact be equal. However, it is clear that in both fibers,  $n$  and  $\tau$  are significantly greater than in fiber 26.

As is apparent from fiber 28, which has the same approximate clad [F] as fiber 29, when the clad [Ge] is high, the recovery behavior appears to be determined by the germanium, and  $n$  and  $\tau$  are similar to that of the other matched clad fibers. When the clad [F] is large, as in fibers 29 and 30, the recovery is then determined by the fluorine, and  $n$  and  $\tau$  increase. Alternatively, the effect on  $n$  and  $\tau$  may be due to the mode being more tightly confined to the Ge-doped core; however, there is no evidence for a correlation of Ge content with  $n$  and  $\tau$  either here or in the Phase I study.

### 5.3 SUMMARY

The results of the one-dimensional study have shown that the composition of single mode fiber claddings can have a significant effect on the recovery of the incremental loss following radiation exposure. It was confirmed that pure silica clad fibers have high initial loss but good recovery, while fibers with clads depressed by F doping show much lower initial attenuation but significantly slower recovery. Addition of Ge and F to maintain the matched clad condition slightly decreases the initial loss while increasing the recovery time relative to fibers with pure silica clads.

Table 5.1. Fiber Dopant Concentrations (wt%) and Recovery Parameters								
Fiber	Core		Clad		Recovery Parameters			
	Ge	F	Ge	F	n	$\tau$ (sec)	$A_o$ (dB/km)	$A_f$ (dB/km)
Matched Clad								
25	7.4	0.01	0.0	0.00	2.6	9.2	82.7	0.5
26	8.4	0.06	0.6	0.17	4.5	112	4.0	0.5
27	8.6	0.07	1.9	0.45	4.6	104	3.0	0.0
28	6.8	0.17	3.5	0.78	4.9	102	2.6	0.0
Depressed Clad								
29	9.1	0.22	0.2	0.84	6.4	680	4.1	0.0
30	6.6	0.31	0.3	1.35	6.0	560	4.0	0.1



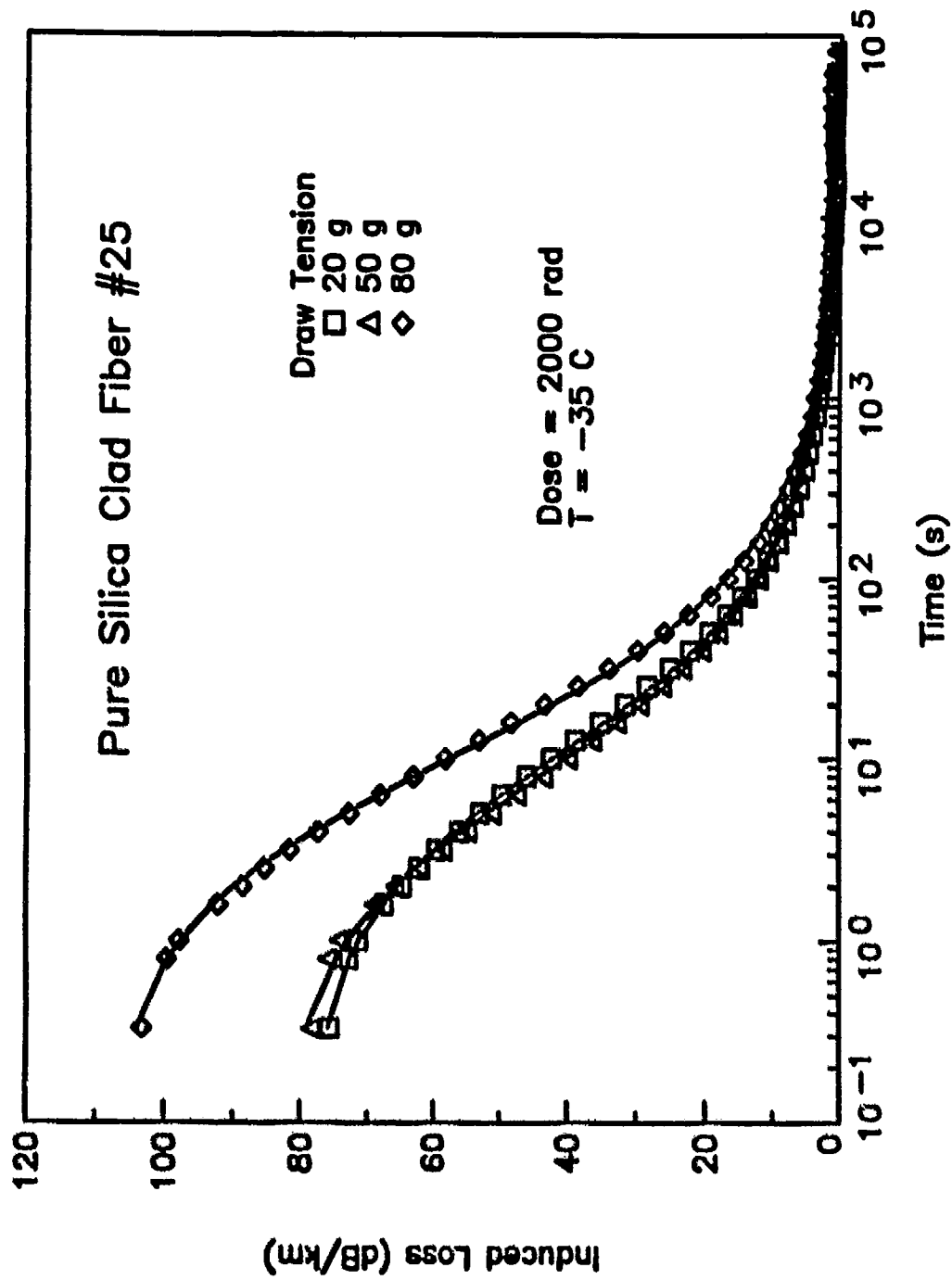


Figure 5.1. Recovery of the 1.3  $\mu\text{m}$  radiation-induced attenuation in the pure silica clad fiber drawn at different draw tensions (points) and fits to Eq. 3.3 using the parameters of Table 5.1.

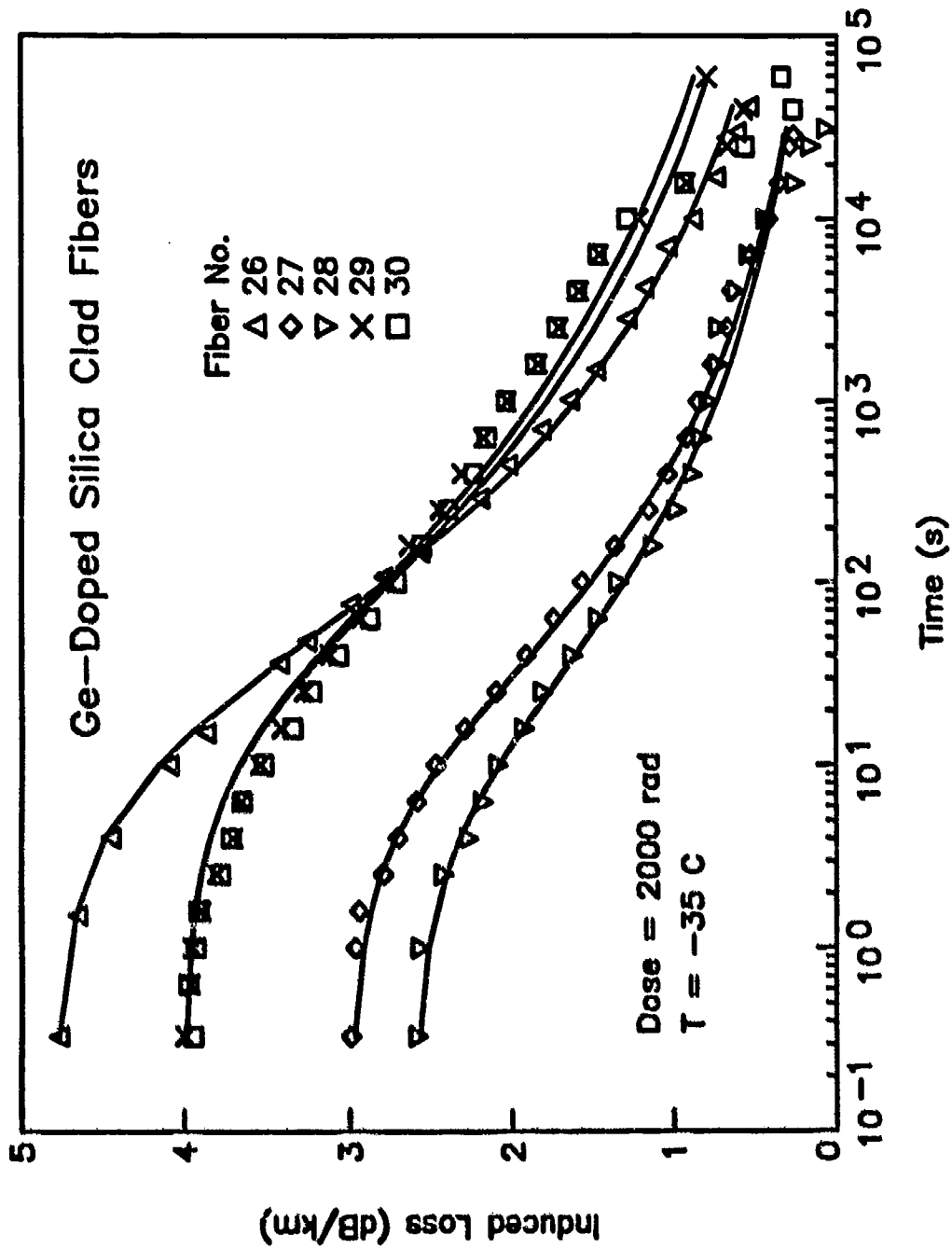


Figure 5.2. Recovery of the 1.3  $\mu\text{m}$  radiation-induced attenuation of the Ge-F-doped silica clad fibers (points) and fits to Eq. 3.3 using the parameters of Table 5.1.

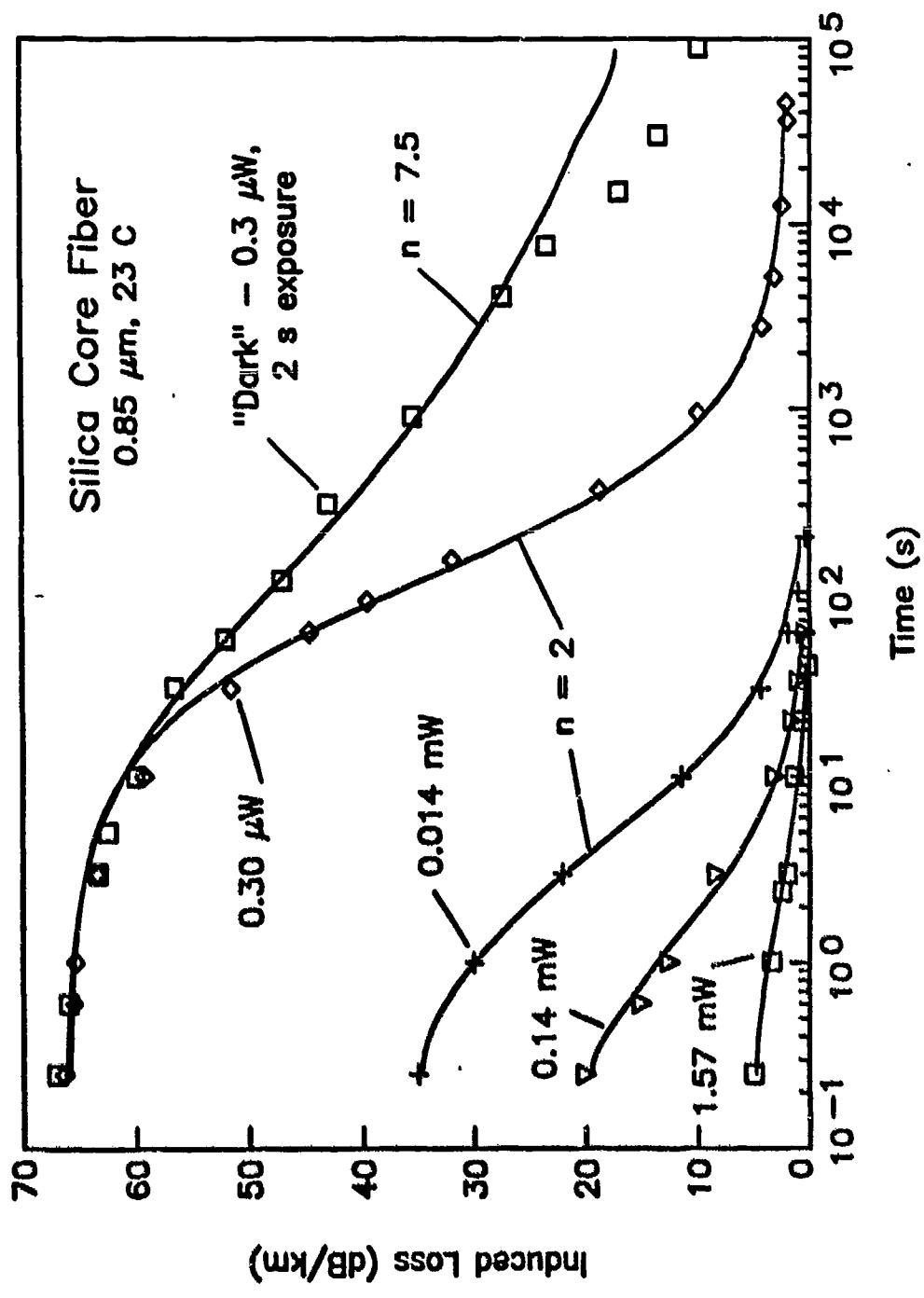


Figure 5.3 Recovery of the radiation-induced attenuation in a multimode pure silica core-polymer clad fiber vs. light power. The data (points) have been fit to  $n^{\text{th}}$ -order kinetic recovery using Eq. 3.3, shown as the lines.

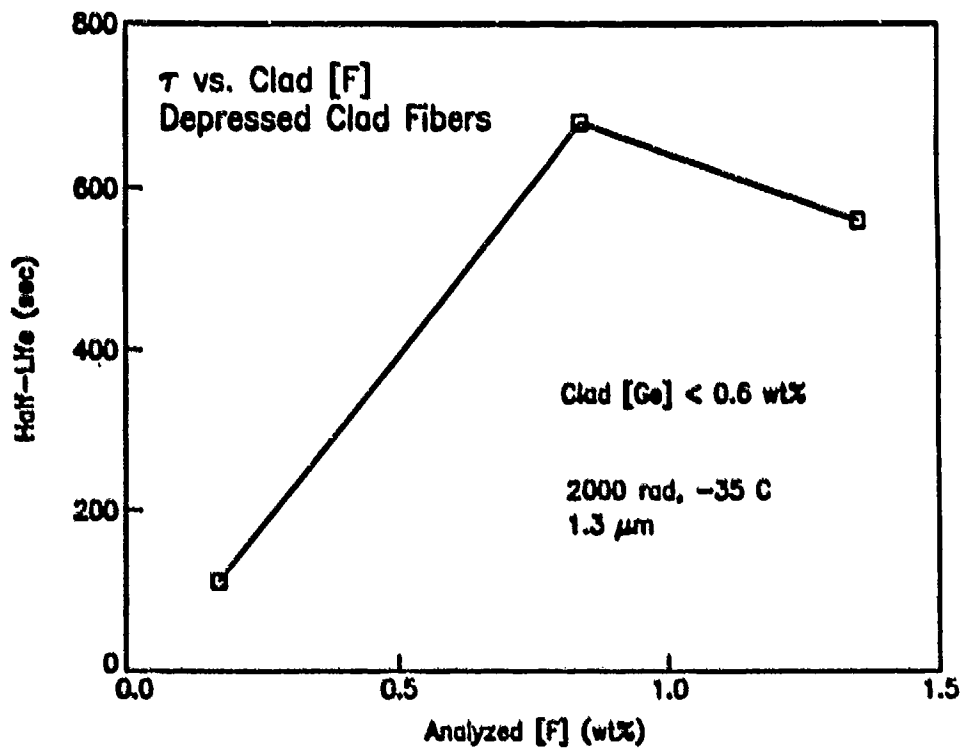
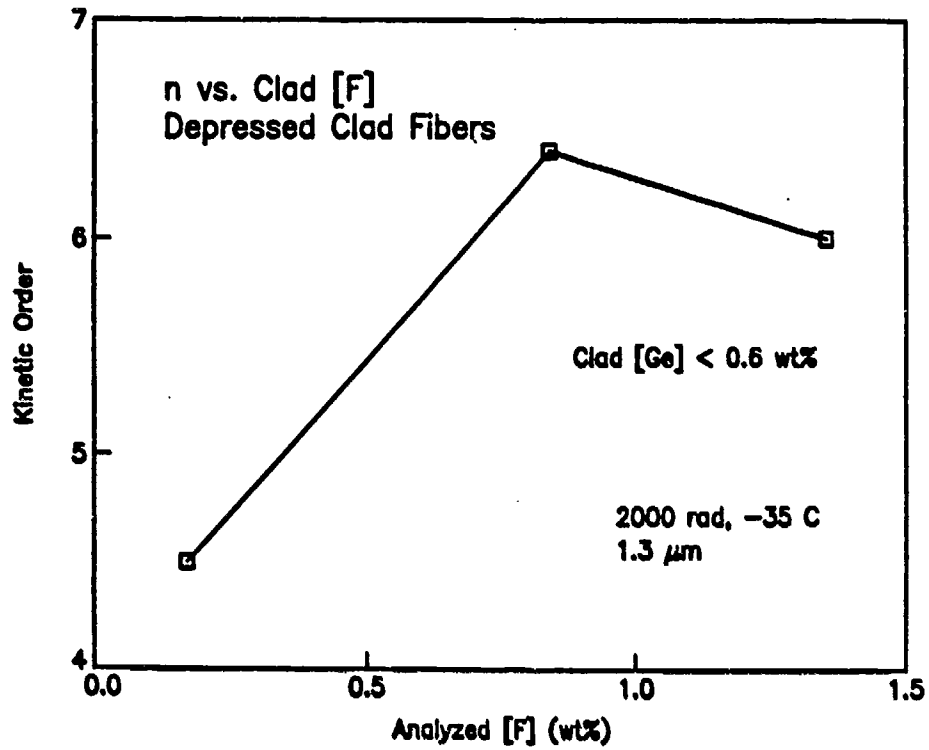


Figure 5.4. Effect of flucrine doping in the clad on  $n$  and  $\tau$ . The points correspond to fibers 26, 29 and 30 (see Table 5.1).

## CHAPTER 6

### RESPONSE-FABRICATION CORRELATIONS

It is clear from the statistical analysis of the Phase I data described in Chapter 3 that there are correlations between fabrication factors and the 1.3  $\mu\text{m}$  radiation response of matched clad single mode fibers. However, the confounding in the Phase I design and the lack of replicates of any experiments have complicated their interpretation and limited their statistical significance. Nevertheless, the fundamental problems in such a study remain, i.e. how to obtain statistically-significant correlations that are unconfounded when there are multiple fabrication factors and when each successful experiment (fiber) requires a minimum of a week's intensive labor to fabricate. Once again, the solution is a factorial experimental design.

#### 6.1 EXPERIMENTAL DESIGN

In the Phase I program, both core and cladding fabrication factors were varied according to the non-orthogonal factorial design shown in Chapter 3. These included for the core: [Ge], and the oxygen-to-reagent ratio used during core deposition; for the clad: [Ge] and the appropriate amount of F codoped with the Ge to maintain the refractive index of the clad identical to that of the silica substrate tube, and the oxygen-to-reagent ratio used during clad deposition; and draw speed and draw tension.

Since the largest fraction (~80-90%) of the light transmitting a single mode fibers is guided in the core, with only a small fraction carried in the clad as an evanescent field, it is to be expected that variations in fabrication factors of the core would have the most effect on radiation response. In addition, the only difference between the materials used for the clad and core is the fluorine doping used in the former to maintain index matching. Although the results discussed in Chapter 5 have shown that excess F doping above that required for a matched clad index has a deleterious effect

on recovery, if the clad composition is maintained constant throughout the study, its effect on the radiation response of the fiber is expected to be constant.

In the Phase I program, 6 different fabrication factors were varied; of these 3 were varied over 3 levels and 3 were varied over 2 levels. A complete experiment varying one factor at a time would have required the fabrication and measurement of  $3^3 \times 2^3 = 216$  fibers. As described in Chapter 3, the reduced design of 16 fibers was not orthogonal, which resulted in confounding of two-way interactions with main effects and other two-way interactions.

It was apparent from Phase I results that there might be two-way interactions which would have a significant effect on the fibers' radiation response. To fully reveal these without confounding, a rigorous experimental design was required. If we chose to vary the same 6 parameters as in Phase I over 2 levels in a full  $2^6$  experiment, 64 fibers would have to be made and measured. Alternatively, a half-replicate of the  $2^6$  design (i.e. 32 fibers) would reveal all main effects and two-way interactions without confounding.[1]

A second problem with Phase I was the lack of any replicates of the fibers, which limited the statistical significance of the correlations. Thus, it was decided that the Phase II design should incorporate 2 replicates of each experiment. To keep the number of fibers within reasonable limits, only the following fabrication factors would be varied: core [Ge], oxygen-to-reagent ratio used during core deposition, draw tension and draw speed, since the effect of clad dopants had been thoroughly elucidated in the one-dimensional studies described in Chapter 5. Each factor was varied over 2 levels, resulting in the  $2^4$  design shown in Table 6.1. Unfortunately, in a half-replicate of a  $2^4$  design, there is confounding among the two-way interactions and main effects, so a full design of 16 different fibers was required. Two replicates of each fiber were fabricated and measured to increase statistical significance.

**6.1.1 Levels of the Core Factors.** The levels for the fabrication factors in the Phase I design, shown in Table 3.1, were chosen to encompass as wide a variation as possible so that any potential correlation between fabrication and radiation response might be revealed. In addition, commercial fiber

fabrication would fall within the range of parameters studied. In some cases this strategy proved to be extreme: (1) fibers fabricated with level 1 core [Ge] = 6.5 wt% were poorly-guiding and suffered considerable microbend loss; and (2) deposition of core and clad with an oxygen-to-reagent ratio of only 5 was quite difficult, resulting in poor Ge incorporation and fibers that were clearly oxygen-deficient. Although the correlation between  $A_o$  and core [Ge] and was found to be statistically significant and unconfounded with two-way interactions in the Phase I study, most of the effect occurred between the first and second levels of core [Ge], i.e. between 6.5 and 10 wt%. Since the statistically significant and unconfounded correlation between  $A_f$  and core  $O_2/R$  was revealed in a 2 level experiment, it was unclear whether the effect occurred uniformly between  $O_2/R = 5$  and 15 or was confined to a lower range of  $O_2/R$ .

Table 6.2 shows the levels of the Phase II fabrication factors, which were chosen to relate this experiment with Phase I. Core [Ge] in Phase II varied over the second and third levels of Phase I, i.e. 10 and 14 wt%; the lower core  $O_2/R$  level of 7 in Phase II allowed fabrication of fibers which were not oxygen-deficient, while  $O_2/R = 15$  was the second level of Phase I; the two Phase II levels of draw tension were the first and third levels of Phase I; but the second level of draw speed in Phase II was limited to 2 m/s by the available draw tower, as described below. The range of levels shown in Table 6.2 encompasses typical commercial telecommunications fibers, with the possible exception of level 2 of draw speed.

**6.1.2 Levels of the Clad Factors.** The clad composition for Phase II was chosen to avoid some of the problems which became evident in Phase I and the one-dimensional study described in Chapter 5. First, phosphorus doping was *not* considered because the lack of recovery of the incremental loss would likely mask any effect of varying core fabrication factors. Few, if any, commercial fiber manufacturers continue to use P-doping in the clad, both because of the deleterious effect on the radiation damage and the additional intrinsic loss which P-doping causes. As before, fibers selected with consideration for the incremental loss in a radiation environment *should not* have any P-doping in the clad.

Phase I demonstrated that fibers with pure silica clads could be considered to be a separate class. Although there was a clear correlation of  $A_0$  with clad [Ge], virtually all of the effect was isolated to the contrast between the first and second levels, i.e. between 0% (pure silica) and 2.4 wt% Ge. Likewise, the one-dimensional study of Chapter 5 showed that doping the clad with even the slightest amount of Ge drastically reduced  $A_0$ . The recovery parameters  $n$  and  $\tau$  were consistently smaller in pure silica clad fibers than in those with Ge-doped clads. Once again, the response of the silica clad would dominate effects of varying core fabrication factors. Thus, the clad chosen for Phase II consisted of Ge-F-doped silica with [Ge] = 2.4 wt% (level 2 of Phase I) deposited with  $O_2/R = 10$  (level 2 of Phase I).

## 6.2 PREFORM FABRICATION

The preforms were fabricated using the NRL MCVD apparatus described in Chapter 2 according to the experimental design shown in Table 6.1 using as target values the Ge dopant concentrations and  $O_2/R$  values shown in Table 6.2.

While preform dopant concentrations influence radiation effects in fibers, their primary role concerns the design of a particular waveguide. The dopant levels selected for this study were bounded by the requirement that the refractive index of the clad be matched to that of the silica substrate tube, that the fibers be single mode at an operating wavelength of 1.3  $\mu\text{m}$  and the outer diameter could range from only 110  $\mu\text{m}$  to 135  $\mu\text{m}$ . These relatively strict constraints necessitated precise control and determination of clad to core diameter ratios, [Ge] and [F] in the clad and [Ge] in the core.

**6.2.1 Reagent Transfer.** The process of germanium and fluorine incorporation into silica glass by the MCVD process can be broken down into two steps. The first involves entrainment of the dopants into a gas stream, while the second concerns the subsequent reaction mechanisms of the reagents in the hot zone.



Delivery of fluorine into the gas stream is achieved by directly controlling and monitoring the mass transport rate of  $\text{SiF}_4$  gas from a pressurized cylinder during the deposition process. Because Ge is delivered by vaporization of  $\text{GeCl}_4$  source liquid into an  $\text{O}_2$  carrier gas flow, control must be achieved by monitoring and controlling all variables determining vaporization conditions. These include bubbler temp, carrier oxygen flow and bubbler liquid level.

Transport of  $\text{GeCl}_4$  vapor is achieved by flowing carrier oxygen through a glass frit submerged in a "bubbler" containing liquid  $\text{GeCl}_4$ . As the oxygen bubbles rise through the liquid, saturation of the carrier gas by the reagent vapor occurs at a rate determined by temperature, transit time and the equilibrium partial vapor pressure of  $\text{GeCl}_4$ . Small temperature variation results in galactic-scale drift in the amount of vapor transported. For this reason, the temperature of the liquid chemicals are allowed up to 24 hours to equilibrate before beginning deposition. If the time for the bubbles to rise through the liquid exceeds that required for saturation, delivery of the reagent vapor will be linear with carrier flow. As a precaution against incomplete saturation, the maintenance of a constant reagent depth was practiced after observing decreased deposition rates as the bubbler contents were consumed.

**6.2.2 Glass Deposition.** Once the reagents have been entrained into the gas stream, reaction kinetics and chemical equilibria govern the formation rate and composition of the glass particulate in the hot zone of the torch. The deposited glass composition continues to evolve through sintering of the particulate deposit into dense glass, the deposition of subsequent layers, and the final collapse of the preform tube into a rod. Detailed discussions of MCVD deposition kinetics are available as works published by several authors,[2,3] however a brief description of two specific processes are included here.

The incorporation of fluorine, which lowers the index of the glass, is proportional to the square root of  $\text{SiF}_4$  flow, but is relatively independent of other variables such as deposition temperature,  $\text{GeCl}_4$  flow,  $\text{SiCl}_4$  flow and additional flow of oxygen. For these reasons  $\text{SiF}_4$  is

considered to be among the most convenient index modifying chemicals utilized in the MCVD process.

**6.2.3 Index Calibration.** In contrast, the deposition of  $\text{GeO}_2$  molecules to raise the core index by forming Ge-doped silica is a complex function of all the above mentioned variables.[3] To determine the effect of oxygen stoichiometry in the gas flow on germanium incorporation efficiency, all deposition variables were held constant with the exception of oxygen flow; i.e., the stoichiometry was varied. Relating this dependence to our equipment was accomplished by generating data points for a calibration curve. Several preforms were fabricated in which the oxygen stoichiometry was varied while all other parameters were held constant.

Once the [Ge] and  $\text{O}_2$  stoichiometries were chosen for the claddings of the preforms of the one-dimensional study described in Chapter 5, a calibration preform was fabricated to determine the proper  $\text{SiF}_4$  flow required to achieve a cladding index matched to the silica substrate tube. Values of [Ge], [F] and  $\text{O}_2/\text{R}$  used in Phase I claddings were adopted for Phase II preforms both for continuity between the data sets, and to obviate the need for additional cladding calibration experiments. However, core parameters for Phase II preforms were sufficiently different to require additional calibration experiments similar to those for defining cladding levels.

After the deposition and collapse of a preform, only destructive elemental analysis can evaluate [Ge] in the cladding region due to the presence of F as a co-dopant to obtain index matching. On the other hand, core [Ge] can be determined simply by measuring the refractive index difference between the core and a known reference, i.e. the  $\text{SiO}_2$  substrate tube. An empirical, linear function relating index change  $\Delta n$  to [Ge] (expressed as wt%  $\text{GeO}_2$ ) was derived by correlating scanning electron microprobe data with preform index profiles performed on the Phase I samples. (See Chapter 3 of the Phase I final report.) Because all preforms are matched clad (relative core index and  $\Delta n$  are identical), Eq. 6.1 may be used to relate  $\Delta n$  to wt%  $\text{GeO}_2$  in the core:

$$\Delta n \times 10^3 = 0.85[\text{GeO}_2] - 1.1. \quad (6.1)$$

The target values for the fiber dimensions were chosen for single mode operation at 1.3  $\mu\text{m}$ , with an outer diameter of 120  $\mu\text{m}$ . By setting the cutoff wavelength (described in Fiber Characterization) near 1.2  $\mu\text{m}$ , operation is guaranteed to be single mode at 1.3  $\mu\text{m}$ . Eq. 6.2 relates the cutoff wavelength  $\lambda_{\infty}$  to the core radius  $a$ , the normalized waveguide index  $V$  (2.4 for single mode) and the numerical aperture NA.

$$\lambda_{\infty} = \frac{2\pi a NA}{V} \quad (6.2)$$

The NA describes the acceptance angle of the fiber in terms of the core and cladding indices  $n_1$  and  $n_2$  as shown in Eq. 6.3.

$$NA = \sqrt{(n_1^2 - n_2^2)} \quad (6.3)$$

The target core [Ge] is converted by Eq. 6.1 to an estimated index so that the NA can be calculated from Eq. 6.3. The required core radius is then derived from Eq. 6.2, and the dimensions of cladding and core dimensions to be generated by MCVD are thereby determined so that an acceptable 120  $\mu\text{m}$  fiber may be drawn. For example, a 120  $\mu\text{m}$  diameter fiber with level 1 [Ge] in the core (10 % by equation 6.1 requires a core index step of 0.0075, and results in an NA of 0.151 and a core diameter of 6.1  $\mu\text{m}$ . Arrival at the appropriate clad-to-core ratio was accomplished by successive trials until the fiber displayed the correct waveguiding characteristics.

Tables 6.3 and 6.4 contain a summary of the preform deposition parameters used in fabricating preforms for both the one-dimensional study of clad effects described in Chapter 5 and the 2<sup>4</sup> orthogonal design with replicates described above. Since 4 preform designs were required for the 16 different fibers, i.e. each preform was drawn using 4 different pairs of draw speed and tension, the preform number is taken as that of the first fiber of each set. The replicates are indicated by the letters A and B. Note that in spite of the fact that there was no intentional deposition of F into the

fiber core, low levels of F are invariably present due to diffusion from the clad and the final etch pass during preform collapse, which uses Freon to remove the layers of core that have become depleted in Ge.

### **6.3 FIBER DRAWING AND MEASUREMENTS**

**6.3.1 In-House Draw Facility.** Preforms produced for determining the optimal cladding dopant levels were drawn on the NRL silica draw tower at the maximum attainable draw rate of 30 meters per minute (0.5 m/s). This upper limit is determined by the time required for the fiber to convectively cool to below the boiling point of the epoxy acrylate coating as the fiber transits the distance from the 2000 C furnace to the coating applicator. On the existing silica draw tower this distance is quite short. However, the future inclusion of a refrigerated-gas flow tube to provide forced-air cooling or drawing on the taller tower in Building 215 will result in significant increase in the maximum draw speed. In all other aspects, the tower accurately reflects the characteristics of industrial towers by the use of a noble-gas-passivated graphite resistance furnace, UV-cured acrylate jacketing application, and closed-loop dimensional control. Additional accessories provide closer monitoring of the process than that available in large scale fiber draw factories (e.g. pyrometer control of furnace temperature vs. current control, and real-time non-contact draw tension measurement).

All preforms at each stage of the study were drawn under conditions kept as identical as possible through extensive monitoring and rigorous procedure. The purging atmosphere of the furnace is routinely dried well below one ppm water, and furnace temperature does not deviate more than one degree from setpoints near 2100 C. The extremities of each preform were excluded from the sample set to preclude irregularities such as deposition taper and altered thermal history where the silica extension handle was welded to the preform proper. The initially-drawn region served to allow precise centering of the fiber in the coating applicator, tuning of the preform feed rate to effect the desired diameter at the target speed, and stabilization of tension, which is a function of both draw speed and temperature. As the central region of the preform reached the hot zone center, a section

of fiber was taken off-line to measure its second-mode cutoff wavelength  $\lambda_{\infty}$  as in Eq. 6.2, thereby exactly determining the required outer diameter. Final stabilization at the indicated setpoints was attained, actual values of speed, tension, diameter and temperature were noted, and the sample section was marked as it wound onto the take-up spool. During the generation of the sample section, tension and speed were recorded, and the controls fine-tuned to maintain the target values. Draw speed was maintained at 30 meters per minute  $\pm 1$  m/min, and the normalized tension was held to within  $\pm 10\%$ . If samples with different values of tension and/or speed were to be generated from a single preform, the transition between settings was intentionally rapid to minimize potential effects due to material variation along the length of the preform. For preforms averaging 17 mm in diameter, 300 m of fiber drawn between successive stabilized setpoints corresponds to an approximately 12 millimeter separation along a 300 mm, nominally uniform section. Not less than 200 meters of each fiber sample was drawn to allow good precision in subsequent characterization testing, and to allow sufficient material for multiple irradiations, as needed.

**6.3.2 Off-Site High Speed Fiber Drawing.** Results from Phase I of the program indicated that contrasting radiation sensitivity against draw speed would require a range of draw speeds not less than 30 - 120 m/min (0.5-4 m/s). Because of the speed limitation of the NRL draw tower (30 m/min), a contract was arranged with Heathway, Inc. in Horsham, Pennsylvania for the use of a tower tall enough to draw fibers at more than 120 meters per minute. Over the course of three separate visits, their tower was upgraded and fitted with our instrumentation, and preforms from the 2<sup>4</sup> experimental design table of Phase II were drawn into fibers at the requisite pairs of two normalized tensions and two speeds.

The condition of the Heathway tower did not satisfy the rental contract at the time of the first visit. Although a capacity for drawing at 240 meters per minute was specified and agreed upon, only after extensive refitting and improvisation was the tower capable of the minimally acceptable value of 120 m/min. Several days were consumed in rearranging components to allow a longer cooling path, diagnosing extensive erosion of the furnace's graphite components, supplementing the existing UV

curing capacity with a lamp driven up from NRL to enable high speed coating, and jury-rigging a coating concentricity monitor to replace the ineffectual commercial version.

After installing additional custom instruments, test rods of silica were drawn to determine specific temperature setpoints for the matrix of two speeds and two tensions. These values needed to be determined before drawing the actual sample preforms so that useful preform material would not be consumed during the often lengthy calibration sequences. From the results, an efficient sequence of varying furnace temperature, testing cutoff wavelength, and stabilizing diameter and speed was derived so that the requisite four distinct samples derived from the two levels each of draw speed and tension could be produced from the useable section of preform. Subsequent sessions at the rental site resulted from a need to refabricate three preforms when either the indicated diameters for satisfying the cutoff wavelength requirement exceeded acceptable limits, or when surface contamination had weakened the fiber.

**6.3.3 Fiber Characterization.** The nominal desired diameter for drawing optical fibers is estimated from profiling the preform's refractive index and structural dimensions, but accurate waveguide parameters and intrinsic loss values may only be ascertained from direct analysis of the fiber. Before the radiation response of any fiber was measured, several properties of the fiber were evaluated for assurance that the quality of the sample compared well with commercial products, and that no obvious variances existed which could cloud comparisons between the samples. A further measurement served to determine the relative importance of loss mechanisms existing at different radii from the fiber axis. Three tests were performed using the Photon Kinetics FOA-2000 Optical Fiber Analyzer acquired since Phase I of the project: intrinsic spectral attenuation, second-mode cutoff wavelength, and mode field diameter. The same Optical Time Domain Reflectometer (OTDR) made by Laser Precision was used in both Phase I and Phase II. Values for fiber dimensions, selected attenuation values and waveguide properties appear for the fibers produced and evaluated in this study in Table 6.5.

**6.3.4 Intrinsic Spectral Attenuation.** The ability of an optical fiber to guide injected light over hundreds of kilometers with losses far below those of any other transmission medium is the

fundamental justification for the technology. Length-dependent transmission loss in optical fibers is an involved function of the frequency of the guided signal. A plot of transmission loss over a range of optical wavelengths gives a detailed and precise description of the material and waveguide properties of the fiber, and it serves to expose any variations which could confuse comparisons of the measured response to radiation in these experiments. A representative loss spectrum measured by the cutback method for one of the fibers from the study (Fig. 6.1) demonstrates the loss mechanisms characteristic of telecommunication fibers. The information plotted is computed from the difference in the amount of light transmitted from a white-light source and scanning monochromator to a detector first through a long (known) length of fiber, and then through a short length of the same fiber. The length-dependent attenuation  $A(\text{dB/km})$  is calculated from the length  $L$  in kilometers, and the sets of transmitted and detected power values at each wavelength through the short length  $I_{\lambda_s}$ , and the long length,  $I_{\lambda_l}$ :

$$A(\text{dB/km}) = -10 \log ( I_{\lambda_l} / I_{\lambda_s} )/L. \quad (6.4)$$

To avoid errors in the measurement due to changing the amount of light launched into the respective lengths, values for the transmitted power through the long length are first recorded, then a break is introduced a short distance from the launch end. The new end is positioned in front of the detector, and the resulting section becomes the short cutback reference length. By not disturbing the launch end, exactly identical amounts of power are injected in both cases. Only a length-dependent difference remains between the two data sets.

In the representative spectrum shown in Fig. 6.1, two strong features near 1.1 and 1.4  $\mu\text{m}$  rest atop a smooth background, which evidences the fundamental material properties limiting the transparency of Ge-doped silica glass: Rayleigh scattering, contributing strong loss at short wavelengths, and the multi-phonon edge, limiting transmission at long wavelengths. If the only scattering sites are density and compositional fluctuations on a scale determined by thermodynamic equilibrium (typically  $\ll 50$  nm), long wavelength light is scattered less than shorter wavelengths with a power law dependence,  $A \propto \lambda^{-4}$ . The desired appearance of this component of loss due only to

Rayleigh scattering is evident in Fig. 6.1 with the background smoothly decreasing from its largest plotted value at  $0.8 \mu\text{m}$ . A large positive offset with little dependence on wavelength would indicate the presence of large scatterers, such as bubbles, inclusion of foreign matter, or sharp fluctuations in the dimensions of the waveguide. Any such evidence would disqualify the sample from consideration or further investigation of radiation effects. The constancy of this scattering mechanism for a given glass system is employed in another measurement (OTDR) discussed below.

The less evident long-wavelength loss mechanism (apparent only as an increase in loss of  $\sim 0.4 \text{ dB/Km}$  from  $1.6$  to  $1.7 \mu\text{m}$ ) reflects the ability of the molecular structure of the glass network to vibrate with energies that correspond to the energy of photons with sufficiently long wavelengths. The pronounced absorption of photons at sufficiently long wavelengths and dissipation into vibrations of the glass lattice is termed the multiphonon absorption. The theoretical total loss due to summing Rayleigh scattering and the multiphonon edge exhibits a minimum of  $\sim 0.15 \text{ dB/Km}$  near  $1.55 \mu\text{m}$ . If the measured loss of a fiber sample greatly exceeds this minimum, excessive loss mechanisms are present, and the sample section is rejected. Loss results at the design wavelength of  $1.3 \mu\text{m}$  for fibers of the Phase II study appear in Table 6.5.

The sharp feature of Fig. 6.1 at  $1.38 \mu\text{m}$  indicates the optical absorption due to the second harmonic of the OH vibration at  $\sim 2.8 \mu\text{m}$  in silica. The inclusion of only 1 ppm of "water" in the form of OH contributes a  $40 \text{ dB/km}$  loss at  $1.38 \mu\text{m}$ , and  $\sim 12$  and  $9 \text{ dB/Km}$  at  $1.25$  and  $0.95 \mu\text{m}$  respectively. The additional  $2.7 \text{ dB/km}$  indicated for this sample corresponds to  $<100 \text{ ppb}$ , which is typical for today's telecommunications fibers. Early studies relating water content to details of radiation response in pure silica multimode fibers compared "wet" silica ( $>100 \text{ ppm OH}$ ) to "dry" fibers containing 1 or 2 ppm. For this study, OH contents well below  $0.5 \text{ ppm}$  ( $<20 \text{ dB/km}$  at  $1.38 \mu\text{m}$ ) is assumed to be irrelevant to radiation response. The OH content for each fiber in the study is shown in terms of additional loss at  $1.38 \mu\text{m}$  in  $\text{dB/km}$  in Table 6.5.

The broad feature around  $1.1 \mu\text{m}$  in the spectrum in Fig. 6.1 is unrelated to any material effects, but it is due instead to the waveguiding properties of the fiber and the nature of the loss



measurement. At the operational wavelength of a single-mode fiber, only one solution exists for the spatial power distribution of the light (for a given polarization state); this solution is called the lowest-order guided mode. Higher modes are not sufficiently guided by the index structure of the fiber, and are therefore lost after a relatively short length. At significantly shorter wavelengths, more than one mode *is* supported, and at sufficiently long wavelengths, *no* modes can be guided over an appreciable distance. The spectral feature noted here results from both second and first modes propagating through the short (~ 1 meter) cutback length below 1.2  $\mu\text{m}$ . The second mode suffers nearly complete extinction after propagating through the original longer length at wavelengths  $>1.0 \mu\text{m}$ , and the short and long length difference constitutes the feature shown. The longest wavelength where there was evidence of optical power traversing the short length (~1.19  $\mu\text{m}$  in the figure) is termed the "second mode cutoff wavelength". The physical origins of cutoff involve the numerical aperture NA (a measure of the relative indices of the core and cladding, see Eq. 6.3), core radius  $a$ , wavelength of the measurement  $\lambda$ , and a normalized waveguide index  $V$  (~2.4 for single-mode), as shown in Eq. 6.2. Once the preform has been fabricated, the wavelength set to 1.3  $\mu\text{m}$  and  $V = 2.4$  for single mode operation, only the core diameter is accessible for variation. Because the ratio of core and outside diameter is constant for a give preform, the overall diameter of the fiber is adjusted during draw to place the cutoff wavelength as desired, with confirmation provided by testing with a specialized rapid measurement instrument during the draw process.

In fibers operated at just greater than the cutoff wavelength, the single-moded power is highly confined in the fiber core and is insensitive to loss due to bending or stressing of the fiber such as is induced by installation in real-world environments, or by the handling and configuring necessary for measuring the effect of exposure to radiation during this project. At wavelengths far from cutoff, spurious loss confuses the data with long term drifting or excessive noise during necessary motion of the sample or as the fiber wound on a spool relaxes and microbends.

Should the fiber be operated at a wavelength below cutoff, the signal is compromised of both the second mode susceptibility to bending loss, and interference of the laser signal with itself through

propagation and recombination of the different optical paths constituted by each mode. A subtler complication also arises when evaluating radiation-induced loss with multiply moded light in a nominally single-mode fiber. The glass volume illuminated by different modes varies in the degree to which each mode interacts with the core and cladding regions. The lowest mode is centered on the fiber axis, and the mode field diameter (described below), completely describes the relative overlap of the optical power with each fiber region. The power distribution of higher order modes can vary significantly along the length of a bent or strained fiber. A study which would resolve the contribution of loss mechanisms originating in a particular region of the fiber requires an unambiguous knowledge of the relative amounts of signal propagated in each region. Because the selected wavelength for operation was  $1.3 \mu\text{m}$  throughout the study, the fibers were screened to have a cutoff wavelength near, but less than,  $1.3 \mu\text{m}$ . Explicit measurements of cutoff wavelength are tabulated for the experimental fibers in Table 6.5.

Incorporation of impurities such as transition metals is detectable as broad absorption bands in the visible to near-IR. The presence of these spectral features distort the background described above, and indicates the possibility of complicating effects on radiation response. The presence of ppm-concentrations of metals such as iron, nickel or cobalt results in prominent losses over the hundred meter lengths of the samples. The absence of features other than modal loss or water absorption peaks in the studied fibers obviates any concern over the role of these impurities.

**6.3.5 Mode Field Diameter.** The lowest order optical mode propagates in a fiber with the highest intensity along the center axis of the core of the circular optical waveguide and decreases exponentially as a function of the distance from the axis. A significant fraction of the power extends into the cladding material as an evanescent wave. As a result, attenuation of light in a fiber occurs by loss mechanisms in both core and cladding, with relative contributions proportional to the amount of light in each of the regions. For the 2<sup>4</sup> experimental design the radiation sensitivity of a set of fibers with identical claddings was compared as only the core parameters were varied. By knowing the contribution to optical loss of the cladding, the loss due to core-localized mechanisms may be

separated once the fraction of optical power in each region is known. Based on the concept that the lowest order guided mode of a simple cylindrical dielectric waveguide (e.g., a matched-clad fiber) has a simple and well-defined radial power distribution, the intensity as a function of radius can be measured and employed to determine the core/cladding power ratio. The Photon Kinetics FOA-2000 fiber analyzer performs the measurement, and produces a result called the "mode field diameter" (MFD). This value indicates the distance in  $\mu\text{m}$  from the fiber axis where the optical intensity falls to  $1/e^2$  of the peak, central value. By fitting this number to a Gaussian approximation of the power distribution and then integrating inside and outside of the known core radius, the power fractions in core and cladding can be calculated. The results of the MFD measurement and the core power fraction calculation appear in table 6.5.

**6.3.6 Optical Time Domain Reflectometry.** Variations in either waveguide properties or loss mechanisms along the length of a fiber may result from anomalous material characteristics capable of skewing the results of the comparative study. Because components of the net loss in a fiber simply add together as the total loss at a wavelength, the cutback method of measuring attenuation is incapable of sensing length dependent variation. Optical time domain reflectometry (OTDR), an optical instrument analogous to radar, utilizes the phenomenon of Rayleigh backscatter to generate a graphical representation of loss as a function of position along a fiber. A short optical pulse ( $\sim 20$  ns) is launched into the fiber, then the backscattered signal ( $\sim 1$  ppm of the forward power) returned to the same end of the fiber is recorded versus time. Since a laser is typically used to launch the pulse, OTDR measurements are limited to specific wavelengths. The logarithm of the returned signal plotted against time reveals a profile of loss per length (as indicated by local slope) along the fiber. Discontinuities such as breaks or bends and regions of high loss may then be avoided when sample lengths are selected. Although such gross faults are rarely encountered, uniformity in the experimental sample set is further assured.

An example OTDR trace presented in Fig 6.2 shows three distinct regions: The left most edge to just before cursor A represents signal backscattered from a lead-in fiber, then the sudden rise

indicates reflection from an oil-matched butt-coupling to the sample. From cursor *A* to *B* the signal from the sample falls by 0.16 dB over a distance of 0.301 km for a loss at 1.3  $\mu\text{m}$  of  $<0.6$  dB/km. After *B* the trace goes off screen where the reflection from the end of the sample saturates the detector. Of particular importance is the lack of features over the length of the sample, indicating no local loss anomalies greater than 0.025 dB.

## 6.4 IRRADIATIONS

The Phase II fibers were irradiated in the  $^{60}\text{Co}$  pool to a total dose of 2500 rad at a dose rate of  $\sim 3500$  rad/min. The increase in optical attenuation at 1.3  $\mu\text{m}$  was monitored *in-situ* during the exposure and for approximately  $10^4$ - $10^5$  sec following removal of the fibers from the source. The fibers were maintained at  $-35$  C, and 1  $\mu\text{W}$  of optical power was transmitted during the exposure and recovery. Two fibers were irradiated simultaneously, and as described in Chapter 2, to minimize the effects of fluctuations in laser power, a small amount of the injected light was used as a reference. The output of each fibers was ratioed to the reference channel. In other respects the test procedure conformed that developed by the NATO Nuclear Effects Task Group.[4]

A typical set of raw data is shown in Fig. 6.3. The experiment begins  $\sim 60$  min after the fibers have reached  $-35$  C and variations in transmitted power due to thermal effects have ceased. The initial data acquisition,  $\sim 30$  s in this case, is the baseline, which is slightly offset from zero; this offset will be subtracted from the growth and recovery data. The fiber is inserted into the source at 30 s, and the radiation-induced loss increases monotonically until it is removed,  $\sim 100$  s. The recovery data from  $10^2$  to  $3 \times 10^4$  s show good stability; there is a slight amount of instrumental drift at longer times. Much of the noise evident on the recovery data is simply the digitizing steps. These recovery data are then extracted from the raw data, and the point at which the fiber has been removed from the source is set to  $t = 0$ . For convenience, a limited number of data points are extracted from the recovery data, as shown by the points in Fig. 6.4.

Each set of recovery data has been fit to the equation for  $n^{\text{th}}$  order kinetic recovery described by Eq. 3.3. A typical fit of the recovery data is shown as the solid line in Fig. 6.4. It is apparent that the agreement between data and theory is quite good, and the recovery can be described satisfactorily by the four recovery parameters:  $A_0$ ,  $A_f$ ,  $n$  and  $\tau$ .

Table 6.6 contains the complete set of recovery parameters for the fibers of the  $2^4$  experimental design. There is good agreement between the two replicates for each experiment, with the exception of the values for  $A_f$ ,  $n$  and  $\tau$  for #37 and #38. Unfortunately, the data of #37B and #38B contained a substantial amount of drift, which prevented a confident fit to Eq. 3.3 and adequate determination of  $A_f$ ,  $n$  and  $\tau$ . These fibers were irradiated a second time, but the drift and noise problems were equally bad. Because of insufficient length, a third irradiation was not attempted. However, the raw data of #37A and #38A were quite good, as shown for #37A in Fig. 6.4.

## 6.5 ANALYSIS OF DATA

As in the case of the Phase I data described in Chapter 3, the PC version of Multivariate was used to perform MANOVA on the fabrication factors and radiation response parameters on the 30 fibers of Phase II shown in Table 6.6. The data of fibers 37B and 38B were discarded because of excessive drift and noise, but in spite of the lack of replicates of these two fibers, the MANOVA revealed a high degree of association between fabrication factors and radiation response parameters, as described below. The initial analysis involved main effects, two-way, three-way, and four-way interactions. However, the significance of the three-way and four-way interactions was negligible, so the degrees of freedom associated with them was pooled with the error term for subsequent analyses. A summary of the probabilities of no effects of the factors showing statistical significance is contained in Table 6.7.

$\Delta_0$ . The main effect of  $A_0$  on core [Ge] is highly significant with a probability of no effect  $p < 0.0001$ . This result substantially strengthens the same conclusion of the Phase IA study described in Chapter 3, where  $p < 0.05$  for the first contrast of core [Ge] between 6.5 and 14% (Table 3.11). In

Phase II, the contrast in core [Ge] is between 8.5 and 15 wt%, but the effect of the second contrast of [Ge] in Phase I between 10 and 14% was *not* significant with  $p < 0.45$ , as shown in Table 3.11. Although one conclusion from comparing the Phase I and II results is that the significant effect falls between core [Ge] = 6.5 and 8.5%, it seems reasonable that the lack of significance of the  $A_2$ - $A_3$  contrast in Phase I is due to confounding with two-way interactions, as shown in Table 3.5.

The substantially increased significance of  $A_0$  on core [Ge] in Phase II is due to the improved, unconfounded experimental design and the replicates of all but two fibers. Note that a preliminary analysis of the Phase II data using just one replicate of each design yielded  $p < 0.0005$  for  $A_0$  on core [Ge].

Although the only significant main effect on  $A_0$  was of core [Ge] in Phase IA, the rigorous  $2^4$  experimental design has revealed additional main effects of core oxygen-to-reagent ratio and draw speed on  $A_0$ , and two-way interactions of draw speed-draw tension and, to a lesser extent,  $O_2/R$ -draw speed with  $A_0$ , as shown in Table 6.7. With the exception of the  $O_2/R$ -draw speed interaction, all are significant within the conventional criterion of  $p < 0.05$ . The significance of the latter is nominal and may be only a reflection of the significant main effects of  $O_2/R$  and draw speed individually.

$A_f$ . The multivariate analysis of the Phase II showed no correlation between  $A_f$  and core  $O_2/R$ , in marked contrast to Phase I where  $p < 0.09$  for the main effect of core  $O_2/R$  on  $A_f$ . There,  $A_f$  decreased with increasing  $O_2/R$  from 5 to 15 (Table 3.11). However, the two results are not inconsistent since different levels of core  $O_2/R$  were used in Phase II, i.e. 7 and 15. Apparently, all the decrease in  $A_f$  occurs on increasing  $O_2/R$  from 5 to 7 with no effect of further increase.

As shown in Table 3.11, the Phase II design has revealed a statistically significant two-way interaction of core [Ge]-draw tension on  $A_f$ , which was not evident in Phase I because of confounding.

$n$ . The main effect of core  $O_2/R$  with  $n$  and draw speed with  $n$  were found to be significant with  $p < 0.10$  and  $p < 0.13$ , respectively, and the two-way interaction of core  $O_2/R$  and draw speed with  $n$

had  $p < 0.14$ . (Since the sample population is small we relax the criterion for statistical significance to  $p \sim 0.1$ , as was done in the prior study.) Whether the two-way interaction is significant is marginal and may be simply a reflection of the presence of the two main effects. In contrast, analysis of the Phase I data resulted in probabilities for the two main effects of 0.66 and 0.39, respectively. However, it was concluded that the two-way interaction of core  $O_2/R$  and draw speed on  $n$  was significant because  $p$  was relatively small ( $< 0.21$ ). The present work, where the experimental design was rigorous, clearly shows a significant effect of both the main effects and two-way interactions on  $n$ .

**1.** A significant effect of core  $O_2/R$  on  $\tau$  was found with  $p < 0.14$  vs.  $p < 0.43$  in Phase I. The two-way interaction of core  $O_2/R$  and draw speed on  $\tau$  found in Phase I was not significant in Phase II. A possible origin for this discrepancy is the fact that in Phase I the draw speed levels were 0.5 and 4.0 m/s and the oxygen ratio levels were 5 and 15, as compared to 0.5 and 2 m/s and 7 and 15 in Phase II. It is possible that the significant effect occurs between draw speeds of 2 and 4 m/s and  $O_2/R$  of 5 to 7 or that the apparent significance of the two-way interaction in Phase I was due to confounding. It is reasonable to attach more credence to the present study since the design is more rigorous and there is no confounding of main effects and two-way interactions.

## 6.6 ESTIMATED EFFECTS

**A<sub>0</sub>** The estimated effect of core [Ge] on  $A_0$  is shown in Fig. 6.5; increasing [Ge] from 8.5 to 15% results in a decrease in  $A_0$  of 1.1 dB/km. By contrast, the estimated effects of the first and second contrast of core [Ge] between 6.5 and 14% and between 10 and 14% in the Phase I study were 7.3 and 1.2 dB/km, respectively. Thus, the present results are consistent with estimated effect between 10 and 14% from Phase I.

The estimated effects of the main effects of core  $O_2/R$  and draw speed on  $A_0$  are shown in Figs. 6.6 and 6.7. Increasing the oxygen-to-reagent ratio from 7 to 15 results in a decrease in  $A_0$  of 0.38 dB/km, and increasing draw speed from 0.5 to 2 m/s causes a 0.43 dB/km increase in  $A_0$ . The

two-way interaction of  $O_2/R$  and draw speed on  $A_o$  is shown in Fig. 6.8; it is apparent that increasing oxygen has little effect at slow draw speeds, while increasing draw speed has little effect on  $A_o$  if the core was deposited with high  $O_2/R$ . Obviously, high draw speed and low oxygen ratios should be avoided.

The estimated effect of draw tension and draw speed on  $A_o$  is shown in Fig. 6.9. If the fiber is drawn at low speed, a decrease in  $A_o$  occurs with increasing tension, while the opposite trend obtains at high speed.  $A_o$  is relatively insensitive to draw speed at low tension.

**$A_f$ .** The effect of core [Ge] and draw tension on  $A_f$  is shown in Fig. 6.10. Although the trend with increasing [Ge] is quite different depending on whether the fiber is drawn at low or high tension, it should be remembered that the error bars on the determination of  $A_f$  are  $\pm 0.075$  dB/km due to the fact that the long term stability of attenuation measurement apparatus is  $\pm 0.0037$  dB, and a 50 m fiber sample length is used. Although MANOVA revealed a significant interaction of core [Ge] and draw tension on  $A_f$ , determination of the estimated effect is problematic.

**$n$ .** The estimated effects of the fabrication factors on  $n$  are shown in Figs. 6.11-6.13. It is apparent that increasing core  $O_2/R$  from 7 to 15 increases  $n$  by 0.43, while increasing draw speed from 0.5 to 2.0 m/s decreases  $n$  by 0.38. As shown in Fig. 6.13, there is no effect of draw speed on  $n$  in fibers whose preforms are deposited with high  $O_2/R$ , and there is little effect of changing  $O_2/R$  on fibers drawn at 0.5 m/s. In contrast, there is a significant increase in  $n$  of 1.5 in fibers drawn at 2 m/s. Alternatively, the recovery of fibers deposited with low  $O_2/R$  is significantly enhanced if they are drawn at high speed.

**$\tau$ .** The estimated effect of core  $O_2/R$  on  $\tau$  is shown in Fig. 6.14. It is apparent that increasing the oxygen-to-reagent ratio from 7 to 15 results in an increase in  $\tau$  of 58 s.

Figures 6.5-6.14 show the significant effects of varying fabrication factors on the radiation response parameters. Obviously, the dependence is quite complex, and an analysis of the estimated effects in terms of optimizing the hardness of single mode optical fibers against the fallout radiation environment will be given in Chapter 7. However, it should be emphasized at this point that variation



in fabrication factors *does* affect the parameters critical for fallout hardness, i.e.  $A_f$ ,  $n$ , and  $\tau$ , so fiber designs can be optimized, hopefully without significantly increasing the cost or complexity of the fiber.

## REFERENCES

1. C.R. Hicks, *Fundamental Concepts in the Design of Experiments* (Holt, Rinehart and Winston, New York, NY, 1964).
2. W.G. French, R.E. Jaeger, J.B. MacChesney, S.R. Nagel, K. Nassau and A.D. Pearson, "Fiber preform preparation," *Optical Fiber Telecommunications*, S.E. Miller and A.G. Chynoweth, Ed. (Academic Press, New York, 1979), pp. 233-262.
3. D.L. Wood, K.L. Walker, J.B. MacChesney, J.R. Simpson and R. Csencsits, "Germanium chemistry in the MCVD process for optical fiber fabrication," *J. Lightwave Tech.* LT-5 (1987) 277-285.
4. NATO Panel IV, RSG 12, Nuclear Effects Task Group, "Procedure for measuring steady state gamma radiation-induced attenuation in optical fibers and optical cables," Report No. LA-UR-90-1901, P.B. Lyons, Ed. (Los Alamos National Laboratory, Los Alamos, NM, 1990).

Table 6.1 2<sup>4</sup> Experimental Design

N	Core [Ge]	Core O <sub>2</sub> /R	Draw Speed	Draw Tension
31	1	1	1	1
32	1	1	1	2
33	1	1	2	1
34	1	1	2	2
35	2	1	1	1
36	2	1	1	2
37	2	1	2	1
38	2	1	2	2
39	1	2	1	1
40	1	2	1	2
41	1	2	2	1
42	1	2	2	2
43	2	2	1	1
44	2	2	1	2
45	2	2	2	1
46	2	2	2	2

**Table 6.2 Core Fabrication Variables and Levels**

	<b>Factor</b>	<b>Level 1</b>	<b>Level 2</b>
<b>A.</b>	<b>Core [Ge]</b>	<b>8.5</b>	<b>15 wt%</b>
<b>B.</b>	<b>Core O<sub>2</sub>/R</b>	<b>7</b>	<b>15</b>
<b>C.</b>	<b>Draw Speed</b>	<b>0.5</b>	<b>2 m/s</b>
<b>D.</b>	<b>Draw Tension</b>	<b>20</b>	<b>80 g</b>

Table 6.3 Parameters Used in Depositing the Core of Matched Clad Single Mode Fiber Preforms and the Glass Composition (wt% Oxide) Determined by Electron Microprobe

Fiber	Preform	SiCl <sub>4</sub>		GeCl <sub>4</sub>		F	O <sub>2</sub>	He	Temp
		g/m	flows ccm	g/m	flows ccm	wt%	flow/p m	flow lpm	C
25	NRL901002	0.26	44	0.077	60	0	2.0	0.4	1970
26A	NRL900726	0.26	44	0.070	54	--	2.0	0.4	1950
26B	NRL900803	0.26	44	0.070	54	0.6	2.0	0.4	1960
27	NRL900928	0.26	44	0.084	65	2.0	2.1	0.4	1970
28	NRL900926	0.26	44	0.077	60	3.5	2.2	0.4	1940
29A	NRL901024	0.26	44	0.077	60	--	2.0	0.4	1960
29B	NRL901026	0.26	44	0.077	60	0.2	2.0	0.4	1960
30	NRL901030	0.26	44	0.064	50	0.3	2.0	0.4	1960
31A	NRL910206	0.26	44	0.122	95	2.0	2.1	0.1	1990
31B	NRL910320	0.26	44	0.122	95	2.0	2.1	0.1	2020
33A	NRL910213	0.26	44	0.174	125	1.7	2.1	0.2	1990
35B	NRL910215	0.26	44	0.181	140	1.9	2.1	0.2	1990
39A	NRL910416	0.26	44	0.077	60	2.0	2.1	0.4	1990
39B	NRL910417	0.26	44	0.077	60	2.0	2.1	0.4	1990
43A	NRL910212	0.26	44	0.116	90	2.0	2.1	0.4	1985
43B	NRL910219	0.26	44	0.116	90	1.7	2.1	0.4	1980

Table 6.4 Parameters Used in Depositing the Clad of Matched Clad Single Mode Fiber Preforms and the Glass Composition (wt% Oxide) Determined by Electron Microprobe

Fiber	Preform	SiCl <sub>4</sub>		GeCl <sub>4</sub>		SIF <sub>4</sub>		O <sub>2</sub>		He flow lpm	Temp C
		g/m	flow sccm	wt%	g/m	flow sccm	wt%	flow lpm	ratio		
25	NRL901002	1.5	245	106	0	0	0	2.0	10	0	1990
26A	NRL900726	1.5	245	--	0.025	20	--	2.0	10	0	1950
26B	NRL900903	1.5	245	99.2	0.025	20	0.17	2.0	10	0	1970
27	NRL900928	1.5	245	97.5	0.1	77	0.45	2.1	10	0	1970
28	NRL900926	1.5	245	95.6	0.18	146	0.78	2.2	10	0	1920
29A	NRL901024	1.5	245	--	0.025	20	--	2.0	10	0	2980
29B	NRL901026	1.5	245	98.5	0.025	20	1.31	2.0	10	0	2970
30	NRL901030	1.5	245	98.5	0.025	20	1.24	2.0	10	0	2960
31A	NRL910206	1.5	245	97.5	0.1	77	0.50	2.1	10	0.3	2020
31B	NRL910320	1.5	245	97.5	0.1	77	0.48	2.1	10	0.3	2020
33A	NRL910213	1.5	245	97.5	0.1	77	0.46	2.1	10	0.3	2020
33B	NRL910215	1.5	245	97.5	0.1	77	0.44	2.1	10	0.3	2020
39A	NRL910416	1.5	245	97.5	0.1	77	0.47	2.1	10	0.3	2020
39B	NRL910417	1.5	245	97.5	0.1	77	0.46	2.1	10	0.3	2020
43A	NRL910212	1.5	245	97.5	0.1	77	0.46	2.1	10	0.3	2020
43B	NRL910219	1.5	245	97.8	0.1	77	0.46	2.1	10	0.3	2020

Table 6.5. Optical and Physical Properties of the Phase II Fibers

Preform	Optical Attenuation				$\lambda_{co}$ ( $\mu\text{m}$ )	NA	MFD ( $\mu\text{m}$ )	OD ( $\mu\text{m}$ )	Core Power (%)	Clad/Core Dia Ratio	Core Dia ( $\mu\text{m}$ )
	1.3 $\mu\text{m}$	1.38 $\mu\text{m}$	1.38 $\mu\text{m}$	1.38 $\mu\text{m}$							
25	911003	2.52	40.06	1.16	0.162	6.99	132	71	24.0	5.5	
26	900803	1.06	61.82	1.08	0.148	7.99	130	60	24.1	5.4	
27	900928	3.04	11.95	1.13	0.153	7.74	105	67	18.1	5.8	
28	900926	4.77	6.04	1.12	0.132	8.98	128	74	17.3	7.4	
29	901026	0.53	2.25	1.18	0.162	7.03	120	76	20.3	5.9	
30	901030	0.55	4.14	1.17	0.158	7.32	118	72	20.3	5.8	
31A	910206	0.70	0.80	1.19	0.143	7.69	125	80	18.1	6.9	
31B	910320	1.13	5.02	1.14	0.145	7.51	110	79	16.6	6.7	
35A	910213	0.97	2.20	0.96	0.173	6.87	135	71	25.0	5.4	
35B	910215	0.66	0.71	1.10	0.170	6.66	135	68	26.5	5.1	
39A	910416	0.53	4.07	1.18	0.144	6.84	130	88	18.6	7.0	
39B	910417	1.50	8.00	1.17	0.156	7.46	115	76	18.1	6.4	
43A	910212	0.71	1.58	1.05	0.187	6.60	130	65	27.2	4.8	
43B	910219	0.61	0.77	1.16	0.180	6.27	135	72	26.9	5.0	

Table 6.6a. Levels of Fabrication Factors and Radiation Response Parameters

N	Core [Ge]	Core O <sub>2</sub> /R	Speed	Tension	A <sub>0</sub> (dB/km)	A <sub>f</sub> (dB/km)	n	τ (s)
31A	1	1	1	1	4.1	0.0	6.2	260
31B	1	1	1	1	4.4	0.0	5.6	232
32A	1	1	1	2	3.8	0.1	6.2	312
32B	1	1	1	2	3.9	0.0	5.9	264
33A	1	1	2	1	3.2	0.1	5.2	360
33B	1	1	2	1	5.4	0.0	5.0	212
34A	1	1	2	2	4.8	0.0	5.4	244
34B	1	1	2	2	5.0	0.0	5.4	224
35A	2	1	1	1	3.2	0.0	5.7	316
35B	2	1	1	1	3.0	0.0	6.6	304
36A	2	1	1	2	2.8	0.6	5.2	207
36B	2	1	1	2	2.6	0.0	6.4	304
37A	2	1	2	1	3.8	0.0	5.1	195
37B	2	1	2	1	3.3	0.0	2.4	107
38A	2	1	2	2	3.6	0.0	5.6	207
38B	2	1	2	2	6.2	1.0	2.4	90
39A	1	2	1	1	4.5	0.0	6.0	308
39B	1	2	1	1	4.0	0.5	4.8	152
40A	1	2	1	2	4.0	0.0	7.1	420
40B	1	2	1	2	3.8	0.0	6.2	360
41A	1	2	2	1	4.0	0.0	6.7	420
41B	1	2	2	1	3.9	0.4	5.8	200
42A	1	2	2	2	4.0	0.0	6.7	336
42B	1	2	2	2	4.1	0.0	6.2	252
43A	2	2	1	1	2.7	0.0	6.4	377
43B	2	2	1	1	2.8	0.1	6.0	356
44A	2	2	1	2	2.4	0.5	5.2	182
44B	2	2	1	2	2.7	0.0	6.8	550
45A	2	2	2	1	3.0	0.0	6.2	243
45B	2	2	2	1	2.8	0.0	5.2	350
46A	2	2	2	2	3.2	0.0	6.2	243
46B	2	2	2	2	3.2	0.2	5.2	220

**Table 6.7**  
**Probability of no effect between radiation response parameters and fabrication variables derived from 2<sup>4</sup> experimental design**

Parameter	Variable	p
A <sub>o</sub>	[Ge]	< 0.0001
	O <sub>2</sub> /R	< 0.05
	Draw Speed	< 0.02
	Draw Speed X Tension	< 0.06
	O <sub>2</sub> /R X Speed	< 0.09
A <sub>f</sub>	[Ge] X Tension	< 0.04
n	O <sub>2</sub> /R	< 0.10
	Draw Speed	< 0.13
	O <sub>2</sub> /R X Speed	< 0.14
τ	O <sub>2</sub>	< 0.14



SPECTRAL ATTENUATION LENGTH: .4770 km  
ID: NRL901026 5-NOV-90 10:42:48

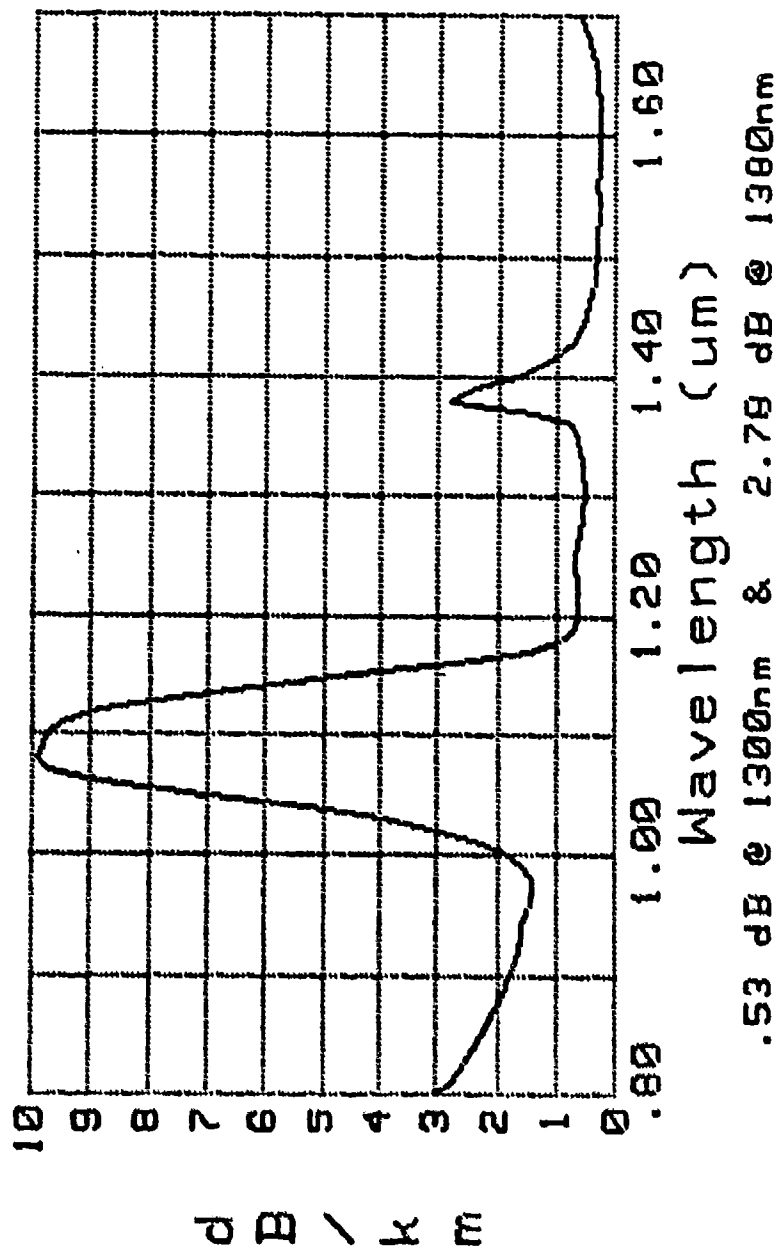


Figure 6.1. Attenuation of a typical matched clad single mode fiber fabricated during the Phase II study. The large attenuation peak near 1.1  $\mu\text{m}$  is the second mode cutoff; the fiber is designed to work at 1.3  $\mu\text{m}$ .

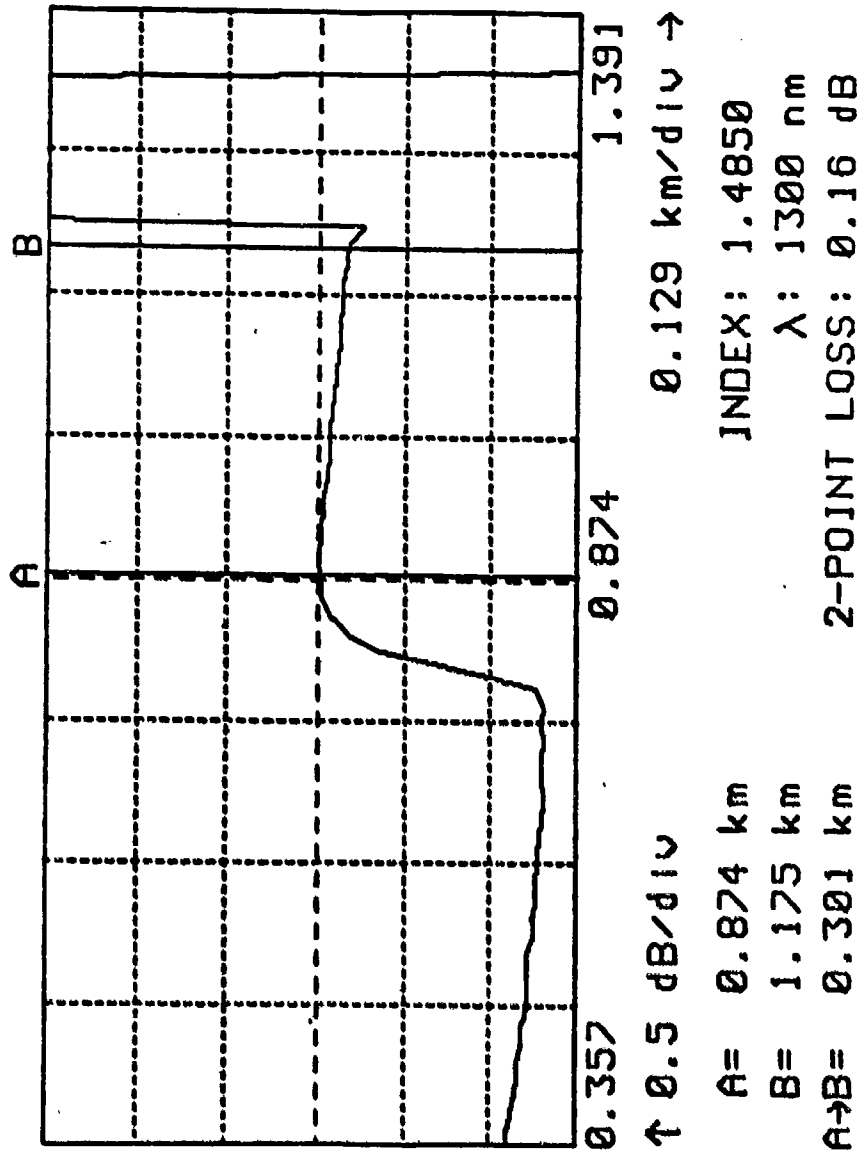


Figure 6.2 Optical time domain reflectometry trace of a matched clad single mode fiber fabricated during the Phase II study. The fiber data are contained between cursors A and B.

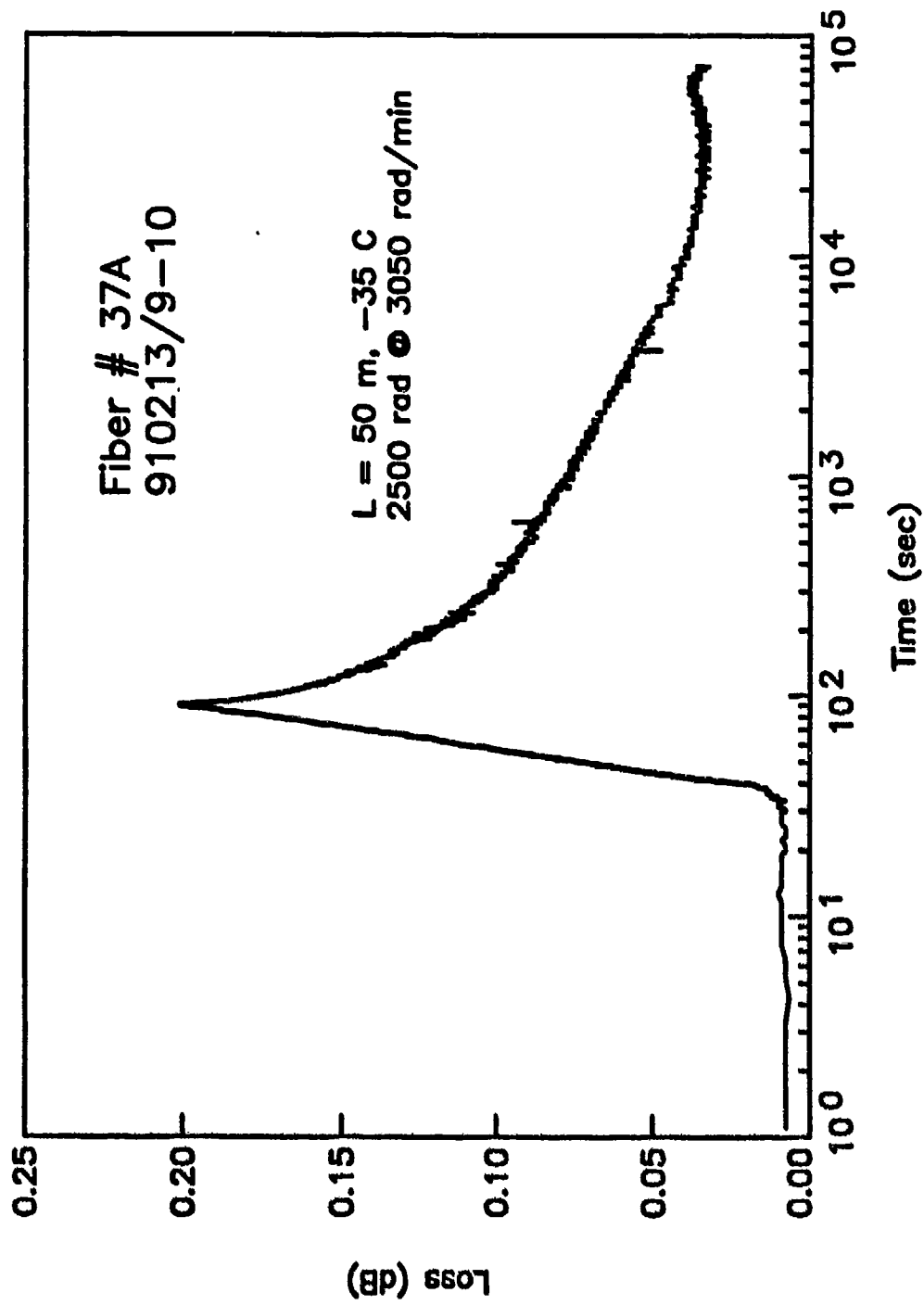


Figure 6.3. Raw data showing the growth of the radiation-induced attenuation of a fiber during exposure and the recovery following removal from the  $^{60}\text{Co}$  source.

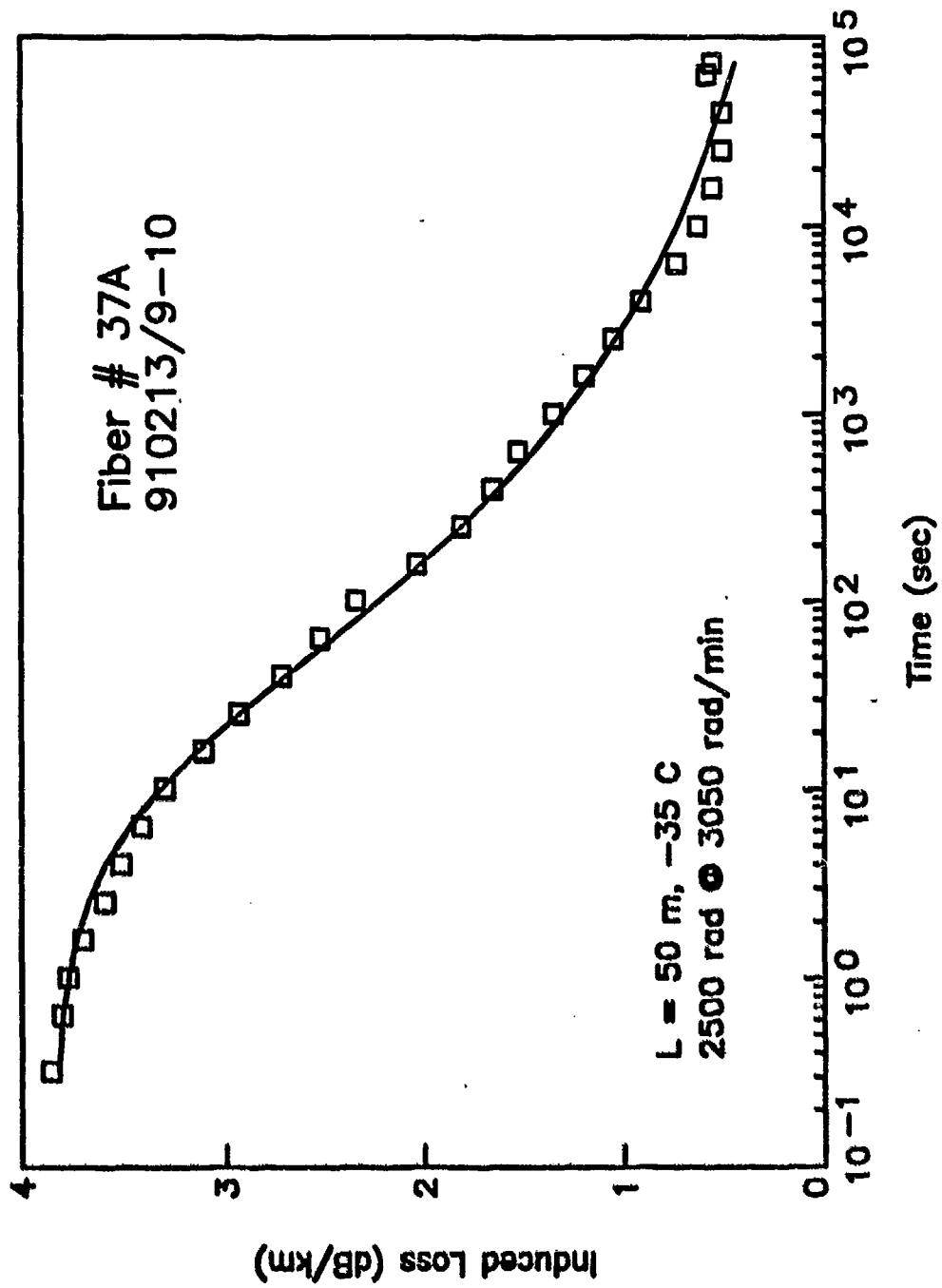


Figure 6.4 Recovery data extracted from the raw data of Fig. 6.3 (points) and the fit of the data to  $n^{\text{th}}$  order kinetic behavior as in Eq. 3.3 (line).

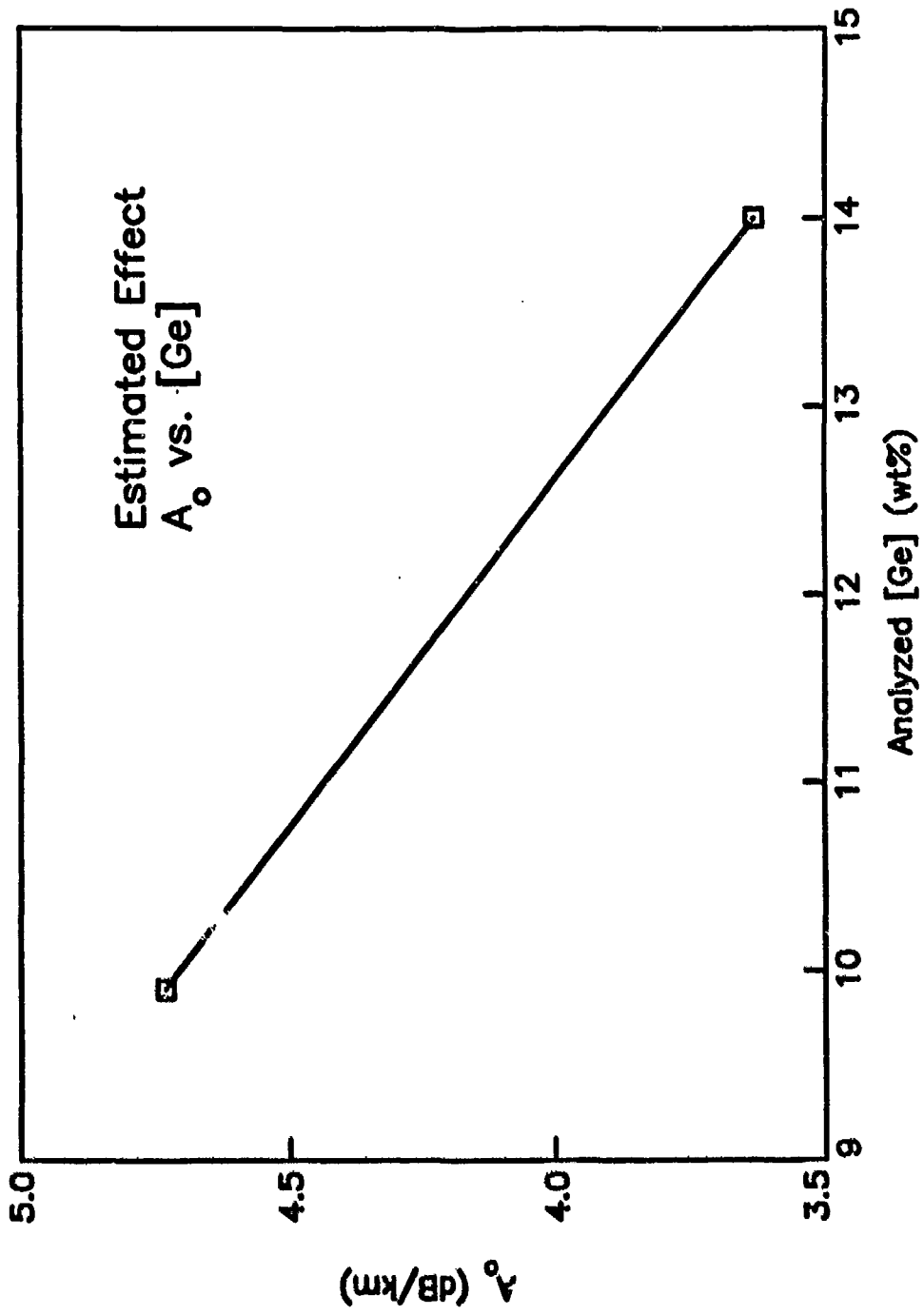


Figure 6.5 Estimated effect of core [Ge] analyzed by electron microprobe on  $A_0$ .

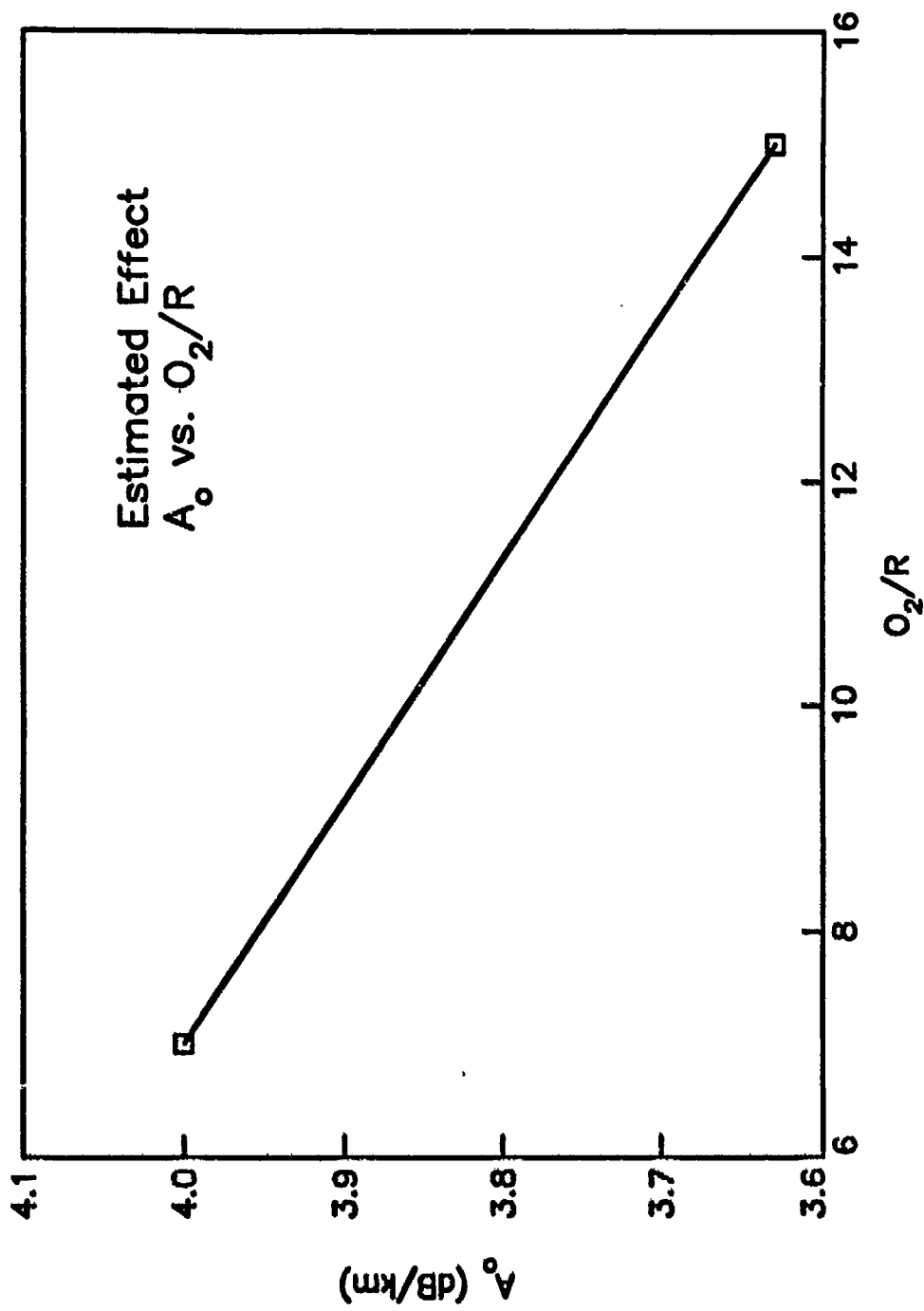


Figure 6.6 Estimated effect of oxygen-to-reagent ratio used during core deposition on  $A_0$ .

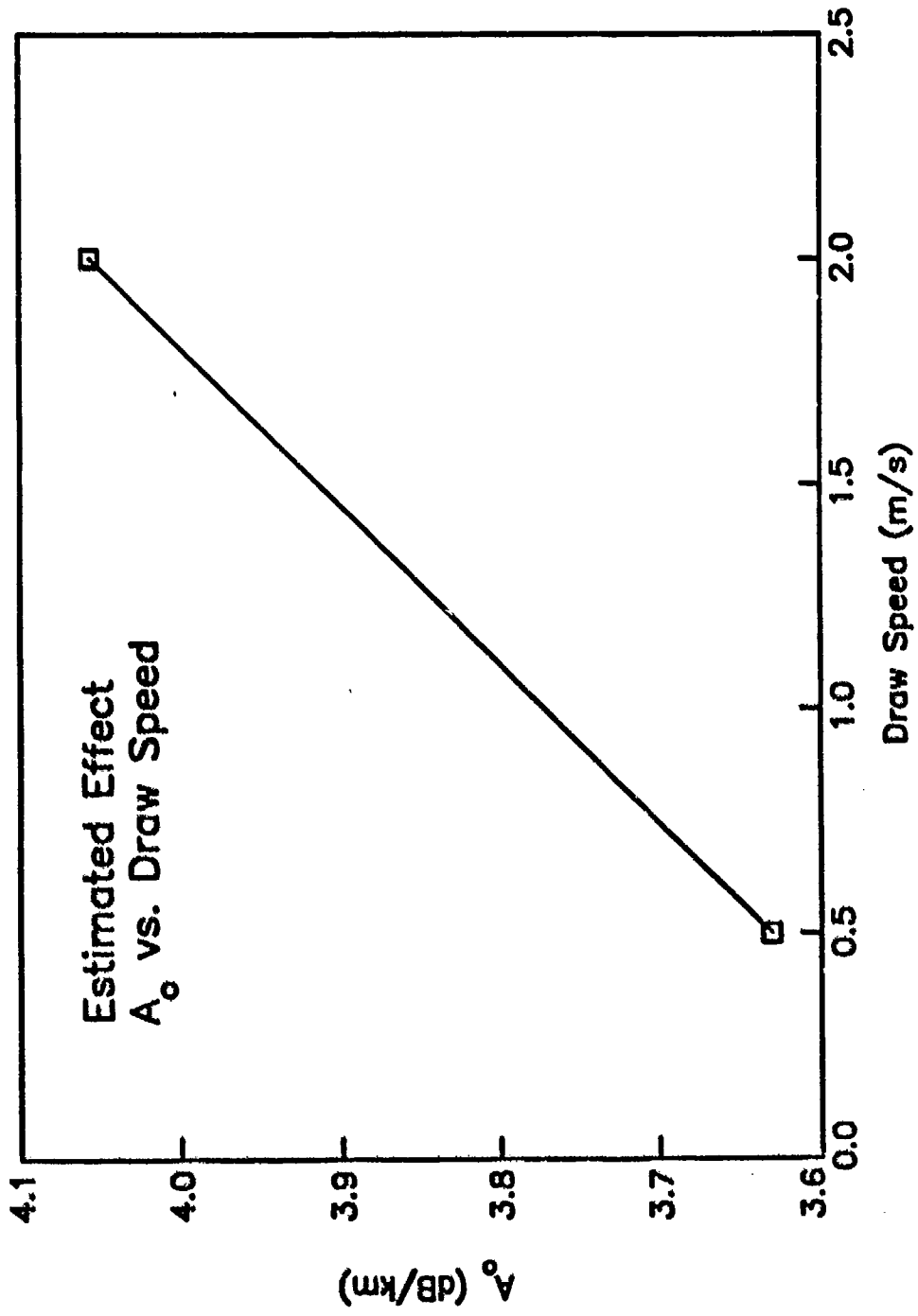


Figure 6.7 Estimated effect of draw speed on  $A_0$ .

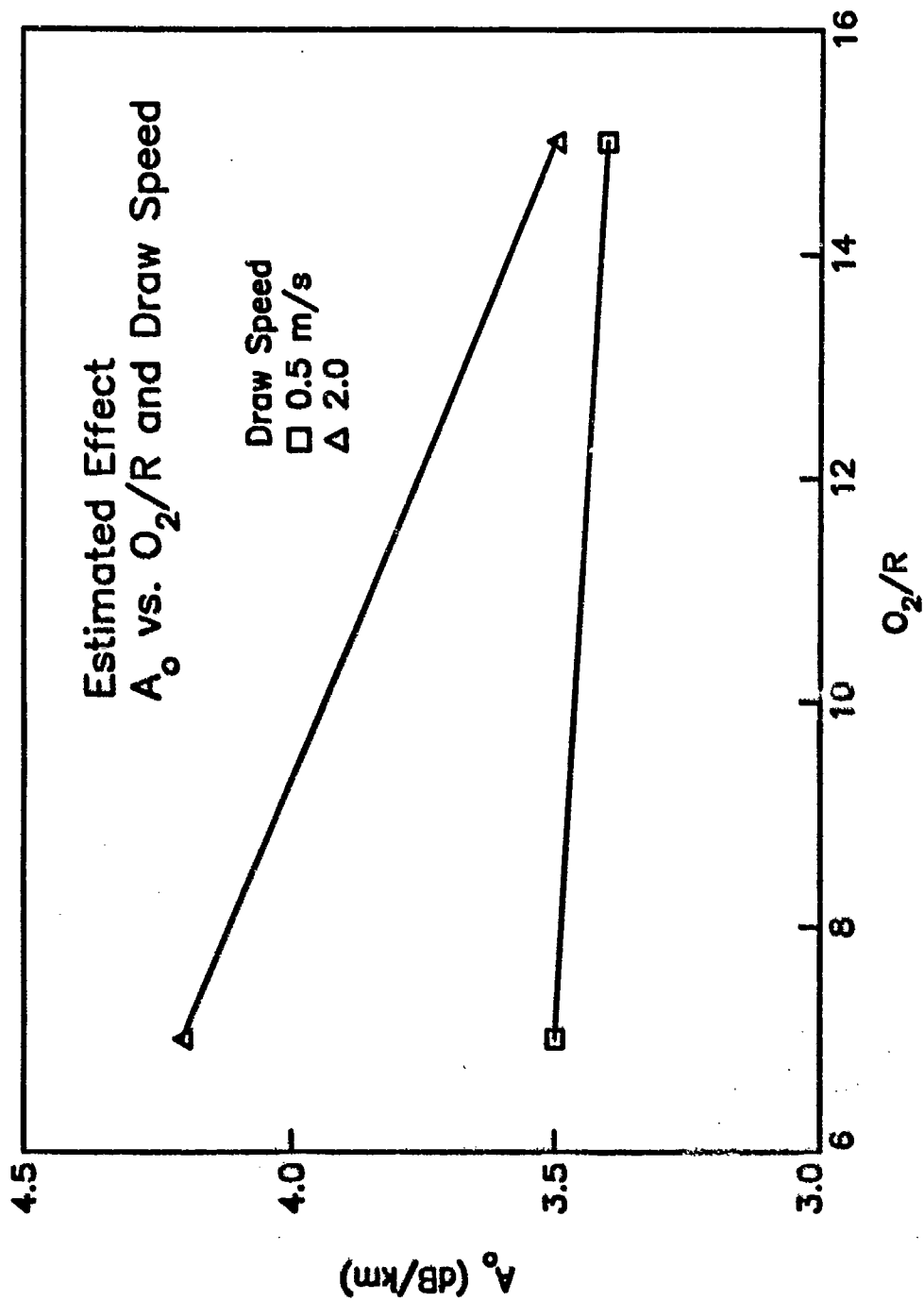


Figure 6.8. Estimated effect of the two-way interaction of oxygen-to-reagent ratio used during core deposition and fiber draw speed on A<sub>o</sub>.



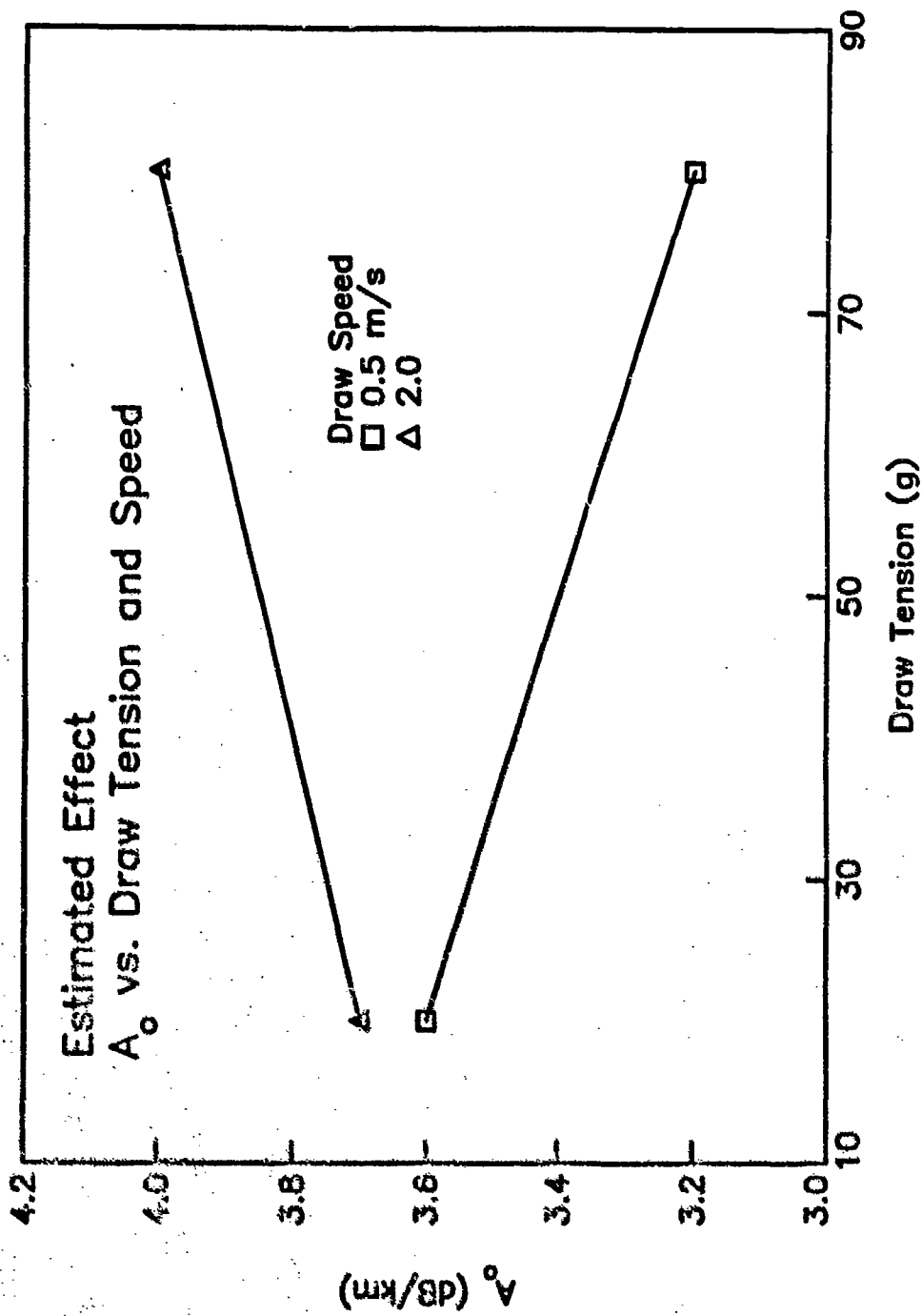


Figure 6.9. Estimated effect of the two-way interaction of fiber draw speed and draw tension on A<sub>0</sub>.

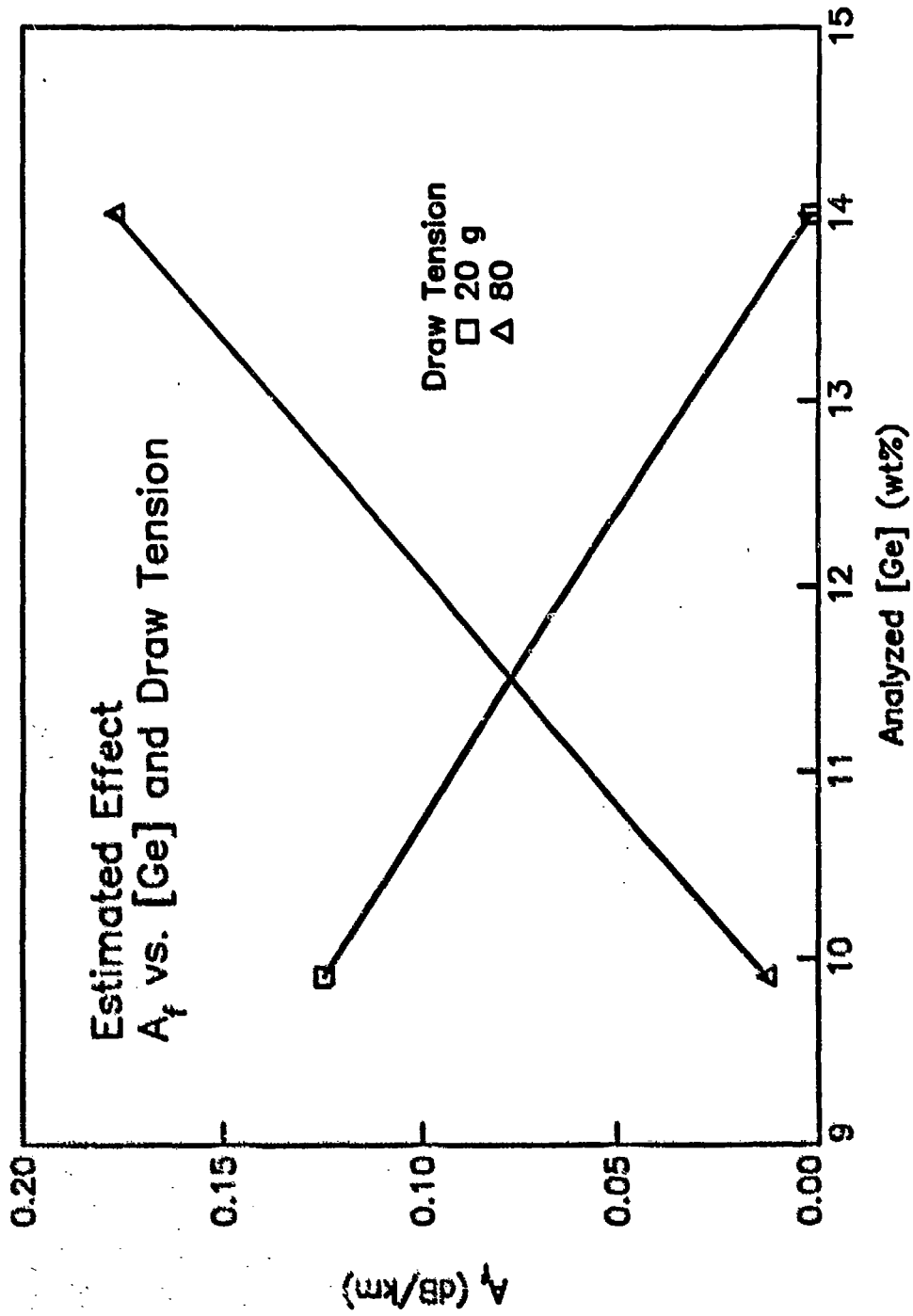


Figure 6.10. Estimated effect of the two-way interaction of core [Ge] and draw tension on  $A_f$ .

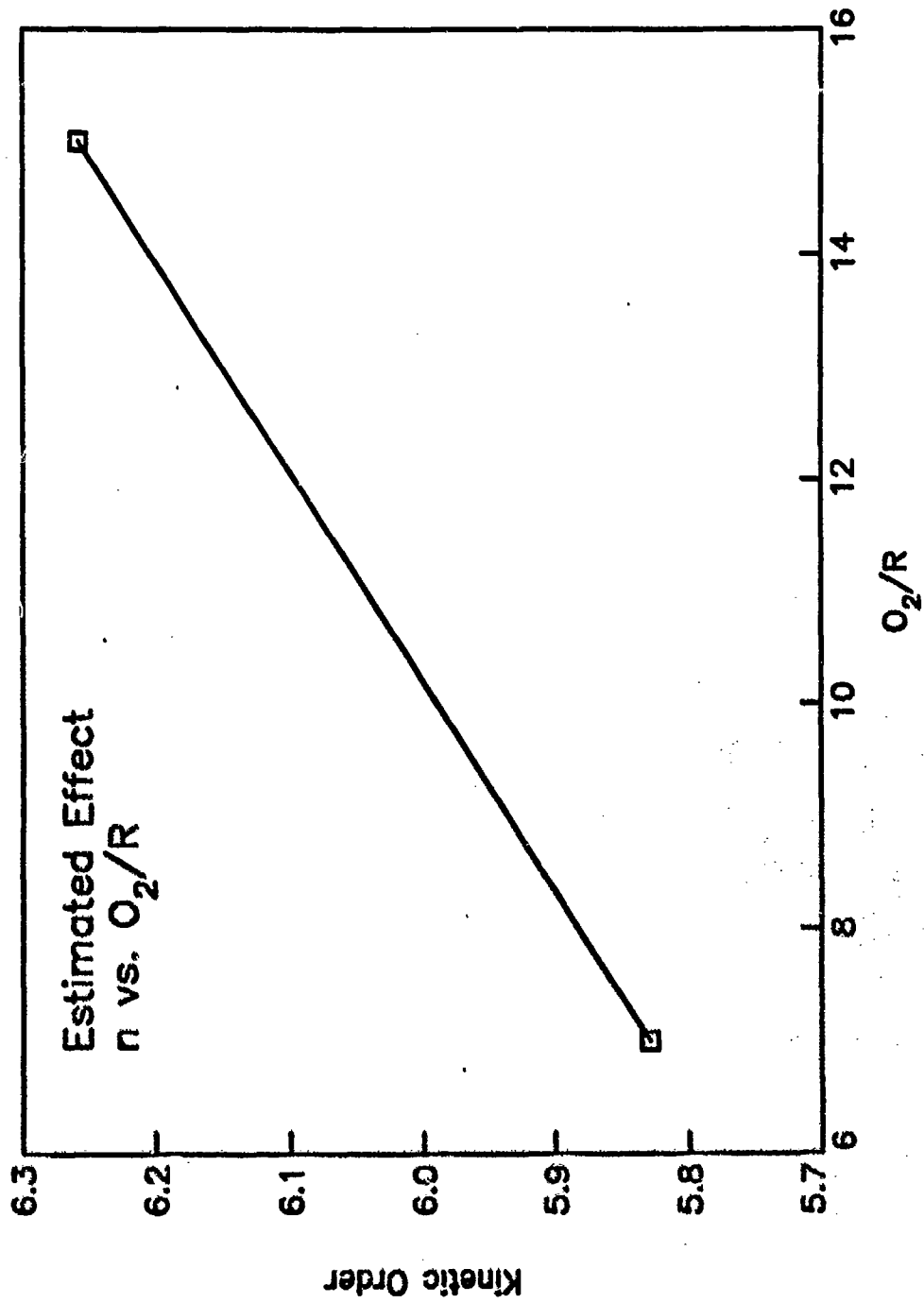


Figure 6.11. Estimated effect of oxygen-to-reagent ratio used during core deposition on n.

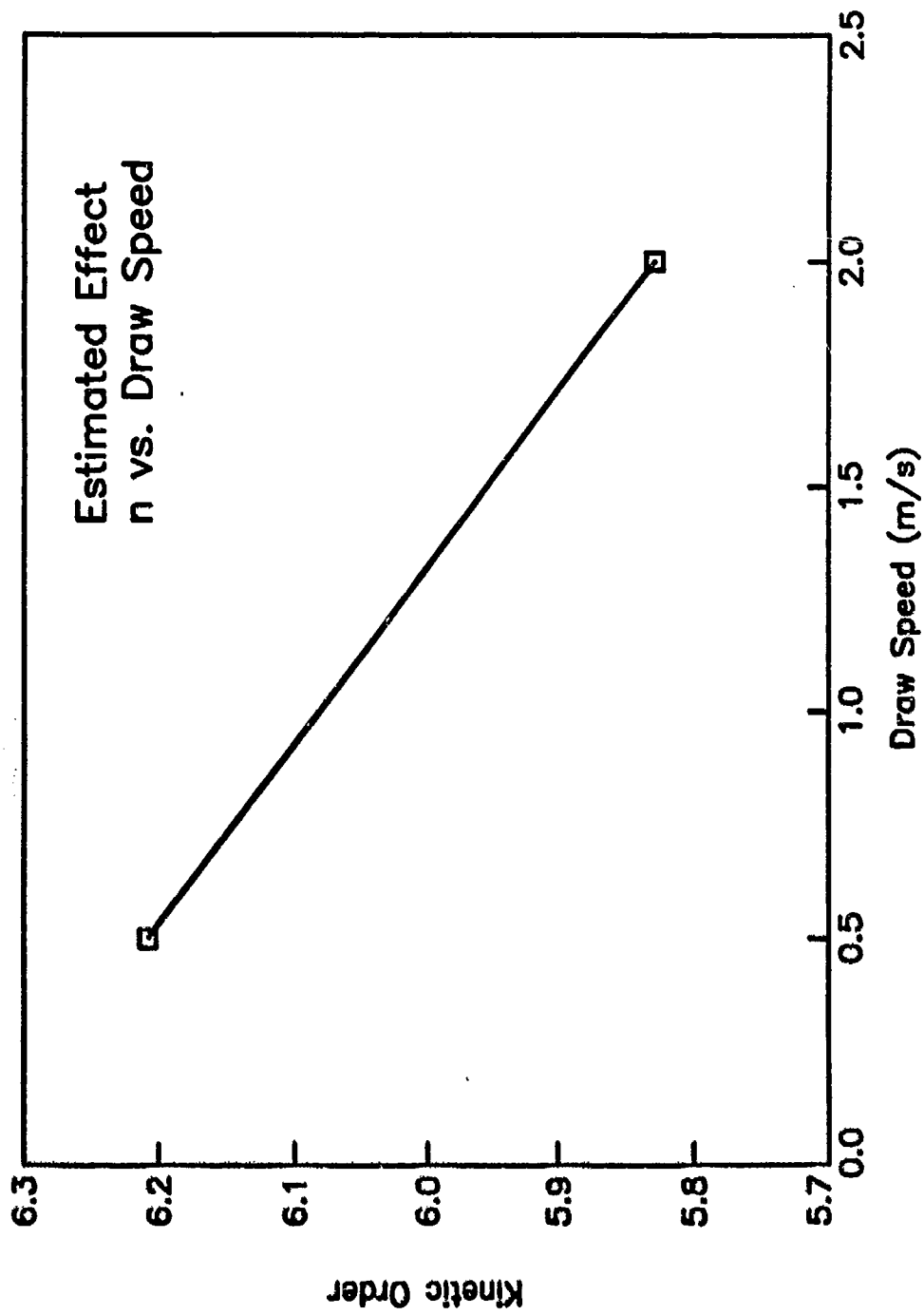


Figure 6.12. Estimated effect of fiber draw speed on n.

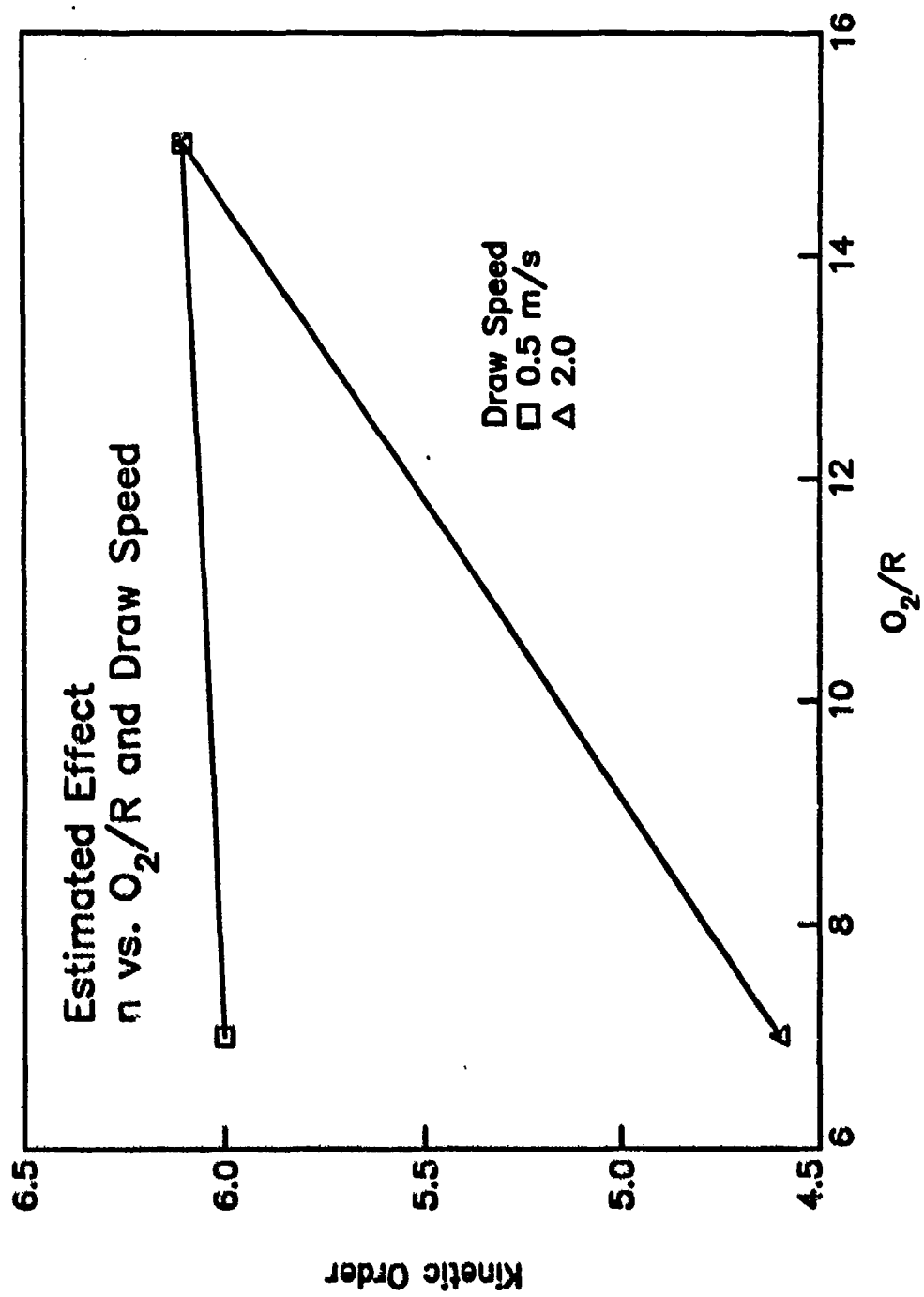


Figure 6.13. Estimated effect of the two-way interaction of oxygen-to-reagent ratio used during core deposition and draw speed on  $n$ .

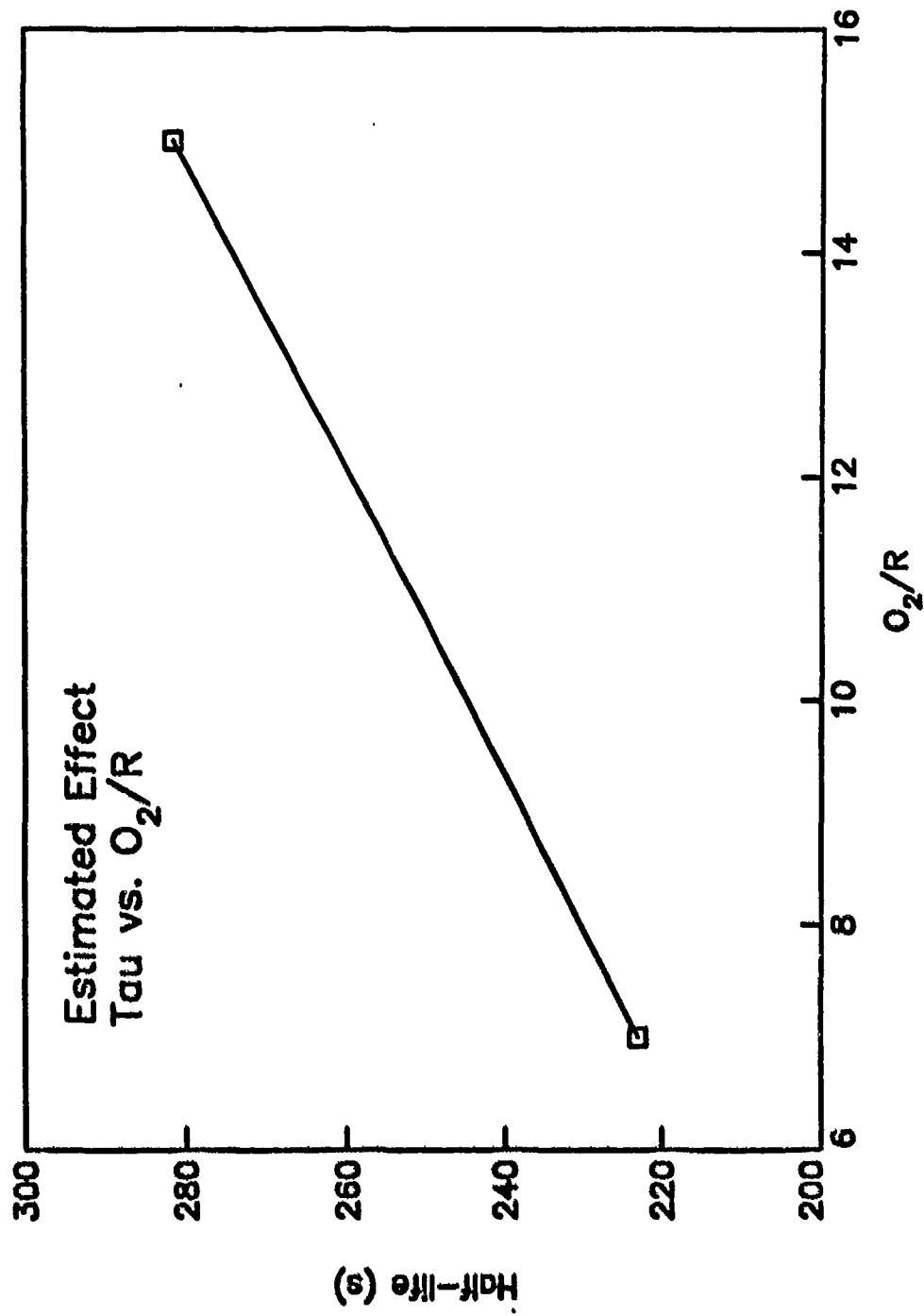


Figure 6.14. Estimated effect of oxygen-to-reagent ratio used during core deposition on  $\tau$ .

## CHAPTER 7

### CONCLUSIONS

The present investigation of the relationship between single mode fiber fabrication variables and the recovery of the induced attenuation following radiation exposure has established a number of statistically significant correlations which have important implications for the selection and fabrication of optical fiber cables that are hardened against radiation environments. Because a rigorous  $2^4$  experimental design was used in Phase II, there is no confounding of the main effects and two-way interactions. The Phase II results are in general consistent with those of Phase I, and where discrepancies are evident, they may be attributed to either differences in the levels chosen for the fabrication factors or confounding in the Phase I design. Interestingly, because of the absence of confounding, several additional main effects and two way interactions were revealed to have statistical significance in Phase II. For example, draw speed has been shown to play a critical role through  $A_0$ ,  $A_T$ , and  $n$  through both main effects and two way interactions.

#### 7.1 SUMMARY OF RESULTS

The present study has clearly shown the relationship between single mode fiber core and clad fabrication factors and radiation response. Although the principal determinant of radiation response is the core since the largest fraction of the optical power is guided in the core, variations in clad fabrication can be used to advantage to further decrease the radiation response of fibers. A summary of the core effects follows:

##### 7.1.1 Core Effects.

1.  $A_0$  decreases with increasing core [Ge] or  $O_2/R$  but increases with increasing draw speed. Due to a two way interaction of draw speed and  $O_2/R$  on  $A_0$ , there is no effect of high  $O_2/R$  and no effect of  $O_2/R$  at low draw speed. Similarly, because of the two way interaction of draw tension and draw speed, there is no effect of draw speed on  $A_0$  at low tension.

2. Although  $A_f$  decreases substantially upon decreasing  $O_2/R$  from 5 to 7, there is no further decrease between 7 and 15. Thus, the use of moderate amounts of oxygen during core deposition is sufficient to minimize  $A_f$ . There is a weak two way interaction of core [Ge] and draw tension, which shows that  $A_f$  is minimized for either low [Ge] and high tension or high [Ge] and low tension.
3. Both  $n$  and  $\tau$  increase with increasing  $O_2/R$ , while  $n$  decreases with increasing draw speed. Due to a two way interaction of  $O_2/R$  and draw speed on  $n$ , there is no effect of  $O_2/R$  on  $n$  at low draw speed and no effect of draw speed at high  $O_2/R$ .

#### 7.1.2 Clad Effects.

1. For the silica clad fibers,  $A_0$  is large, but  $n$  and  $\tau$  are both substantially smaller than in the doped silica clad fibers. Although the incremental attenuation is high, recovery is rapid.
2. Doping the clad with even the smallest amount of Ge (and the appropriate amount of F to maintain index matching to the silica substrate tube) greatly decreases  $A_0$  and increases  $n$  and  $\tau$ . As expected from Phase I and the core studies,  $A_0$  decreases slightly with increasing Ge.
3. In fibers with low clad Ge content, increasing the amount of F above the matched clad condition, which depresses the cladding index below the silica substrate, results in significant increases in  $n$  and  $\tau$ , but now change in  $A_0$  or  $A_f$ . Hence, the level of incremental attenuation is unchanged, but the recovery is substantially slowed.

7.1.3 Temperature Dependence. Studies of the temperature dependence of the recovery of the radiation-induced attenuation in commercial single mode fibers have shown that the color center concentration is temperature dependent, which causes  $A_0$ , and to a lesser extent  $A_f$ , to be thermally activated. Although the kinetic order is independent of temperature, the half-life  $\tau$  is thermally activated due to its dependence on the rate constant for diffusion. An interesting observation is that the activation energy of  $\tau$  is *negative* in both the phosphorus doped silica clad Northern Telecom fiber and in the pure silica core Sumitomo Z fiber. In the former, this is due to relative thermal stabilities of the phosphorus-related color centers contributing to the incremental loss, while the effect is not



understood in the latter. Nevertheless, these data provide the first quantitative analysis of the temperature dependence of the radiation-induced loss in single mode fibers.

## 7.2 RADIATION HARD FIBER DESIGN.

The results of the Phase II study indicate variations in the fabrication factors for matched clad 1.3  $\mu\text{m}$  single mode fibers which can substantially increase their radiation hardness. However, in some cases these are contradictory, and appropriate measures must be selected for the intended application and environment of the fiber.

**7.2.1 Fallout Radiation Environment.** The primary concern for fibers exposed to the fallout from a nuclear weapons detonation is their low dose rate response. The net incremental attenuation in a fiber is the sum of the competing processes of darkening due to radiolytic electron and hole trapping and resultant color center formation and recovery due to thermal and light-induced annealing. Thus, it is important to maximize the recovery, i.e. to minimize  $A_p$ ,  $n$  and  $\tau$ .

The results discussed above and in Chapter 6 have shown that for the Ge-doped silica core, low  $O_2/R = 7$  will decrease  $n$  and  $\tau$ , while further decreases in  $O_2/R$  will result in unacceptably high values of  $A_p$ . Because of the two way interactions, the kinetic order will be minimized at a 2 m/s draw speed (and low  $O_2/R$ ), low draw tension (20 g) and high core [Ge].

For the matched clad fiber design, the best recovery is offered by pure silica clad, although the processing difficulty and  $A_0$  are substantially increased. As Ge and F are more heavily doped, while still maintaining the matched clad condition,  $n$  increases slightly. So, the most cost effective design for doped clads seems to be slight Ge and F doping.

Depressed clad fiber design are required for shifting the zero pulse dispersion to longer wavelength or for dispersion flattening for wavelength division multiplexing. In these cases, doping levels of F above that required for matched clad are used, and the one-dimensional study has shown that this results in a substantial increase in both  $n$  and  $\tau$ . This retardation of the recovery may have severe consequences for both WDM and long wavelength systems. Depressed clads can and should

be avoided for 1.3  $\mu\text{m}$  fibers; they are not required to minimize pulse dispersion since the zero dispersion wavelength is near 1.3  $\mu\text{m}$ .

**7.2.2 Delayed Gamma Radiation Environment.** The incremental loss induced by the delayed gamma component and the time required for a system to clear following a detonation is determined the initial attenuation  $A_0$  as well as the recovery parameters and to a lesser extent  $A_f$ . The most significant effect on  $A_0$  is core [Ge], and maximizing this is not in conflict with the requirements of good recovery described above. Likewise, heavily doping the clad with Ge and F will further decrease  $A_0$  while only slightly increasing  $n$ . A more significant clad effect occurs in the pure silica clad fiber, which has extremely large values of  $A_0$  but excellent recovery. The question in this case is whether the recovery is sufficiently fast that the system can be restored within the requisite time period in spite of the large initial loss.

Increasing core  $O_2/R$  to 15 will further decrease  $A_0$ , but at the expense of increasing  $n$  and  $r_i$ ; decreased draw speed, which decreases  $A_0$  is not only cost-ineffective but also increases  $n$ ; but low draw tension is compatible with minimizing both  $A_0$  and  $A_f$ .

Thus, it is apparent that some tradeoffs must be made to optimize hardness to both the delayed gamma and fallout radiation environments. The parameters which must be optimized are the core  $O_2/R$ , draw speed, and clad [Ge], and it remains to the fiber designer to select appropriate values. Nevertheless, the results of Phase II have provided sufficient information for fiber manufacturers to optimize their product, especially for the fallout radiation environment which is likely of more import for long line telecommunications. It should be emphasized, that most of the indicated variations in fabrication factors can be made with little additional expense to the manufacturing process and without degrading the intrinsic properties of the fiber. Nevertheless, radiation hard fibers can be made in a cost-effective manner.

### 7.3 FUTURE DIRECTIONS

The studies completed under Phases I and II of this program have demonstrated a high degree

of correlation between matched clad single mode fiber fabrication factors and the recovery of the radiation-induced attenuation at 1.3  $\mu\text{m}$ . The estimated effects derived from the statistical analysis in Phase II can be used to develop a rudimentary capability for predicting the radiation response of deployed fiber from knowledge of the core and clad compositions, deposition conditions and draw parameters. The predictive capability could be more fully developed by fabricating additional preforms and fibers with levels of factors intermediate between those used in Phase II. Likewise, the two-level experimental design used in Phase II could derive only first order dependencies, and there is no *a priori* reason to suspect that the dependence is not of higher order. Additional studies at intermediate levels would resolve these issues.

Of more importance is the fact that 1.3  $\mu\text{m}$  lightwave systems are now being installed and retrofitted with erbium-doped fiber amplifiers pumped by semiconductor laser diodes because of their high gain, reliability, and broadband amplification. There is virtually no data on the effects of nuclear radiation on the attenuation, gain, or spontaneous emission of these devices. Because of their intended widespread application in the telecommunications network, there is a critical need to establish a data base of their radiation response, and if necessary, study ways to improve their radiation hardness.

Although the Phases I and II studies have demonstrated fabrication-response relationships at 1.3  $\mu\text{m}$ , the next generation of lightwave communications systems will operate either at the single wavelength of 1.55  $\mu\text{m}$  to take advantage of the lower intrinsic loss and higher bandwidth or wavelength-division multiplexed between 1.3  $\mu\text{m}$  and 1.55  $\mu\text{m}$ . To achieve high bandwidth in these fibers, complex core designs and depressed clads are typically used. As indicated in Chapter 5, the presence of excess F in the clad to obtain the cladding depression seems to have a deleterious effect on the recovery following radiation exposure. Yet, these are only preliminary results.

There are critically important knowledge gaps with respect to the newer 1.55  $\mu\text{m}$  single mode cables envisioned for the next generation of inter-city high data rate transmission links. There are 3 urgent needs if we are to have the tools necessary to assess the vulnerability future fiber optic

**systems operating at 1.55  $\mu\text{m}$ :**

- 1. The existing data base of single mode fiber radiation responses must be expanded to include 1.55  $\mu\text{m}$  fibers, which are significantly different in structure from those designed for 1.3  $\mu\text{m}$ , so that a systems designer will have the capability of choosing fibers which will survive an anticipated environment.**
- 2. A protocol must be developed for fabricating 1.55  $\mu\text{m}$  single mode optical fibers with greatly enhanced radiation hardness, and the effect of excess F must be thoroughly characterized and studied.**
- 3. As a spin-off of the experiments performed to develop the protocol, a model for predicting fiber radiation response at 1.55  $\mu\text{m}$  with statistical confidence over a wide range of doses, dose rates, and temperatures should be developed so that the survivability of both new and existing installed cables can be quantitatively determined from the fiber fabrication parameters without explicit radiation damage measurements or further sample generation.**

**Because the WDM and long wavelength systems are just now being designed, it is a critical time to perform assessments and studies so that the fiber parameters necessary for system radiation hardness can be implemented in the early stages of fabrication.**

**SUPPLEMENTARY**

**INFORMATION**

Naval Research Laboratory

Washington, DC 20375-5000



NRL/MR/6505-92-6939

NCS Technical Information Bulletin 91-11

ADA 247301

**Correlation of Single Mode Fiber  
Fabrication Factors and Radiation Response**

**Final Report  
November 1991**

E. J. FRIEBELE

*Optical Sciences Division  
Optical Materials Research Group*

Sponsored by

National Communications System  
Arlington, VA

February 28, 1992



Approved for public release; distribution unlimited.

Fabrication sheet  
in Handbook

Erratum Sheet  
 Correlation of Single Mode Fiber Fabrication Factors and Radiation Response  
 NRL Memorandum Report 92-6939  
 NCS Technical Information Bulletin 91-11

Table 6.3, Page 112

Table 6.3 Parameters Used in Depositing the Core of Matched Clad Single Mode Fiber Preforms  
 and the Glass Composition (wt% Oxide) Determined by Electron Microprobe

Fiber	Preform	SiO <sub>2</sub> g/m	SiO <sub>2</sub> flow ccm	wt%	SiO <sub>2</sub> g/m	GeCl <sub>4</sub> flow ccm	wt%	F wt%	O <sub>2</sub> flow lpm	O <sub>2</sub> /R	He flow lpm	Temp C
25	NRL901002	0.26	44	91.6	0.077	60	9.4	0.0	0.60	15	0.4	1970
26A	NRL900726	0.26	44	—	0.070	54	—	—	0.60	15	0.4	1950
26B	NRL900803	0.26	44	91.0	0.070	54	9.0	0.0	0.60	15	0.4	1960
27	NRL900928	0.26	44	91.2	0.084	65	9.8	0.0	0.60	15	0.4	1970
28	NRL900926	0.26	44	91.9	0.077	60	5.0	0.1	0.60	15	0.4	1940
29A	NRL901024	0.26	44	—	0.077	60	—	—	0.60	15	0.4	1960
29B	NRL901926	0.26	44	90.6	0.077	60	9.3	0.1	0.60	15	0.4	1960
30	NRL901930	0.26	44	92.5	0.064	50	7.3	0.2	0.60	15	0.4	1960
31A	NRL910206	0.26	44	88.6	0.122	95	11.3	0.1	0.33	7	0.1	1990
31B	NRL910330	0.26	44	88.9	0.122	95	11.0	0.1	0.33	7	0.1	2020
32A	NRL910213	0.26	44	84.8	0.174	135	15.0	0.2	0.37	7	0.2	1990
32B	NRL910215	0.26	44	85.6	0.181	140	14.5	0.1	0.37	7	0.2	1990
33A	NRL910416	0.26	44	90.4	0.077	60	9.5	0.1	0.60	15	0.4	1990
33B	NRL910417	0.26	44	89.4	0.077	60	10.5	0.1	0.60	15	0.4	1990
43A	NRL910212	0.26	44	93.9	0.116	90	16.0	0.1	0.66	15	0.4	1985
43E	NRL910219	0.26	44	85.9	0.116	90	14.0	0.1	0.66	15	0.4	1980